BOUNDARY ELEMENT-FINITE ELEMENT ACOUSTIC ANALYSIS OF COUPLED DOMAINS

A THESIS SUBMITTED TO
THE GRADUATE SCHOOL OF NATURAL AND APPLIED SCIENCES
OF
MIDDLE EAST TECHNICAL UNIVERSITY

BY

BÜLENT İRFANOĞLU

IN PARTIAL FULFILLMENT OF THE REQUIREMENTS
FOR
THE DEGREE OF DOCTOR OF PHILOSOPHY
IN
MECHANICAL ENGINEERING

AUGUST 2004

Approval of the Graduate School of Natural and Applied Sciences

_____

Prof. Dr. Canan ÖZGEN
Director

I certify that this thesis satisfies all the requirements as a thesis for the degree of Doctor of Philosophy.

_____

Prof. Dr. S. Kemal İDER
Head of Department

This is to certify that we have read this thesis and that in our opinion it is fully adequate, in scope and quality, as a thesis for the degree of Doctor of Philosophy.

_____

Prof. Dr. Mehmet ÇALIŞKAN
Supervisor

Examining Committee Members

Prof. Dr. Y. Samim ÜNLÜSOY (METU-ME) _____

Prof. Dr. Mehmet ÇALIŞKAN (METU-ME) _____

Prof. Dr. Yalçın MENGİ (METU-ES) _____

Prof. Dr. A. Erman TEKKAYA (METU-ME) _____

Dr. A. Hakan ARGEŞO (Baskent Unv.) _____

I hereby declare that all information in this document has been obtained and presented in accordance with academic rules and ethical conduct. I also declare that, as required by these rules and conduct, I have fully cited and referenced all material and results that are not original to this work.

Name, Last name : Bülent, İrfanoğlu

Signature :

ABSTRACT

BOUNDARY ELEMENT-FINITE ELEMENT ACOUSTIC ANALYSIS OF COUPLED DOMAINS

Bülent İrfanoğlu

Ph.D., Department of Mechanical Engineering

Supervisor : Prof. Dr. Mehmet Çalışkan

August 2004, 124 pages

This thesis studies interactions between coupled acoustic domain(s) and enclosing rigid or elastic boundary. Boundary element-finite element (BE-FE) sound-structure interaction models are developed by coupling frequency domain BE acoustic and FE structural models using linear inviscid acoustic and elasticity theories.

Flexibility in analyses is provided by discontinuous triangular and quadrilateral elements in the BE method (BEM), and a rectangular plate and a triangular shell element in the FE method (FEM).

An analytical formulation is developed for an extended fundamental sound-structure interaction problem that involves locally reacting sound absorptive treatment on interior elastic boundary. This new formulation is built upon existing analytical solutions for a configuration known as the cavity-backed-plate problem. Results from developed analytical formulation are compared against those from independent BE-FE analyses.

Analytical and BE-FE analysis results for a selection of cavity-plate(s) interaction cases are given.

Single- and multi-domain BE analyses of cavity-Helmholtz resonator interaction are provided as an alternative to modal method of acoustoelasticity.

A discrete-form of the existing BE acoustic particle velocity formulation is presented and demonstrated on a basic case study. Both the existing and the discretized BE acoustic particle velocity formulations could be utilized in acoustic studies.

A selection of case studies involving fundamental configurations are studied both analytically and computationally (by BE or BE-FE methods). These studies could provide a basis for benchmark case development in the field of acoustics.

Keywords: Boundary Element Method, Finite Element Method, Structural-Acoustic Coupling, Fluid-Structure Interaction, Helmholtz Resonator

ÖZ

BAĞLAŞIKLI ORTAMLARIN SINIR ELEMAN-SONLU ELEMAN AKUSTİK ANALİZİ

Bülent İrfanoğlu
Doktora, Makina Mühendisliği Bölümü
Tez Yöneticisi: Prof. Dr. Mehmet Çalışkan

Ağustos 2004, 124 sayfa

Bu tez bağlaşıklı ortam(lar) ile çevrelerindeki rijit veya esnek cidarlar arasındaki etkileşimi inceler. Sınır eleman-sonlu eleman (BE-FE) ses-yapı etkileşim modelleri frekans alanında BE akustik ve FE yapısal eleman modellerinin lineer, viskoz olmayan akustik ve elastisite teorileri kullanılarak geliştirilmişlerdir.

BE metodunda sürekli olmayan ücgen ve dörtgen elemanlar, FE metodunda da dörtgen plaka ve üçgen kabuk elemanların kullanımı yaklaşıma esneklik sağlamayı amaçlamaktadır.

Yerel tepki gösteren türde ses yutumu uygulanmış elastik cidarları içerecek şekilde genişletilmiş temel bir ses-yapı etkileşim problemine analitik bir çözüm geliştirilmiştir. Bu yeni çözüm plaka-destekli-oyuk (cavity-backed-plate) olarak bilinen problem için mevcut çözümler üzerine inşa edilmiştir. Geliştirilmiş analitik çözümün sonuçları bağımsız BE-FE analiz sonuçları ile karşılaştırılmıştır.

Seçilmiş oyuk-plaka(lar) etkileşimli durumlar için analitik ve BE-FE analiz sonuçları verilmiştir.

Oyuk-Helmholtz rezonatör etkileşimi için tek- ve çok-ortamlı BE analizleri, bir titreşim biçimi analiz yöntemi olan akustoelastisite yöntemine seçenek olarak

sunulmuşlardır.

Mevcut BE akustik parçacık hız formülasyonu ayrık formunda verilmiş ve basit bir durum çalışması örneğine uygulanmıştır. Mevcut bütünleşik ve ayrık formülasyonun akustik çalışmalarda kullanılabileceği gösterilmiştir.

Temel konfigürasyonlar içeren seçilmiş vaka çalışmaları analitik ve sayısal (BE ve BE-FE yöntemleri) olarak incelenmiştir. Bu vaka çalışmaları ile akustikte esas-örnek geliştirme çalışmalarına temel oluşturmak amaçlanmıştır.

Anahtar Kelimeler: Sınır Eleman Yöntemi, Sonlu Eleman Yöntemi, Yapısal-Akustik Bağlaşıklık, Akışkan-Yapı Etkileşimi, Helmholtz Rezonatörü

To My Family

ACKNOWLEDGMENTS

I wish to express my sincere appreciation to my supervisor Prof. Dr. Mehmet Çalışkan for his guidance and providing the oppurtunities to conduct thesis study.

I would also like to express my gratitude to Ph.D. advisory and examining committee members Prof. Dr. Yalçın Mengi and Prof. Dr. A. Erman Tekkaya for their suggestions and help throughout my research; to examining commitee members Prof. Dr. Y. Samim Ünlüsoy for his comments and to Assist. Prof. Dr. A. Hakan Argeşo for his kind help.

Furthermore, I would like to express my sincere thanks to Assoc. Prof. Dr. Yusuf Özyörük for his comments and thoughtful help.

Last but not least, I am indebted to my parents and brothers for their support and unceasing patience and encouragement.

TABLE OF CONTENTS

CHAPTER 1

INTRODUCTION

1.1 General

Acoustic field analysis within enclosed spaces in audio frequency range is the subject of many engineering applications. Passenger cabins of transportation vehicles are typical examples to the type of structures considered in some of the acoustic studies. Elimination or at least reduction of any possible physical damage to humans and improvement of the quality of our lives might be considered as two particular reasons for the need of engineering acoustic studies.

The variety in possible shapes of an enclosed space (cavity, enclosure) and physical conditions require use of flexible engineering analysis tools. Along with the engineering approach, there exist limited closed form analytical solutions to some fundamental configurations and experimental studies that provide further insight to acoustic research studies.

In computational acoustic studies, boundary element (BE) and finite element (FE) analyses are now being widely used. The FE method (FEM) is at a more developed state compared to the BE method (BEM). However, each method has its own distinct advantageous characteristics, which makes them invaluable to engineering studies. The boundary element-finite element (BE-FE) method utilizes respective merits of the BEM and the FEM. In the BE-FE method, acoustic medium is modeled by the BEM and solid medium (structure) is modeled by the FEM. The BE-FE method is a robust engineering tool to investigate sound-structure interaction problems.

Acoustic field within the domain of analysis is always in interaction with its enclosing rigid or elastic solid boundary. Depending on the treatment of the interaction mechanism, coupled dynamic behavior for the two media will be referred

to as partially or fully coupled. In the partially coupled situation, dynamic behavior of only one of the two media is affected due to interaction. However, in the fully coupled case, dynamics of each medium is affected due to behavior of the other medium. In some cases, configuration for the domain of analysis explicitly permits only partial coupling. In other cases, both partial and full coupling treatment may be utilized for analysis. In this study, for these latter cases, fully coupled interaction analysis is considered without concerning whether it is necessary i.e., weak or strong interaction occurs. Full interaction analyses can be carried out by either BE or BE-FE methods. In this study the BEM is used to model acoustic domain. Hence, if elastic boundary is fully coupled to acoustic domain, then BE full coupling analysis can be performed if a relation between acoustic field variables and boundary displacements are known. However, there may be only a few fundamental configurations for which such relations might be known. Considering the diversity of engineering applications BE-FE method provides a general treatment to fully coupled interaction studies.

1.2 Review of Previous Studies

In the following, a brief summary of some previous research work relevant to this study is given.

Books on acoustics and sound-structure interaction edited by Blackstock [1], Fahy [2], Junger and Feit [3], Kinsler, et al. [4], Morse and Ingard [5], Morse and Feshbach [6], Ohayon and Soize [7], Pierce [8] and Skudrzyk [9] provided invaluable information on fluid-structure coupling. Several publications devoted to BEM and its various applications are available in literature; those edited by Wrobel [10], Aliabadi [11], Brebbia and Dominguez [12], Bonnet [13], Ciskowski and Brebbia[14], Gaul, et al. [15] and lecture notes of Mengi [16] have been utilized throughout this study. The books on FEM edited by Bathe [17], Cook, et al. [18], Petyt [19], Weaver and Johnston [20], Zienkiewicz [21] are also utilized to conduct this research work.

In case of steady-state dynamic conditions, acoustic analysis involves solutions of Helmholtz equation. Analytical solutions to Helmholtz equation can be obtained by

separation of variables technique, which involves series expansions of the solution in terms of eigenfunctions of the system. However, solutions are available only for special coordinate systems and boundary conditions [4].

Different dynamical responses in sound-structure problems lead to three frequency ranges of analysis: Low-, medium- and high-frequency ranges. These ranges are defined as: low-frequency range is the modal domain for which the associated system has a low modal density; medium-frequency range is the intermediate frequency band for which modal density exhibits large variations over the band; and high-frequency range is the frequency band for which there exists a uniform high modal density. From acoustical analysis point of view, method used to determine acoustic characteristics of a cavity depends upon the size of the cavity in relation to the wavelength of sound. If the wavelength is considerably less than cavity dimensions, then a statistical approach is used since there are many acoustic resonances. When the wavelength of sound is greater than about one third of the shortest dimension of the cavity the basic assumptions of the statistical approach are no longer valid, hence other non-statistical methods need to be employed in this case [7, 14].

Dowell, et al. [22] introduced a modal method based on the general theory of acoustoelasticity. Their study provided a comprehensive theoretical model to the interaction between internal acoustic pressure field and elastic wall of an enclosure. In this modal method, acoustic pressure or velocity potential is expanded in terms of normal modes of the rigid wall cavity, and elastic wall motion is expressed in terms of uncoupled (*in vacuo*) structural normal modes, and full coupling between acoustic domain and elastic boundary is considered. Furthermore, based on the general theory, an approach to analyze multiply connected cavities is presented. Comparisons of their theory with some experiments were also provided, and the main remaining uncertainty was stated to be the structural and/or cavity damping mechanisms. In most coupled sound-structure problems that involve interaction of interior acoustic field to its flexible boundary, the governing equations of motion are coupled through velocity terms, which result in skew-symmetric coupling matrices [22, 23]. Extraction of coupled system modes requires complex eigenvalue

extraction routines. Bokil and Shirahatti [23] introduced a formulation to obtain coupled system modes using real eigenvalue extraction routines. They presented their study by using Dowell's modal method with some comparisons to experimental data available in literature. They stated that structural damping and/or acoustic wall absorption were the limitations of their study. Jayachandran, et al. [24] pointed that modal expansion approaches for sound-structure interaction analysis, in which rigid wall acoustic modes are used in the formulations, yield accurate solution for the interior pressure but not for the velocity field. The inaccuracy in the velocity field was stated to be considerable in the vicinity of vibrating elastic boundaries. They presented quantitative studies illustrating this inaccuracy.

Development of energy formulations by Gladwell and Zimmermann [25], and Gladwell [26] were followed by finite element applications to sound-structure interaction problems. Some FE studies until early 1980's are the works of Craggs [27], Shuku and Ishihara [28], Petyt, et al. [29], Craggs and Stead [30], Petyt and Lim [31], Richards and Jha [32], and Nefske, et al. [33] which provided various aspects of FE acoustic analysis. Until late 1970's FEM was the dominant engineering tool in acoustic studies compared to BE or BE-FE methods. However, progress in BE and BE-FE methods changed this trend in computational acoustics. This observation is in agreement to a study published by Mackerle [34]. On the other hand, FE is still used widely and a recent review paper by Everstine [35] summarizes several FE formulations of structural acoustic problems.

Sound-structure interaction analysis is an active research area involving numerous engineering applications with multidisciplinary work. Mackerle [36] presented a comprehensive bibliography of recent studies on fluid-structure interaction problems that were investigated by FEM and BEM. His study included a list of references for general solution techniques and problem-specific applications. Ciskowski and Brebbia [14] presented various formulations of BE integral equation and BE methods together with applications to some acoustic problems. They also provided a comprehensive review of research studies in acoustics.

An integral solution approach to predict the acoustics of arbitrarily shaped bodies was presented by Bell, et al. [37]. Their study is viewed as one of the earliest publications on which current BE acoustic analysis are based on. In their study, they provided formulation for acoustic analysis of only two-dimensional problems. Bernhard, et al. [38] presented two distinct BEM's, namely, direct and indirect BEM's. The formulations were based on the Helmholtz integral equation for direct BEM and Huygen's principle for indirect BEM. They described the primary variables for the two formulations as acoustic pressure and particle velocity for direct method, and a fictitious distribution of acoustic sources at the boundary for indirect method. They provided interior acoustic field analysis of enclosures with spherical geometries, and described details related to computational analysis, which included polar coordinate transformation for the treatment of singular integrals, boundary discretization using compatible and incompatible elements, wall treatments and compact (point) acoustic source modeling.

Sestieri, et al. [39] investigated sound-structure interaction in complex shaped cavities. They stated that interior acoustic studies were proven not to possess any trouble or uniqueness problem. They illustrated case studies which were analyzed by BE and modal methods, along with some experimental results. Their study did not involve full coupling of the acoustic medium and vibrating elastic surfaces. Mariem and Hamdi [40] introduced a boundary FEM to study fluid-structure interaction problems. They used a mixed formulation which coupled the classical functional of the structure with a variational formulation by integral equations for the fluid. Their formulation avoided the discretization of the fluid domain, hence was advantegous compared to FEM. They illustrated some case studies involving interaction of structures to both limited and unlimited acoustic domains. Ciskowski and Royster [14, 41] presented BE formulation to analyze fluid-solid interaction problems. In their study acoustic field in the fluid medium was described by the scalar wave equation and displacement field of elastic structure was described by Navier's vector wave equation. Laplace transformed BE equations were coupled to develop a model that could be used for both steady-state and transient response. They illustrated their method in a biomedical application, human ear canal with and without a protective-

ear-plug. Tanaka and Masuda [42] presented BE and boundary-domain element analysis of some sound-structure interaction problems. In their study, interior acoustic field of enclosures were modeled by BEM and elastic enclosure surfaces were modeled by boundary-domain element method. They stated that boundary-domain element method was similar to FEM, and did not present details of this method. Suzuki, et al. [43] dealt with the application of BEM to noise problems inside complex-shaped cavities having complicated boundary conditions. They considered formulations due to prescribed boundary conditions, fully interacting boundaries and apertures where sound leakage was allowed. They presented BE formulation to model sound-absorptive linings, a particular treatment of singular integrals, a brief description of BE-FE analysis using direct, modal and mobility methods, and some case studies by comparing to analytic and/or experimental data. Mathews [44] presented BE-FE analysis of vibrating elastic, arbitrary-shaped, three-dimensional structures in an infinite media. He utilized isoparametric interpolation functions to model both boundary surface and acoustic variables. Coupled system equations were solved using fluid-variable and structural-variable approaches, while the former approach was found to be computationally more efficient and accurate. Non-unique solution of exterior acoustic field at internal cavity modes was assessed, and a method to handle this problem was presented. In his study, only a configuration with spherical geometry was investigated. Jeans and Mathews [45] developed BE-FE formulation to model elasto-acoustic interaction problems applicable to submerged, open, curved, elastic, thin shells. A variational BE formulation of acoustic medium was coupled to a FE formulation of elastic structure. Coupled system equations were solved using fluid-variable-approach, in which elimination of structural displacements yielded reduced matrix sizes. They listed the advantages of variational formulation as reduction of high singularity to weak singularity in integral formulation, which allowed accurate numerical approximation, applicability to non-closed thin shells, and resulting symmetrical fluid matrix. They presented two applications of their study, a cantilever plate problem and a fluid filled thin spherical shell problem. Rajakumar, et al. [46] formulated an acoustic 2-D interface element to couple the BE and FE

discretizations for fluid-structure interaction problems. They illustrated the applications of the interface element with some fundamental 2-D problems. Everstine and Henderson [47] described a computational capability for calculating sound-pressure field radiated or scattered by a harmonically excited, submerged, arbitrary, three-dimensional elastic structure. Their approach coupled FE models of structures with BE models of surrounding fluid. They stated that their study allowed analysis of large-scale interaction problems using available commercial FE software, hence existing FE structural models could be adapted for acoustic analysis with ease. Kopuz and Lalor [48] presented interior acoustic field analysis of a rectangular closed cavity and a modified configuration due to addition of a smaller coupled cavity. Their study revealed that collocation or variational BEM analysis, and the direct and modal superposition FEM analyses yielded almost identical results. Their study illustrated that modification of the initial configuration and the influence of interface properties between coupled cavities yielded considerable changes to interior acoustic field. Kopuz, et al. [49] presented an integrated FEM/BEM approach to predict interior acoustic radiation of open-ended box structures. Dynamic response of the structure due to excitation by a point force was obtained using FEM, then BE acoustic analysis was carried out using surface displacements that were obtained from FE analysis. Numerical analysis results were compared to experimental results, which revealed quite good agreement of theory and real data. Seybert, et al. [50] presented a coupled FEM/BEM for fluid-structure interaction using Ritz vectors and eigenvectors. They considered exterior radiation and scattering problems, for which they stated that for these problems Sommerfeld radiation condition was automatically incorporated in the boundary integral equation. Also, they briefly mentioned the nonuniqueness difficulty at critical frequencies which was an inherent characteristic of BE analysis for exterior acoustic problems. They treated this problem by a formulation that was called CHIEF. Structural displacements were approximated by a linear combination of either Ritz vectors or eigenvectors, which yielded a reduced size for the coupled system of equations. Their study revealed that Ritz vector synthesis was much more efficient than eigenvector synthesis. Cheng, et al. [51] presented a multi-domain boundary

element analysis technique and illustrated its application to muffler problems. In their formulation, acoustic domain was first considered to be composed of separate domains, then, BE formulation of each subdomain was obtained, later, using continuity of pressure and velocity interface conditions separate BE formulations of subdomains were coupled to each other. They briefly stated that multi-domain BE formulation has advantages in modeling acoustic domains involving thin obstacles or involving slender ducts (pipes), and in solution due to resulting banded BE system matrices. They illustrated transmission loss curves for different muffler configurations obtained by multi-domain BE analysis. Their comparisons with FE analysis indicated good agreement. Wu and Dandapani [52] presented a multi-domain BE-FE method to model sound transmission through thin structures. Their formulation differed from conventional multi-domain BE formulation in the way that they used pressure jump across thin structure, which was the interface between two separate acoustic domains. Bai and Wu [53] investigated free vibration of thin spherical shells filled with compressible fluid using BE-FE method. Three approaches to model coupled system behavior, namely, mixed-variable, fluid-variable and structural variable approaches were mentioned briefly. They illustrated their study using structural-variable approach. They calculated natural frequencies and mode shapes of coupled systems using singular value decomposition technique and pointed out that this method was computationally expensive. Lee, et al. [54] presented a direct coupling procedure of the FE and BE methods for structure-acoustic cavity problems. The Laplace transformed matrix equations for acoustic medium and structure were coupled using interface conditions. They illustrated some case studies involving a box-type cavity and an earmuff-earcanal system, for which both steady-state and transient-state acoustic responses were given. Pates, et al. [55] presented BE-FE interior acoustic field analysis of some sound-structure interaction problems, which involved a cavity backed by a composite or isotropic thin elastic panel. They pointed out the acoustic research needs of automotive and aerospace industries. Their results revealed that the transmission loss values for composite panels were very sensitive to the lamination angle of fibers in different layers of composite panels. Niyogi, et al. [56] presented BE-FE acoustic field

analysis within a partly flexible laminated composite enclosure. Flexible wall was modeled as a folded composite plate with fixed boundary along its peripheral to enclosure. Several case studies involving different fold angles, thicknesses, fiber stacking angles and sequences and modal damping ratios for the laminated composite panels were considered. Enclosure dimensions were selected to enable a 1-D acoustic analysis, and interior acoustic field was excited with a rigid piston representing one of the walls of the enclosure. They concluded that stacking sequence and thickness had the most significant effect on interior acoustic field, while fiber orientation and damping could also be utilized to attenuate interior sound pressure levels further. Gaul and Wenzel [57] presented a coupled symmetric BE-FE method to analyze acoustic fluid-structure interaction both in time and frequency domains. In their study, acoustic domain was modeled using a hybrid BE formulation, which was only outlined in their study, while transformation of domain integrals into boundary integrals were emphasized. Both hybrid BEM and FEM were derived from variational principles. One disadvantage in hybrid BE formulation was stated as the need in treatment of hypersingular integrals. They presented an application of their method by a fluid-structure interaction problem involving wave propagation in a fluid filled pipe.

Singular integrals and their treatments are currently one of the major concerns of BE related research studies. Huang and Cruise [58] reviewed several numerical techniques used to calculate singular and near-singular integrals in BE analysis, proposed another solution and provided some convergence studies. Guiggiani and Gigante [59] presented a general method for the direct evaluation of Cauchy principal value integrals in several dimensions. Later, Guiggiani, et al. [60] formulated a general technique for the numerical solution of hypersingular boundary integral equations. Telles [61] formulated a self-adaptive coordinate transformation technique for efficient numerical evaluation of general BE integrals. Later, this technique was implemented by Silva, et al. [62] for acoustic analysis involving continuous or discontinuous three dimensional boundary elements.

Interest in dynamic behavior of plates in relation to their aeroelastic stability and excitation by noise in aerospace applications led to studies involving model response

of the cavity-backed-plate problem. The first study on the subject is by Dowell and Voss [63], followed by the work of Lyon [64]. Research studies on the subject by Pretlove [65, 66], Ketter [67], Kihlman [68], Bhattacharya and Crocker [69], Guy and Bhattacharya [70], Guy [71-73] improved the theoretical and physical understanding of the structural-acoustical interaction problem. These researchers are the pioneers whose works provided significant contributions to the structural-acoustic studies. Work conducted in their studies involved: steady state and transient closed form solutions to cavity-plate interaction problems involving enclosures backed by a single or two plates; effects of plate properties (i.e., geometric and material properties) and boundary conditions (i.e., simply-supported or clamped) on coupled system response; weak and strong coupling configurations (i.e., shallow or deep cavity effects); low-, medium- or high frequency considerations; normal, grazing or different angle of incidence conditions for external excitations; and, some experimental data and verifications. Theoretical and experimental studies by Pan and Bies [74-76], Pan [77-78], Ih and Lee [79], Scarpa and Curti [80] are some recent studies on the coupled system available in literature.

Interaction of acoustic field within enclosures and Helmholtz resonators has some similarities to the coupled system behavior of mechanical structures involving vibration absorbers. However, in the former case, interaction mechanism is more complicated. The work of Fahy and Schofield [81] investigated this enclosure-resonator interaction problem. Their work involved the analysis of a single resonator coupled to an enclosure and tuned to a natural frequency of one of its low order acoustic modes. They provided both free and forced vibration analysis of the coupled system. In their single-mode interaction formulation, a Helmholtz resonator was considered as a point source and coupled to the modal model of the rigid wall enclosure. They presented a design chart illustrating the acoustic response of the coupled system behavior and provided experimental verification of their formulations. Cummings [82] improved the work of Fahy and Schofield by formulating a multi-mode analysis to the interaction problem. Later, Gonenc-Sorguc [83] investigated the enclosure-resonator interaction problem using a multi-mode modal approach based on the theory of acoustoelasticity.

1.3 Scope, Objectives and Achievements

This thesis investigates sound-structure interaction within small enclosures in low audio frequency range. Study aims: to implement general means of analysis tools for practical acoustic applications; to present some case studies involving fundamental configurations, however with general complexity to some extent which may be found in many engineering applications; to provide comparative analyses for some interaction studies by means of analytical, numerical techniques developed and implemented in this study, and by means of some experimental and computational data available in literature.

In this study, BE and BE-FE techniques are the two computational tools, which are used in acoustic analyses. Scientific and technical material used in the formulations of BE and BE-FE approaches are either available in literature or can be obtained with minor modifications to the existing material. However, presented material is the product of research conducted throughout the thesis study and is a composition of various related research studies. Most of the acoustic studies to be presented in here are performed by computer implementation of BE, BE-FE approaches and a new analytical solution developed for a particular sound-structure interaction problem.

Contributions of this thesis study to engineering acoustic studies can be collected under two main headings. This grouping is based on analytical and numerical points of view of the work conducted and as given below.

Based on existing analytic solutions to a sound-structure interaction study known as cavity-backed-plate problem, sound absorptive treatment on the fully coupled interaction boundary is taken into consideration, which yielded an extended formulation to the cavity-backed-plate problem. This analytic solution is verified by comparing analysis results to published data in literature for acoustically perfect reflective wall conditions. Analytical results for the cases of sound absorptive treatment and structural damping are also presented.

Some details of acoustic analysis using BEM are provided. An application is used to illustrate the applicability of BE acoustic particle velocity computations within analysis domain, which might be utilized in sound intensity related studies.

BE-FE method is utilized to investigate the cavity-backed-plate study with and without sound absorbing treatment on the interaction surface. Its agreement to the developed analytic solution is illustrated. Hence, BE-FE analysis of the cavity-backed-plate study involving sound absorptive treatment on interior plate surface is provided as an alternative numerical solution to the developed analytical solution. This sound-structure interaction study is a new and unique study for which both analytical and numerical solutions are given in this study.

BE-FE sound-structure interaction analyses of two studies involving additional full interaction surfaces are given. One of these studies is a modified configuration of the cavity-backed-plate study and involved addition of another full interaction boundary. This sound-structure interaction study can be described briefly as a cavity backed by two plates study and analytical solutions are available in literature. BE-FE analysis results of the cavity backed by two plates study are in good agreement to the analytical solutions. Hence, an alternative solution to this interaction problem by by BE-FE method is provided. The other sound-structure interaction study involved a more general structural behavior. This study involves a fundamental cavity configuration, for which most of its boundary is rigid except an elastic region formed by a L-shaped folded plate. This configuration provides to some extent the complexity of a thin-walled shell-like structure behavior, both in-plane and out-of-plane displacements, coupled to enclosed acoustic field. This study may provide a basis to research studies involving the above stated general structural behavior coupled to acoustic field.

Interaction between an enclosed acoustic field and a modally tuned Helmholtz resonator configuration is analyzed by BEM. Comparative results by the BEM and a modal method based on the theory of acoustoelasticity are presented. An application of multi-domain BE analysis to cavity-resonator interaction and a study involving positioning effects of resonators is presented. In this way, an alternative analysis approach to existing modal based analysis approaches is provided.

1.4 Outline of the Thesis

Contents of this study are presented in seven chapters. Chapter 2 introduces BEM to be used for steady-state dynamic acoustic analysis in three-dimensional finite closed domains. Both BE integral equations and their discrete forms are presented. Multi-domain BE formulation, two families of discontinuous BE patches and numerical treatment of regular and singular BE integrals are provided. Chapter 3 introduces FEM to model thin plate or shell-like structure dynamics. Formulations for a rectangular plate element and a triangular shell element are given. In Chapter 4, BEM and FEM are combined to form BE-FE method to analyze sound-structure interaction problems. Three approaches to BE-FE coupling, namely mixed-, structural- and fluid-variable approaches are provided. An enhanced analytical solution to a fundamental sound-structure interaction problem is developed. Chapter 5 assesses the developed analytical solution and presents sound-structure applications involving sound absorptive treatments and structural damping. Chapter 6 presents computational case studies analyzed by BE and BE-FE methods. Case studies cover a wide spectrum of sound-structure interaction configurations. Discussion and conclusions of the thesis and possible future research based on the current study are given in Chapter 7.

CHAPTER 2

BOUNDARY ELEMENT ACOUSTIC ANALYSIS

This chapter introduces the BE method to be used for computational acoustic analysis in three-dimensional finite closed domains. BEM presented in this chapter is known as direct BEM. Content of this chapter is presented into two main sections.

First section of the chapter presents: assumptions for acoustic medium and behavior of state variables; governing equations for linear acoustic analysis which are state equation, conservation of mass equation, and Euler's equation of motion; wave equation and its form reduced to Helmholtz equation due to harmonically varying dynamic state conditions in time; boundary conditions.

The second section of the chapter presents, in order: notation and fundamental solutions to be used in BE formulation; BE integral equations; discrete form of the BE integral equations and their matrix form representation; implementation of boundary conditions into the BE equations with emphasis on admittance and impedance type conditions; formulation of multi-domain BE analysis; two families of boundary elements, namely, discontinuous triangular and quadrilateral surface patch elements. The chapter concludes with a treatment of regular and singular integrations in the BE formulations and presentation for numerical evaluation of these integrals.

This chapter can be considered as the backbone for acoustic analysis by BEM. Illustrated BE formulations will be integrated later with FE formulations, given in Chapter 3, to form BE-FE method, presented in Chapter 4. In Chapter 6, BE computational acoustic analysis will be illustrated with some case studies.

2.1 Governing Equations of Acoustic Domain

Acoustic medium is assumed to have homogenous, inviscid, compressible and thermally non-conducting fluid characteristics, in which body forces are not significant. Deviations of fluid pressure, density and particle velocity from their respective initial values are assumed to be small. Acoustic state variables can be expressed as

$$p_f = p_o + p$$
$$\rho_f = \rho_o + \rho$$
$$\underline{v}_f = \underline{v}_o + \underline{v}$$

where p_f, ρ_f, $\underline{v}_f$ are instantaneous values of acoustic pressure, fluid density and particle velocity, respectively, p_o, ρ_o, $\underline{v}_o$ represent initial values and p, ρ, $\underline{v}$ represent small amplitude fluctuations of the variables. Instantaneous value and fluctuation of acoustic variables are functions of both position and time.

Propagation of sound waves with no mean flow condition ($\underline{v}_o$=0) is governed by the following set of linear acoustic equations [1-6, 8, 9].

State equation:

$$p = c_o^2 \rho \tag{2.1}$$

Conservation of mass:

$$\frac{\partial \rho}{\partial t} + \rho_o \underline{\nabla} \bullet \underline{v} = \frac{\partial m}{\partial t} \tag{2.2}$$

Euler's equation of motion:

$$\rho_o \frac{\partial \underline{v}}{\partial t} + \underline{\nabla} p = 0 \tag{2.3}$$

where c_o is the speed of sound in the medium, m is the distributed mass source per unit volume, $\underline{\nabla}$ is the gradient operator, t is time and $\underline{\nabla} \bullet \underline{v}$ represents the divergence of particle velocity.

Above governing equations can be reduced to a single differential equation in terms of acoustic pressure as follows: first, rewrite equation 2.2 by expressing density fluctuation in terms of pressure fluctuation using equation 2.1; then, take time derivative of the resulting expression and utilize equation 2.3. These mathematical manipulations yield the wave equation:

$$\nabla^2 p - \frac{1}{c_o^2}\frac{\partial^2 p}{\partial t^2} = -\frac{\partial^2 m}{\partial t^2} \tag{2.4}$$

where ∇^2 is the Laplacian operator.

Rate of acoustic mass source per unit volume can be expressed as

$$\frac{\partial m}{\partial t} = \rho_o Q \tag{2.5}$$

where Q represents volume velocity source strength per unit volume and called source strength density [1, 8, 9].

If the dynamic state of acoustic medium varies harmonically in time, by separating the time and position dependencies, acoustic fluctuations can be considered to have the forms

$$\begin{aligned} p &\equiv p(\underline{x}, t) = \hat{p}(\underline{x})e^{i\omega t} \\ \underline{v} &\equiv \underline{v}(\underline{x}, t) = \hat{\underline{v}}(\underline{x})e^{i\omega t} \\ \rho &\equiv \rho(\underline{x}, t) = \hat{\rho}(\underline{x})e^{i\omega t} \end{aligned} \tag{2.6}$$

where i is the imaginary constant and ω is angular frequency.

Therefore, for harmonic excitation and response conditions, wave equation 2.4 in view of expressions in equation 2.6 reduces to the Helmholtz equation:

$$\nabla^2 \hat{p} + k^2 \hat{p} = -\hat{f} \tag{2.7}$$

where in view of the relation in equation 2.5, acoustic excitation is expressed as

$$\hat{f} \equiv \hat{f}(\underline{x}) = -\omega^2 \hat{m}(\underline{x}) = i\omega\rho_o \hat{Q}(\underline{x}) \tag{2.8}$$

with $k = \omega/c_o$ being the wave number.

In this study, acoustic domain in consideration occupies a finite closed three-dimensional region. Analyses will be carried out in frequency domain by assuming harmonic steady-state vibration conditions.

In order to have a well-posed problem, boundary conditions have to be specified. At a point on the boundary one can prescribe either acoustic pressure or normal component of acoustic particle velocity, or combination of these two acoustic field variables. It may be noted that at a boundary point, one can write

$$\hat{q}_n = \frac{\partial \hat{p}}{\partial n} = -i\omega\rho_o \hat{v}_n \tag{2.9}$$

where n is normal axis at boundary point and $\hat{v}_n$ represents normal velocity component. This equation shows that as boundary condition one can also specify normal component of pressure gradient ($\hat{q}_n = \frac{\partial \hat{p}}{\partial n}$) instead of normal velocity ($\hat{v}_n$).

2.2 Boundary Element Formulation

2.2.1 Boundary Integral Equations

An arbitrary three-dimensional acoustic domain with the interior region V and boundary S is illustrated in Figure 2.1. The domain is referred to an (x_1, x_2, x_3) cartesian coordinate system. In BE formulation, there are two types of points, namely, field (observation) and source points, which are denoted respectively by $\underline{x}$ and $\underline{x}_o$ in the figure. Let r be the distance between $\underline{x}_o$ and $\underline{x}$; $\underline{r}$, unit vector directed from $\underline{x}_o$ to $\underline{x}$ and $\underline{n}$, outer unit normal at field point $\underline{x}$ when it is on S.

In BE formulation, a set of special functions called fundamental solutions (FS) is used. For acoustic problems in frequency domain, the first fundamental solution, also known as free-space Green's function, is the solution of Helmholtz equation in unbounded domain when there is a concentrated unit excitation at source point, that is, the first FS $\tilde{p}$ satisfies

$$\nabla^2 \tilde{p}(\underline{x}_o, \underline{x}) + k^2 \tilde{p}(\underline{x}_o, \underline{x}) = -\Delta(\underline{x}_o, \underline{x})$$

where $\Delta(\underline{x}_o, \underline{x})$ is three-dimensional Dirac-delta function. On the other hand, the second FS $\tilde{q}_n$ is, associated with $\tilde{p}$, the normal pressure gradient at a field point on S, that is

$$\tilde{q}_n(\underline{x}_o, \underline{x}) = \frac{\partial \tilde{p}(\underline{x}_o, \underline{x})}{\partial n}$$

These FS's are already derived in literature [10,14-16]. They are

$$\tilde{p}(\underline{x}_o, \underline{x}) = \frac{e^{-ikr}}{4\pi r} \tag{2.10}$$

and

$$\tilde{q}_n(\underline{x}_o, \underline{x}) = -\frac{e^{-ikr}}{4\pi r^2}(ikr + 1)\frac{\partial r}{\partial n} \tag{2.11}$$

with $r = |\underline{x} - \underline{x}_o|$.

Fundamental solutions are non-local functions due to their dependence on both source and observation point coordinates. They become singular as the distance between source and observation points diminishes.

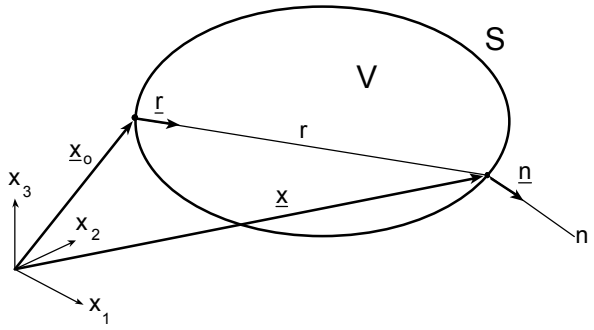

Figure 2.1 Illustration of enclosed three-dimensional acoustic domain

BE integral equations for acoustic analyses are available in literature [14, 16]. It is

$$b(\underline{x}_o)\hat{p}(\underline{x}_o) + \int_S \tilde{q}_n(\underline{x}_o, \underline{x})\hat{p}(\underline{x})da = \int_S \tilde{p}(\underline{x}_o, \underline{x})\hat{q}_n(\underline{x})da + \int_V \hat{f}(\underline{x})\tilde{p}(\underline{x}_o, \underline{x})dv \qquad (2.12)$$

with coefficient $b(\underline{x}_o)$ defined as

$$b(\underline{x}_o) = \begin{cases} \dfrac{\theta}{4\pi} & \text{if } \underline{x}_o \text{ is on S} \\ 1 & \text{if } \underline{x}_o \text{ is within V} \\ 0 & \text{if } \underline{x}_o \text{ is outside of V} \end{cases}$$

where θ is referred as the solid angle subtended by the acoustic fluid at the source point. For a smooth surface point, that is where a unique tangent plane can be defined, $\theta = 2\pi$; hence, $b(\underline{x}_o) = ½$ [14-16]. Explicit expression for θ is available in literature [14, 50, 52].

Acoustic particle velocity components at an interior point $\underline{x}_o$ in V can be obtained by evaluating gradient of acoustic pressure at that point using equation 2.12, which yields [16]

$$\begin{aligned}\hat{v}_j(\underline{x}_o) &= -\frac{1}{i\omega\rho_o}\frac{\partial\hat{p}(\underline{x}_o)}{\partial x_{oj}} \qquad , \quad j = 1\text{-}3 \\ &= \int_S d_j(\underline{x}_o,\underline{x})\hat{q}_n(\underline{x})da - \int_S t_j(\underline{x}_o,\underline{x})\hat{p}(x)da + \int_V \hat{f}(\underline{x})d_j(\underline{x}_o,\underline{x})dv\end{aligned} \tag{2.13}$$

where the two new kernels d_j and t_j are given by

$$\begin{aligned} d_j(\underline{x}_o,\underline{x}) &= -\frac{1}{i\omega\rho_o}\frac{\partial\tilde{p}(\underline{x}_o,\underline{x})}{\partial x_{oj}} \\ &= -\frac{1}{i\omega\rho_o}\frac{e^{-ikr}}{4\pi r^2}(1+ikr)r_j \\ t_j(\underline{x}_o,\underline{x}) &= -\frac{1}{i\omega\rho_o}\frac{\partial\tilde{q}_n(\underline{x}_o,\underline{x})}{\partial x_{oj}} \\ &= -\frac{1}{i\omega\rho_o}\frac{e^{-ikr}}{4\pi r^3}[(1+ikr)n_j - (3+3ikr+(ikr)^2)r_j\frac{\partial r}{\partial n}] \end{aligned}$$

with r_j and n_j representing components of unit vector $\underline{r}$ and outer unit normal vector $\underline{n}$, respectively. It should be noted that gradient of pressure with respective to varied source point is negative of that with respect to varied field point.

BE integral equation 2.12 has a volume integral, whose integrand involves the distributed acoustic excitation and the first fundamental solution. Hence, it does not contain any unknown. It may be noted that there are methods, such as, particular integral method, by which the volume integral can be carried to the boundary, thus, the boundary-only nature of BEM can be preserved [10, 12, 15, 16].

2.2.2 Discrete Form of Boundary Integral Equations

BEM can be interpreted as a method for obtaining numerical solution of the BE integral equation, which requires writing this integral equation in discrete form.

In this study, it will be assumed that acoustic excitation is due to compact sources. This implies that for the source distribution one can write, in view of equation 2.8,

$$\hat{f}(\underline{x}) = \sum_{l=1}^{L}\hat{f}_l\Delta(\underline{x}_l,\underline{x}), \qquad \hat{f}_l = -\omega^2\hat{m}_l = i\omega\rho_o\hat{Q}_l \tag{2.14}$$

where L is the number of compact sources and $\hat{f}_l$ is the strength of compact source

located at $\underline{x}_l$.

In BEM, boundary surface is represented by sum of finite number of surface patches which are referred as boundary elements. If boundary surface is discretized into M boundary elements, integral equation 2.12 can be expressed as, in view of equation 2.14,

$$b(\underline{x}_o)p(\underline{x}_o) + \sum_{m=1}^{M} \int_{S_m} \tilde{q}_n(\underline{x}_o, \underline{x})\hat{p}(\underline{x})da = \sum_{m=1}^{M} \int_{S_m} \tilde{p}(\underline{x}_o, \underline{x})\hat{q}_n(\underline{x})da + \sum_{l=1}^{L} \hat{f}_l \tilde{p}(\underline{x}_o, \underline{x}_l) \quad (2.15)$$

where S_m represents the boundary associated with m^{th} element.

Over each element, geometry and acoustic variables are described by interpolation functions and nodal values of related variables, which are of the form:

$$x_i = \sum_{k=1}^{K} N_k(\xi_1, \xi_2)\, x_i^k \quad , \quad i = 1-3 \quad (2.16)$$

$$\hat{p}(\underline{x}) = \sum_{k=1}^{K} M_k(\xi_1, \xi_2)\, \hat{p}^k \quad (2.17)$$

$$\hat{q}_n(\underline{x}) = \sum_{k=1}^{K} M_k(\xi_1, \xi_2)\, \hat{q}_n^k \quad (2.18)$$

$$\hat{v}_n(\underline{x}) = \sum_{k=1}^{K} M_k(\xi_1, \xi_2)\, \hat{v}_n^k \quad (2.19)$$

where K is the number of geometric or nodal points used for each BE, x_i are global coordinates, ξ_1 and ξ_2 are local coordinates, x_i^k are coordinates of geometric points, and $\hat{p}^k$, $\hat{q}_n^k$ and $\hat{v}_n^k$ are nodal point values of field variables.

Substitution of the expressions in equations 2.16, 2.17 and 2.18 into equation 2.15 yields

$$b(\underline{x}_o)\hat{p}(\underline{x}_o) + \sum_{m=1}^{M}\sum_{k=1}^{K} h^{mk}(\underline{x}_o, \underline{x})\hat{p}^{mk} = \sum_{m=1}^{M}\sum_{k=1}^{K} g^{mk}(\underline{x}_o, \underline{x})\hat{q}_n^{mk} + \sum_{l=1}^{L} \hat{f}_l \tilde{p}(\underline{x}_o, \underline{x}_l) \quad (2.20)$$

where the superscripts m and k denote respectively the element and nodal point, and

$$h^{mk}(\underline{x}_o, \underline{x}) = \int_{S_m} M_k(\underline{\xi})\tilde{q}(\underline{x}_o, \underline{x})\, J d\xi_1 d\xi_2 \quad (2.21)$$

$$g^{mk}(\underline{x}_o, \underline{x}) = \int_{S_m} M_k(\underline{\xi})\, \tilde{p}(\underline{x}_o, \underline{x})\, J d\xi_1 d\xi_2 \quad (2.22)$$

with $\underline{\xi} \equiv (\xi_1, \xi_2)$.

In equations 2.21 and 2.22, prime on S_m is used to indicate domain of integration on m^{th} element expressed in terms of local coordinates, J represents the Jacobian of the global to local coordinate transformation. Hence, the differential area d*a* in global coordinates can be expressed in local coordinate system as

$$da = Jd\xi_1 d\xi_2$$

where the Jacobian and its components are defined as [12]

$$\begin{aligned} J &= \sqrt{J_1^2 + J_2^2 + J_3^2} \\ J_1 &= \frac{\partial x_2}{\partial \xi_1}\frac{\partial x_3}{\partial \xi_2} - \frac{\partial x_2}{\partial \xi_2}\frac{\partial x_3}{\partial \xi_1} \\ J_2 &= \frac{\partial x_3}{\partial \xi_1}\frac{\partial x_1}{\partial \xi_2} - \frac{\partial x_1}{\partial \xi_1}\frac{\partial x_3}{\partial \xi_2} \\ J_3 &= \frac{\partial x_1}{\partial \xi_1}\frac{\partial x_2}{\partial \xi_2} - \frac{\partial x_2}{\partial \xi_1}\frac{\partial x_1}{\partial \xi_2} \end{aligned} \tag{2.23}$$

Discrete BE integral equations obtained for each surface source point using equation 2.20 yield a system of equations which may be written in matrix form as

$$\mathbf{Hp} = \mathbf{G'q} + \mathbf{f} \tag{2.24}$$

or using the relationship between normal components of particle velocity and gradient of pressure given in equation 2.9,

$$\mathbf{Hp} = \mathbf{Gv} + \mathbf{f} \tag{2.25}$$

where **G** and **G'** are related by

$$\mathbf{G} = -i\omega\rho_o\mathbf{G'}$$

In equations 2.24 and 2.25, **H, G'** and **G** are called influence matrices; **p**, **q**, **v** and **f** are vectors of nodal acoustic pressure, normal pressure gradient, normal particle velocity and loading due to acoustic compact sources, respectively. It should be noted that influence matrices are complex valued, densely populated and non-symmetric.

Substituting boundary conditions, above matrix equations 2.24 or 2.25 can be solved for the remaining unknown variables on the boundary surface. Then, acoustic pressure at interior points can be evaluated using, in view of equation 2.20,

$$\hat{p}(\underline{x}_o) = -\sum_{m=1}^{M}\sum_{k=1}^{K} h^{mk}(\underline{x}_o, \underline{x})\hat{p}^{mk} - \sum_{m=1}^{M}\sum_{k=1}^{K} g^{mk}(\underline{x}_o, \underline{x})\hat{q}_n^{mk} + \sum_{l=1}^{L} \hat{f}_l \tilde{p}(\underline{x}_o, \underline{x}_l)$$

and particle velocity can be evaluated from the discrete form of equation 2.13:

$$\hat{v}_j(\underline{x}_o) = \sum_{m=1}^{M}\sum_{k=1}^{K} d_j^{mk}(\underline{x}_o, \underline{x})\hat{q}_n^{mk} - \sum_{m=1}^{M}\sum_{k=1}^{K} t_j^{mk}(\underline{x}_o, \underline{x})\hat{p}^{mk} + \sum_{l=1}^{L} \hat{f}_l d_j(\underline{x}_o, \underline{x}_l)$$

where

$$d_j^{mk}(\underline{x}_o, \underline{x}) = \int_{S_m} d_j(\underline{x}_o, \underline{x}) M_k J d\xi_1 d\xi_2$$

$$t_j^{mk}(\underline{x}_o, \underline{x}) = \int_{S_m} t_j(\underline{x}_o, \underline{x}) M_k J d\xi_1 d\xi_2$$

Solution of BE equations 2.24 and 2.25 in the case of prescribed acoustic pressure or normal velocity boundary conditions is quite straightforward. Comparatively more involved situation exists when combination of acoustic pressure and normal velocity is specified as a boundary condition. In acoustic studies, this latter type of boundary condition is utilized to model sound absorptive treatments.

Admittance or impedance boundary conditions are combination type of boundary conditions stated above. Considering locally reacting surface conditions, admittance and impedance boundary conditions can be expressed in matrix form as [14, 43]

$$\mathbf{v}_r = \mathbf{Y}\mathbf{p} \tag{2.26}$$

$$\mathbf{p} = \mathbf{Z}\mathbf{v}_r, \qquad \mathbf{Z} = \mathbf{Y}^{-1} \tag{2.27}$$

where $\mathbf{Y}$ and $\mathbf{Z}$ are diagonal admittance and impedance matrices, respectively; $\mathbf{v}_r$ is the normal acoustic particle velocity $\mathbf{v}$ relative to prescribed boundary surface normal velocity $\mathbf{v}_s$:

$$\mathbf{v}_r = \mathbf{v} - \mathbf{v}_s \tag{2.28}$$

Admittance boundary conditions can be implemented in equation 2.25 as, in view of equations 2.26 and 2.28,

$$(\mathbf{H} - \mathbf{G}\mathbf{Y})\mathbf{p} = \mathbf{G}\mathbf{v}_s + \mathbf{f} \tag{2.29}$$

and similarly, when the impedance boundary conditions in equation 2.27 are used, the BE equation in equation 2.25 takes the form as

$$(\mathbf{H}\mathbf{Z} - \mathbf{G})\mathbf{v} = \mathbf{Z}\mathbf{v}_s + \mathbf{f} \tag{2.30}$$

It should be emphasized that boundary conditions considered up to now should

be interpreted as partially interacting boundary conditions. In other words, acoustic domain dynamics is influenced by the prescribed surface boundary conditions; however, acoustic domain does not alter the prescribed behavior of surface boundary. Full interaction between acoustic domain and boundary surface will be considered in Chapter 4.

2.2.3 Multi-Domain Boundary Element Formulation

The geometric considerations or changes in acoustic properties may dictate that an acoustic domain be subdivided into sub-domains. When this is the case, BE analyses can be performed by writing the BE equation for each sub-domain separately, then, combining BE equations in view of interface conditions between sub-domains [12, 15, 51].

Decomposition of an arbitrary three-dimensional domain into two sub-domains is illustrated in Figure 2.2, where the outer unit normal of two sub-domains are designated by $\underline{n}_1$ and $\underline{n}_2$.

In view of equation 2.25, BE equations for the two sub-domains can be written as

$$\begin{bmatrix}\mathbf{H}_1 & \mathbf{H}_{1i}\end{bmatrix}\begin{bmatrix}\mathbf{p}_1 \\ \mathbf{p}_{1i}\end{bmatrix} = \begin{bmatrix}\mathbf{G}_1 & \mathbf{G}_{1i}\end{bmatrix}\begin{bmatrix}\mathbf{v}_1 \\ \mathbf{v}_{1i}\end{bmatrix} + \mathbf{f}_1 \tag{2.31}$$

$$\begin{bmatrix}\mathbf{H}_{2i} & \mathbf{H}_2\end{bmatrix}\begin{bmatrix}\mathbf{p}_{2i} \\ \mathbf{p}_2\end{bmatrix} = \begin{bmatrix}\mathbf{G}_{2i} & \mathbf{G}_2\end{bmatrix}\begin{bmatrix}\mathbf{v}_{2i} \\ \mathbf{v}_2\end{bmatrix} + \mathbf{f}_2 \tag{2.32}$$

where subscript i is used to identify the nodes at interface; and pressure, velocity vectors, and influence matrices are partitioned accordingly. Interface conditions between sub-domains due to force equilibrium and velocity continuity are, respectively,

$$\mathbf{p}_{1i} = \mathbf{p}_{2i} = \mathbf{p}_{int} \tag{2.33}$$

and

$$\mathbf{v}_{1i} = -\mathbf{v}_{2i} = \mathbf{v}_{int} \tag{2.34}$$

It may be noted that the velocity interface condition in equation 2.34 can also be written in terms of normal pressure gradient as

$$\mathbf{q}_{1i} = -\mathbf{q}_{2i} = \mathbf{q}_{int} \tag{2.34}$$

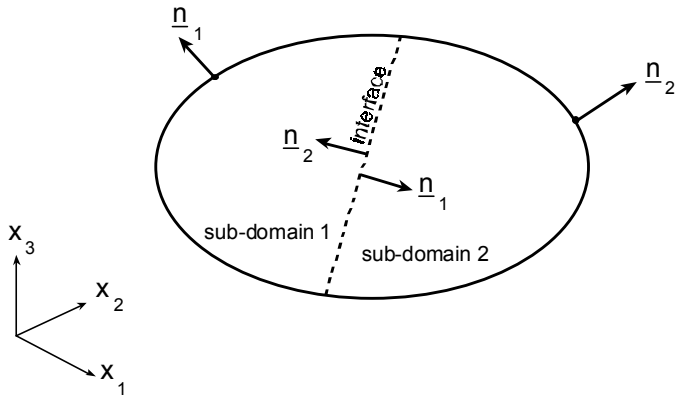

Figure 2.2 Illustration of a multi-domain configuration

Total acoustic behavior of the coupled system can be obtained by combining equations 2.31 and 2.32 in view of equations 2.33 and 2.34, which gives

$$\begin{bmatrix} \mathbf{H}_1 & \mathbf{H}_{1i} & \mathbf{0} \\ \mathbf{0} & \mathbf{H}_{2i} & \mathbf{H}_2 \end{bmatrix} \begin{bmatrix} \mathbf{p}_1 \\ \mathbf{p}_{int} \\ \mathbf{p}_2 \end{bmatrix} = \begin{bmatrix} \mathbf{G}_1 & \mathbf{G}_{1i} & \mathbf{0} \\ \mathbf{0} & -\mathbf{G}_{2i} & \mathbf{G}_2 \end{bmatrix} \begin{bmatrix} \mathbf{v}_1 \\ \mathbf{v}_{int} \\ \mathbf{v}_2 \end{bmatrix} + \begin{bmatrix} \mathbf{f}_1 \\ \mathbf{f}_2 \end{bmatrix} \tag{2.36}$$

Solution of the coupled system in equation 2.36 yields the results for the unknowns both on the boundary of the combined system and on the interface.

Treating a single-domain problem as a multi-domain one introduces additional unknowns at interfaces between sub-domains. However, modeling advantages may be gained and computational efficiency may be improved because of the banded structure of influence matrices as seen from equation 2.36. These improvements may be important for large-scale problems. As mentioned previously, the multi-domain BEM can also be used, in addition to the above stated purpose, to accommodate the heterogeneities that may exist in an acoustic medium [15, 51].

2.2.4 Discontinuous Boundary Elements

In numerical solution of BE equation, boundary surface is discretized by a finite number of boundary elements. As already mentioned, over each element, geometry and the distribution of acoustic variables are approximated in terms of interpolation

functions as shown in equations 2.16 through 2.19.

Discontinuous BE's refer to those elements over which the distribution of an acoustic variable is described in terms of its values at some nodes, all of which lie inside the element; thus, the acoustic variable may suffer jumps across interfaces between elements. However, it may be noted that some of the geometric points x_i^k in equation 2.16 are on the border line of the element and are chosen so that the geometric continuity is insured at interfaces between elements.

Families of three-dimensional triangular and quadrilateral elements implemented in this study are illustrated in Figure 2.3. Each element is abbreviated by a three-letter code, in the order, indicating shape of the element (T: triangular, Q: quadrilateral), element geometry interpolation functions (L: linear, Q: quadratic) and acoustic variable interpolation functions (C: constant, L: linear, Q: quadratic).

Geometry interpolation functions used in TLC, TLL, TLQ elements are linear and in TQQ elements are quadratic. Geometry interpolation functions used in QLC, QLL, QLQ elements are bilinear and in QQQ elements are biquadratic. Variable interpolation functions can be obtained from related geometry interpolation functions by using a scale factor λ, which is a measure for the distance between geometric points and collocation nodes. Geometric and variable interpolation functions used in triangular and quadrilateral elements are listed in Table 2.1 [10-16, 62].

Geometric and nodal point information is given in Figure 2.4 for triangular elements. Local coordinates of geometric and nodal points for these elements are listed in Tables 2.2 and 2.3, respectively. Similar information for quadrilateral elements is illustrated in Figure 2.5, and in Tables 2.4 and 2.5. As can be seen in Figures 2.4 and 2.5, the scale factor λ used in the description of acoustic variable interpolation functions represents displaced location of collocation nodes relative to geometric points. The values of the scale factor λ used in this study are 0.25, 0.25 and 0.15 for TLL, TLQ and TQQ elements, respectively, and 0.15 for QLL, QLQ and QQQ elements. These values are chosen in view of published data in literature [62].

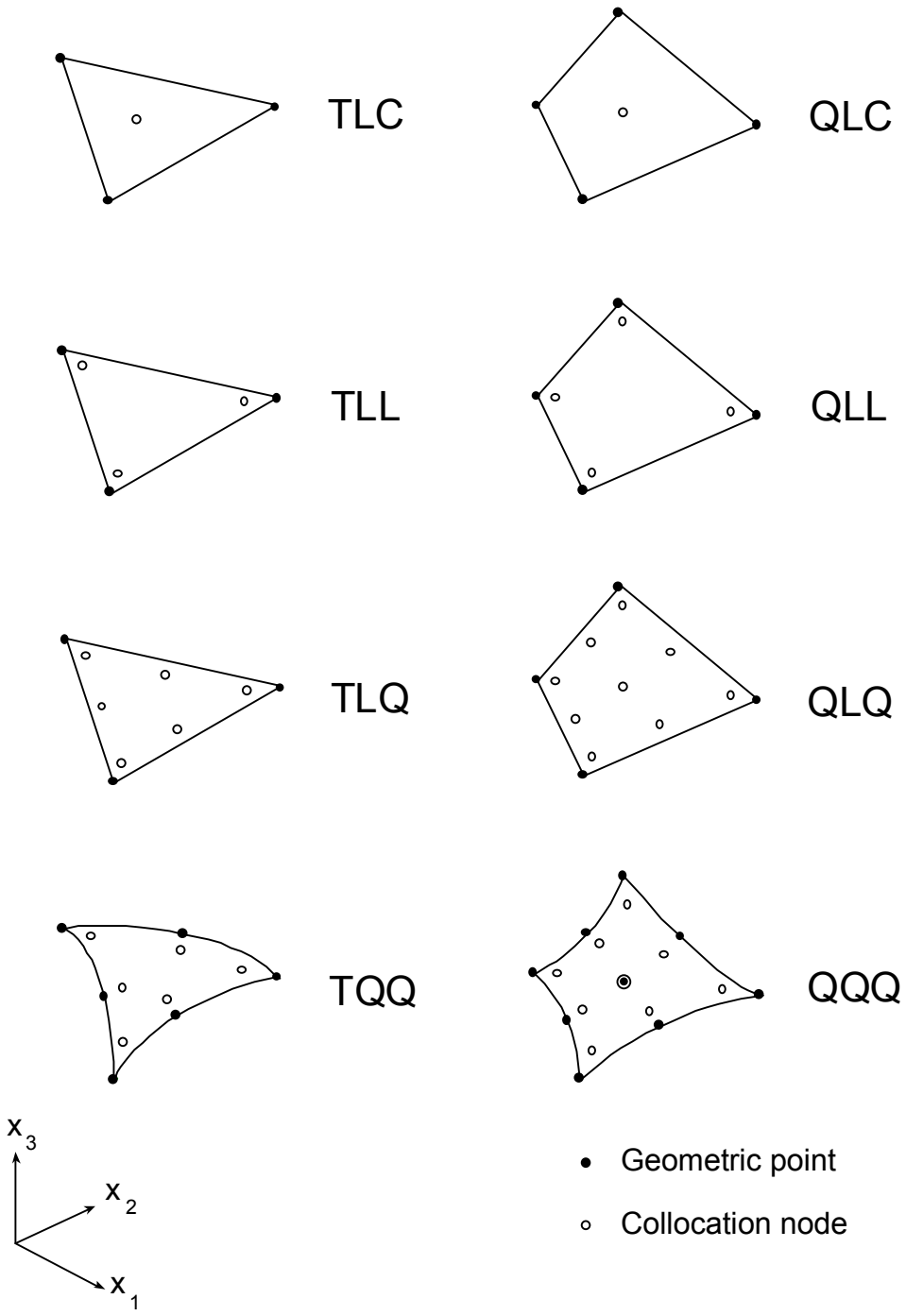

Figure 2.3 Triangular and quadrilateral boundary elements

Table 2.1 Interpolation functions

Element Type	Triangular	Quadrilateral
Geometry Interpolation Functions	Linear $N_1 = \xi_3 = 1 - \xi_1 - \xi_2$ $N_2 = \xi_1$ $N_3 = \xi_2$	Bilinear $N_1 = \frac{1}{4}(1-\xi_1)(1-\xi_2)$ $N_2 = \frac{1}{4}(1+\xi_1)(1-\xi_2)$ $N_3 = \frac{1}{4}(1+\xi_1)(1+\xi_2)$ $N_4 = \frac{1}{4}(1-\xi_1)(1+\xi_2)$
	Quadratic $N_1 = \xi_3(2\xi_3 - 1)$ $N_2 = \xi_1(2\xi_1 - 1)$ $N_3 = \xi_2(2\xi_2 - 1)$ $N_4 = 4\xi_3\xi_1$ $N_5 = 4\xi_1\xi_2$ $N_6 = 4\xi_2\xi_3$	Biquadratic $N_1 = N_1^1 N_2^1$ $\quad N_1^1 = \frac{1}{2}\xi_1(\xi_1 - 1)$ $N_2 = N_1^2 N_2^1$ $N_3 = N_1^2 N_2^2$ $\quad N_1^2 = \frac{1}{2}\xi_1(\xi_1 + 1)$ $N_4 = N_1^1 N_2^2$ $\quad N_1^3 = (1-\xi_1^2)$ $N_5 = N_1^3 N_2^1$ $N_6 = N_1^2 N_2^3$ $\quad N_2^1 = \frac{1}{2}\xi_2(\xi_2 - 1)$ $N_7 = N_1^3 N_2^2$ $\quad N_2^2 = \frac{1}{2}\xi_2(\xi_2 + 1)$ $N_8 = N_1^1 N_2^3$ $N_9 = N_1^3 N_2^3$ $\quad N_2^3 = (1-\xi_2^2)$
Acoustic Variable Interpolation Functions	Constant M = 1	Constant M = 1
	Linear and Quadratic $M_k = N_k(\xi'_1, \xi'_2, \xi'_3)$ k = 1-3 (or 6) $\xi'_1 = \frac{\xi_1 - \lambda}{1-3\lambda}$, $\xi'_2 = \frac{\xi_2 - \lambda}{1-3\lambda}$ $\xi'_3 = 1 - \xi'_1 - \xi'_2 = \frac{\xi_3 - \lambda}{1-3\lambda}$	Bilinear and Biquadratic $M_k = N_k(\xi'_1, \xi'_2)$ k = 1-4 (or 9) $\xi'_1 = \frac{\xi_1}{1-\lambda}$, $\xi'_2 = \frac{\xi_2}{1-\lambda}$

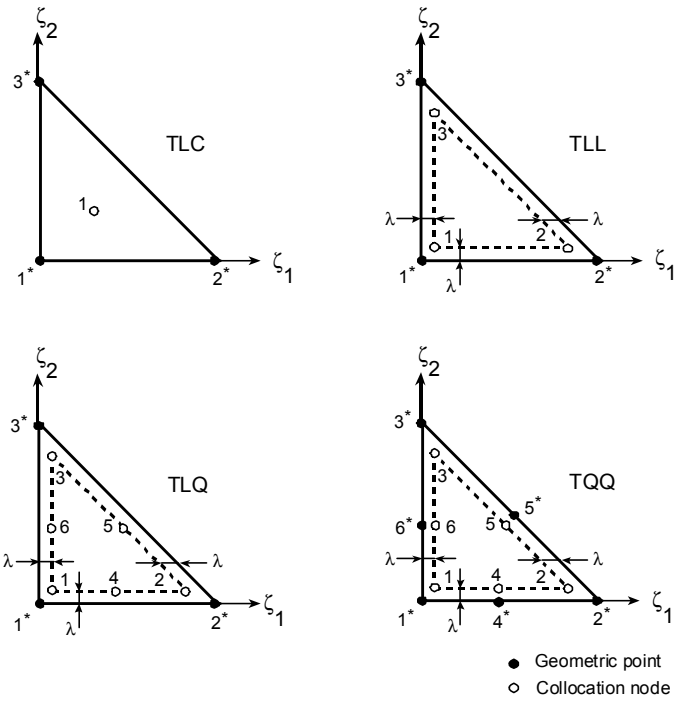

Figure 2.4 Geometric points and collocation nodes for triangular parent elements

Table 2.2 Local coordinates of geometric points for triangular elements

	1^*	2^*	3^*	4^*	5^*	6^*
TLC	(0,0)	(1,0)	(0,1)			
TLL	(0,0)	(1,0)	(0,1)			
TLQ	(0,0)	(1,0)	(0,1)			
TQQ	(0,0)	(1,0)	(0,1)	(0.5,0)	(0.5,0.5)	(0,0.5)

Table 2.3 Local coordinates of collocation nodes for triangular elements

	1	2	3	4	5	6
TLC	$(\frac{1}{3},\frac{1}{3})$					
TLL	(λ,λ)	(1-2λ,λ)	(λ,1-2λ)			
TLQ	(λ,λ)	(1-2λ,λ)	(λ,1-2λ)	$(\frac{1-2\lambda}{2},\lambda)$	$(\frac{1-2\lambda}{2},\frac{1-2\lambda}{2})$	$(\lambda,\frac{1-2\lambda}{2})$
TQQ	(λ,λ)	(1-2λ,λ)	(λ,1-2λ)	$(\frac{1-2\lambda}{2},\lambda)$	$(\frac{1-2\lambda}{2},\frac{1-2\lambda}{2})$	$(\lambda,\frac{1-2\lambda}{2})$

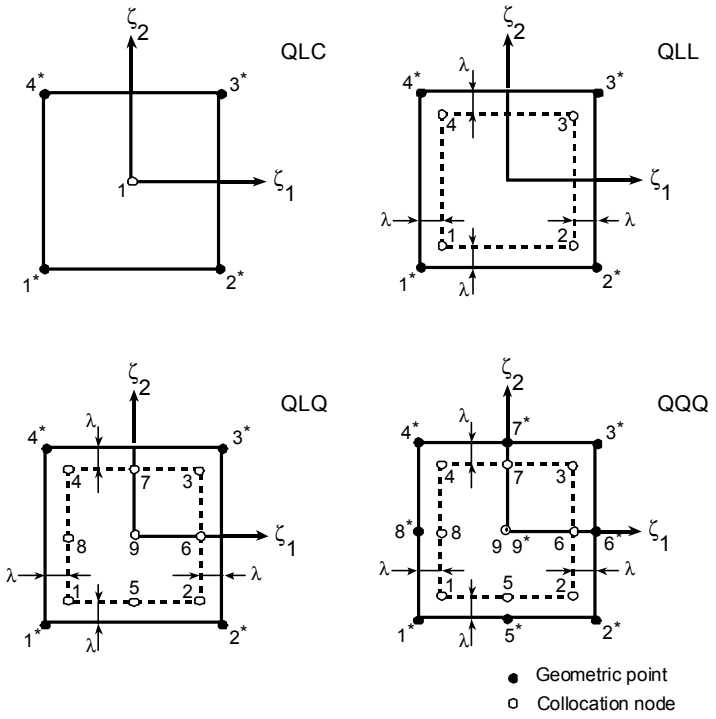

Figure 2.5 Geometric points and collocation nodes for quadrilateral parent elements

Table 2.4 Local coordinates of geometric points for quadrilateral elements

	1^*	2^*	3^*	4^*	5^*	6^*	7^*	8^*	9^*
QLC	(-1,-1)	(1,-1)	(1,1)	(-1,1)					
QLL	(-1,-1)	(1,-1)	(1,1)	(-1,1)					
QLQ	(-1,-1)	(1,-1)	(1,1)	(-1,1)					
QQQ	(-1,-1)	(1,-1)	(1,1)	(-1,1)	(0,-1)	(1,0)	(0,1)	(-1,0)	(0,0)

Table 2.5 Local coordinates of collocation nodes for quadrilateral elements ($\alpha=1-\lambda$)

	1	2	3	4	5	6	7	8	9
QLC	(0,0)								
QLL	$(-\alpha,-\alpha)$	$(\alpha,-\alpha)$	(α,α)	$(-\alpha,\alpha)$					
QLQ	$(-\alpha,-\alpha)$	$(\alpha,-\alpha)$	(α,α)	$(-\alpha,\alpha)$	$(0,-\alpha)$	$(\alpha,0)$	$(0,\alpha)$	$(-\alpha,0)$	(0,0)
QQQ	$(-\alpha,-\alpha)$	$(\alpha,-\alpha)$	(α,α)	$(-\alpha,\alpha)$	$(0,-\alpha)$	$(\alpha,0)$	$(0,\alpha)$	$(-\alpha,0)$	(0,0)

Use of discontinuous elements provides ease of modeling in BEM. If a node at the boundary surface is at an edge or corner there would be no unique outer normal at that location, where, therefore, acoustic particle normal velocity or normal pressure gradient could not be defined uniquely. These difficulties can be eliminated easily by using discontinuous elements. In other words, one can place collocation nodes on smooth boundary surface and use the advantage of inter-element discontinuity for acoustic variables as a remedy to above described problem. On the other hand, the main disadvantage of using discontinuous elements compared to continuous elements is the increase in the number of unknowns due to additional collocation nodes used within elements. It should be noted that one of the most special properties of BEM is that the discontinuities of acoustic variables across interfaces between elements do not invalidate the convergence of the technique [14, 62, 96, 97].

2.2.5 Numerical Evaluation of Boundary Element Integrals

From the study of equations 2.10 and 2.11, it is obvious that the fundamental solutions become singular as $r \to 0$, that is, as observation (field) point approaches source point, which is the case when observation and source points are on the same element.

If no singularity is involved, that is, when source and observation points are on different elements, standard Gaussian quadrature for integrations over triangular or quadrilateral elements can be used. For triangular elements, BE integrals reduce to

$$I = \int_0^1 \left[\int_0^{1-\xi_2} f(\xi_1, \xi_2, \xi_3) d\xi_1 \right] d\xi_2$$

which can be numerically evaluated from [16]

$$I \cong \sum_{i=1}^{N} \sum_{j=1}^{N} w_i w_j (1-\xi_2^j) f(\xi_1^i, \xi_2^j, \xi_3^{ij})$$

where

$$\xi_3^{ij} = 1 - \xi_1^i - \xi_3^j$$

Here, w_i and ξ^i represent weight and evaluation location, respectively, and N

indicates number of integration points.

In literature, the multiplicative coefficients used in numerical integrations over triangular regions are condensed into a single weighting factor, w_k^* with corresponding integration locations ξ_i^{*k} [12, 18, 101], that is

$$I \cong \sum_{k=1}^{N} w_k^* f(\xi_1^{*k}, \xi_2^{*k}, \xi_3^{*k})$$

For quadrilateral elements, BE integrals would be of the form

$$I = \int_{-1}^{1} \left[\int_{-1}^{1} f(\xi_1, \xi_2) d\xi_1 \right] d\xi_2$$

and their numerical evaluation is carried out by [18, 102],

$$I \cong \sum_{i=1}^{N} \sum_{j=1}^{N} w_i w_j f(\xi_1^i, \xi_2^j)$$

As mentioned previously, when source and observation points are both on the same element, BE integrals contain singularities. Diagonal elements of the influence matrices are obtained by evaluating these singular integrals.

In the present study, to evaluate singular integrals, each element is divided into triangular sub-regions (see Figure 2.6) and integrands are expressed in terms of polar coordinates centered at the singular source point. Then, integrations over each sub-region are summed up. Boundary element integrals to be evaluated in this way are of the form

$$h^{mk} = \sum_{t=1}^{T} \int_{\theta_1^t}^{\theta_2^t} \left[\int_{0}^{\bar{\rho}(\theta)} M_k \, \tilde{q} \, J\rho d\rho \right] d\theta \qquad (2.37)$$

$$g^{mk} = \sum_{t=1}^{T} \int_{\theta_1^t}^{\theta_2^t} \left[\int_{0}^{\bar{\rho}(\theta)} M_k \, \tilde{p} \, J\rho d\rho \right] d\theta \qquad (2.38)$$

where T = 3 for triangular elements and T = 4 for quadrilateral elements, and θ_1 and θ_2 are integration limits in θ direction for the triangular sub-region under consideration.

Triangular sub-regions formed in quadrilateral and triangular elements, local coordinates (ξ_i) and polar coordinates (ρ, θ) centered at a typical singular source

point are illustrated in Figure 2.6, which is adopted from available literature [13]. It should be noted that, the location of singular source point ξ_{oi} in the figure represents collocation node of the element.

From the figure it is clear that transformation from local to polar coordinates is given by

$$\begin{aligned} \xi_1 &= \xi_{01} + \rho\cos(\theta) \\ \xi_2 &= \xi_{02} + \rho\sin(\theta) \end{aligned} \tag{2.39}$$

and the radial distance in each triangular sub-region has the limits

$$0 \le \rho \le \bar{\rho}(\theta) = \frac{\rho_m}{\cos(\theta - \theta_m)}$$

where ρ_m is perpendicular distance from singular (source) point to the element boundary, and θ_m represents angular orientation of the perpendicular line as illustrated in Figure 2.6 (c).

Applying the polar coordinate transformation to singular integrals in equations 2.37 and 2.38, resulting integrals over each triangular sub-region can be expressed in the form

$$I = \int_{-1}^{1} \left[\int_{0}^{1} f(\rho,\theta) d\rho \right] d\theta$$

which can be evaluated using standard Gaussian quadrature rules, that is, by

$$I \cong \sum_{i=1}^{N} \sum_{j=1}^{N} w_i w_j f(\rho^i, \theta^j)$$

A treatment of how singular integrals could be eliminated using polar coordinate transformation and Taylor series approximation of the integrand terms in equations 2.37 and 2.38 is given below [59, 60]. Substituting fundamental solutions in equations 2.10 and 2.11 into equations 2.37 and 2.38, explicit form of integrals to be evaluated can be obtained as

$$h^{mk} = -\sum_{t=1}^{T} \int_{\theta_1^t}^{\theta_2^t} \left[\int_{0}^{\bar{\rho}(\theta)} M_k \frac{e^{-ikr}}{4\pi r^2} (ikr+1) \frac{\partial r}{\partial n} J\rho d\rho \right] d\theta \tag{2.40}$$

$$g^{mk} = \sum_{t=1}^{T} \int_{\theta_1^t}^{\theta_2^t} \left[\int_{0}^{\bar{\rho}(\theta)} M_k \frac{e^{-ikr}}{4\pi r} J\rho d\rho \right] d\theta \tag{2.41}$$

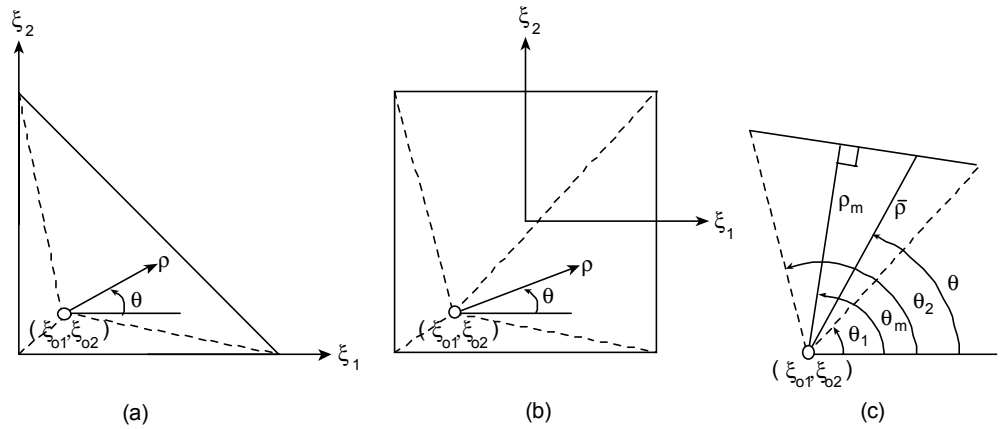

Figure 2.6 Division of parent elements into triangular sub-regions; (a) triangular elements, (b) quadrilateral elements, (c) typical triangular sub-region

Singularities in equations 2.40 and 2.41 are due to fundamental solutions and other terms of the integrands are regular. Furthermore, integrand of equation 2.40 has a higher order of singularity than that of equation 2.41. However, this integrand has a multiplicand of normal derivative of the distance between the singular (source) and integration points, which has a smoothing effect on the singularity.

Taylor series expansion of the parametric equation $x_i = x_i(\xi_k)$ of the element about the singular point or its image point on parent element yields [59, 60]

$$x_i - x_{oi} = \left.\frac{\partial x_i}{\partial \xi_1}\right|_{\xi_o} (\xi_1 - \xi_{o1}) + \left.\frac{\partial x_i}{\partial \xi_2}\right|_{\xi_o} (\xi_2 - \xi_{o2}) + \ldots \quad , \quad i = 1\text{-}3 \qquad (2.42)$$

which leads to, in view of equation 2.39,

$$x_i - x_{oi} = \rho A_i(\theta) + O(\rho^2)$$

where O( ) indicates the order of approximation and

$$A_i(\theta) = \left.\frac{\partial x_i}{\partial \xi_1}\right|_{\xi_o} \cos(\theta) + \left.\frac{\partial x_i}{\partial \xi_2}\right|_{\xi_o} \sin(\theta) \qquad (2.42)$$

Hence, for radial distance between source and field points, one has

$$\begin{aligned} r &= \sqrt{\sum_{i=1}^{3} (x_i - x_{0i})^2} \\ &= \rho A(\theta) + O(\rho^2) \end{aligned} \qquad (2.43)$$

where A(θ) is defined by

$$A(\theta) = \sqrt{\sum_{i=1}^{3} (A_i(\theta))^2} \tag{2.44}$$

For the components of the unit vector $\underline{r}$, one obtains

$$\begin{aligned} r_i &= \frac{\partial r}{\partial x_i} = \frac{x_i - x_{oi}}{r} \\ &= \frac{A_i(\theta)}{A(\theta)} + O(\rho) = d_{i0} + \rho d_{i1} O(\rho^2) \end{aligned} \tag{2.45}$$

where $d_{i0} = A_i/A$ and d_{i1} is a function of θ which may be determined when higher order terms are included in equation 2.42 [59, 60].

Components of the outer unit normal vector may be evaluated from

$$n_i = \frac{J_i}{J} \tag{2.46}$$

where Jacobian J and its components J_i are as defined previously in equation 2.23. Taylor series expansion of Jacobian component J_i yields

$$\begin{aligned} J_i &= J_i\big|_{\xi_o} + \rho\left(\frac{\partial J_i}{\partial \xi_1}\bigg|_{\xi_o} \cos(\theta) + \frac{\partial J_i}{\partial \xi_2}\bigg|_{\xi_o} \sin(\theta)\right) + O(\rho^2) \\ &= J_{i0} + \rho J_{i1} + O(\rho^2) \end{aligned} \tag{2.47}$$

Using summation convention, where a repeated index implies summation over its range, one obtains, for $\frac{\partial r}{\partial n} J$,

$$\begin{aligned} \frac{\partial r}{\partial n} J &= r_i n_i J = r_i J_i \\ &= d_{i0} J_{i0} + \rho(d_{i0} J_{i1} + d_{i1} J_{i0}) + O(\rho^2) \end{aligned} \tag{2.48}$$

However, since $d_{i0}J_{i0}$ is equal to zero, the above expression simplifies to

$$\begin{aligned} \frac{\partial r}{\partial n} J &= \rho(d_{i0} J_{i1} + d_{i1} J_{i0}) + O(\rho^2) \\ &= \rho p_1(\theta) + O(\rho^2) \end{aligned} \tag{2.49}$$

Similarly, expansion of the variable interpolation function M_k results in

$$M_k = M_{k0} + \rho M_{k1} + O(\rho^2) \tag{2.50}$$

When in the BE integral h^{mk} given in equation 2.40, which has a higher order of singularity, the expressions in equations 2.42 through 2.50 are used, one obtains

$$h^{mk} \cong -\sum_{t=1}^{T} \int_{\theta_1^t}^{\theta_2^t} \left[\int_0^{\bar{\rho}(\theta)} (M_{k0} + \rho M_k) \frac{e^{-ik\rho A(\theta)}}{4\pi A^2(\theta)} (ik\rho A(\theta) + 1) p_1(\theta) d\rho \right] d\theta$$

which is regular. Similarly, the other BE integral g^{mk} in equation 2.41, and which has a lower order of singularity, may be reduced to a regular form.

As illustrated above, polar coordinate transformation together with the Taylor series approximation of integrands is an adequate means of removing singularities in the BE integrals considered. However, if orders of singularities are higher than the ones presented in equations 2.40 and 2.41, other techniques should be used for the removal of singularities [13, 58-60].

In the present study, the singularity problems are treated only when source and field points lie on the same element by using the polar coordinate transformation; and the near singularity problems arising from the closeness of the nodes in neighboring elements are disregarded.

CHAPTER 3

FINITE ELEMENT STRUCTURAL ANALYSIS

This chapter introduces the FE formulation for structural vibration analysis. The content of the chapter is presented in two main sections.

In the first section, governing equations for structural analysis is introduced in view of the FE formulations available in literature. Stating assumptions for both elastic solid medium and element formulations to be considered, resulting equations of the FEM are given. Matrix form of the governing equations of motion is obtained by assembling element matrices and vectors. Only, brief information about FEM is presented. Both time-domain and frequency-domain governing structural FE equations are given. The latter one is due to structural vibration in the case of steady-state harmonic excitation and response conditions.

In the second section of the chapter, first, available FE formulation for a rectangular plate element to model out-of-plane (bending) vibration of thin flat plates is presented [85, 86]. Then, the FE formulation is given for a flat facet triangular shell element to model both in-plane (membrane) and out-of-plane (bending) vibration of thin plates or shell-like structures [87-92].

The FE structural equations to be presented in this chapter will be integrated later with the BE equations, presented in Chapter 2, to analyze sound-structure interaction problem, which will be discussed in Chapter 4. Then, in Chapter 6, coupled BE-FE formulation will be used to illustrate some computational acoustic studies.

3.1 Finite Element Formulation for Structural Analysis

FE formulation for structural dynamic analysis is documented in literature [17-21]. In what follows, the FE formulation is reviewed in general terms with the assumptions: homogeneous and isotropic material properties; linear elastic behavior; small strain and deformations; negligible body forces and no initial residual strains.

In FE modeling, the structure is subdivided into a finite number of elements and the displacement field within an element is approximated as

$$\mathbf{w} = \mathbf{N}\mathbf{u}^{e} \tag{3.1}$$

where $\mathbf{w}$ is the displacement vector whose components are the displacements in three orthogonal directions, $\mathbf{N}$ is the displacement interpolation matrix which is a function of spatial coordinates and $\mathbf{u}^{e}$ is the nodal displacement vector which is a function of time.

Displacement field within an element is usually expressed in a local coordinate system. However, total structure behavior is expressed in terms of global coordinates. For each element, the transformation relation for the displacements expressed in local ($\mathbf{u}^{e}$) and global ($\mathbf{u}^{\hat{e}}$) coordinates is of the form [18, 21]

$$\mathbf{u}^{e} = \mathbf{A}^{e}\mathbf{u}^{\hat{e}} \tag{3.2}$$

where $\mathbf{A}^{e}$ is the orthogonal transformation matrix formed by direction cosines relating local to global axes.

Stress-strain and strain-displacement relations are

$$\boldsymbol{\sigma} = \mathbf{D}\boldsymbol{\varepsilon}$$

$$\boldsymbol{\varepsilon} = \Delta\mathbf{w}$$

where $\boldsymbol{\sigma}$ and $\boldsymbol{\varepsilon}$ are the stress and strain tensors, respectively, $\mathbf{D}$ is the elasticity matrix and Δ is a spatial differential operator matrix relating displacements to strains.

Governing FE equations for the structure may be obtained through the use of virtual work principle. They are of the form [17-21]

$$\mathbf{M}\ddot{\mathbf{u}} + \mathbf{C}\dot{\mathbf{u}} + \mathbf{K}\mathbf{u} = \mathbf{f}_{s} \tag{3.3}$$

with the dot indicating time derivative. The assembled mass $\mathbf{M}$, damping $\mathbf{C}$, and stiffness $\mathbf{K}$ matrices, and nodal load $\mathbf{f}_{s}$ and displacement vector defined by $\mathbf{u}$ are

$$\mathbf{M} = \sum_e \mathbf{A}^{e^T} \mathbf{M}^e \mathbf{A}^e \quad , \quad \mathbf{M}^e = \int_{V^e} \rho \mathbf{N}^T \mathbf{N} dv \tag{3.4}$$

$$\mathbf{C} = \sum_e \mathbf{A}^{e^T} \mathbf{C}^e \mathbf{A}^e \quad , \quad \mathbf{C}^e = \int_{V^e} \mu \mathbf{N}^T \mathbf{N} dv \tag{3.5}$$

$$\mathbf{K} = \sum_e \mathbf{A}^{e^T} \mathbf{K}^e \mathbf{A}^e \quad , \quad \mathbf{K}^e = \int_{V^e} \mathbf{B}^T \mathbf{D} \mathbf{B} dv \quad , \quad \mathbf{B} = \Delta \mathbf{N} \tag{3.6}$$

$$\mathbf{f}_s = \sum_e \mathbf{A}^{e^T} \mathbf{f}_s^e \quad , \quad \mathbf{f}_s^e = \int_{S^e} \mathbf{N}^T \boldsymbol{\tau} da \tag{3.7}$$

$$\mathbf{u} = \sum_e \mathbf{A}^{e^T} \mathbf{u}^e = \sum_e \mathbf{u}^{\hat{e}} \tag{3.8}$$

where $\mathbf{M}^e$, $\mathbf{C}^e$, $\mathbf{K}^e$ and $\mathbf{f}^e_s$ are the element mass, damping, stiffness matrices and element load vector, respectively. V^e is element volume, S^e is element surface area, ρ is structural mass density, μ is viscous damping coefficient, $\boldsymbol{\tau}$ is surface traction vector. Summation operation over the $\sum_e$ elements formally implies the FE assembling procedure.

The linear system of equations of motions in equation 3.3 can be solved in time or frequency domain. In the present study, analyses will be carried out in the frequency domain by assuming steady-state harmonic excitation and response conditions, such as, $\mathbf{f}_s(\underline{x}, t) = \hat{\mathbf{f}}_s(\underline{x}) e^{i\omega t}$ and $\mathbf{u}(\underline{x}, t) = \hat{\mathbf{u}}(\underline{x}) e^{i\omega t}$ with $\hat{\mathbf{f}}_s(\underline{x})$ and $\hat{\mathbf{u}}(\underline{x})$ indicating amplitudes of excitation and response at nodal points $\underline{x}$, respectively, and t denotes time and ω is angular frequency. Then, equation 3.3 reduces to

$$(-\omega^2 \mathbf{M} + i\omega \mathbf{C} + \mathbf{K}) \hat{\mathbf{u}} = \hat{\mathbf{f}}_s \tag{3.9}$$

Instead of using viscous dissipation, structural damping can be modeled by using

$$\mathbf{C} = \frac{\eta}{\omega} \mathbf{K} \tag{3.10}$$

where η is the structural loss factor [19]. Rayleigh (proportional) damping model is another possibility, in which damping matrix $\mathbf{C}$ has the form [18]

$$\mathbf{C} = \alpha \mathbf{K} + \beta \mathbf{M} \tag{3.11}$$

where α and β are stiffness and mass proportional damping constants, respectively.

At a point on the structure, boundary condition can be prescribed in the form of displacement or traction, or a combination of them.

3.2 A Plate and a Shell Finite Element Formulation

3.2.1 A Flat Rectangular Plate Element

A rectangular element is utilized to model flexural (bending) vibration of thin flat plates [85, 86]. Figure 3.1 illustrates the plate element in its local Cartesian coordinate system (x_1, x_2, x_3). The element has lateral dimensions of a, b in x_1 and x_2-axis directions, respectively, and uniform thickness h in x_3-axis direction. It has four corner nodes and nine degrees of freedom (dof) at each node.

The plate element is referred to as a conforming element due to its capability to satisfy displacement and slope continuity with the adjacent elements. Displacement component normal to the element plane (w), describing bending motion of the element, is expanded as

$$\begin{aligned}\hat{w}(x_1,x_2)=\sum_{i=1}^{2}\sum_{j=1}^{2}\Big[&h_{0i}(x_1)h_{0j}(x_2)w^{ij} \;+\; h_{1i}(x_1)h_{0j}(x_2)w^{ij}_{x_1}\\ &+\; h_{0i}(x_1)h_{1j}(x_2)w^{ij}_{x_2} \;+\; h_{1i}(x_1)h_{1j}(x_2)w^{ij}_{x_1x_2}\\ &+\; h_{2i}(x_1)h_{0j}(x_2)w^{ij}_{x_1x_1} \;+\; h_{0i}(x_1)h_{2j}(x_2)w^{ij}_{x_2x_2}\\ &+\; h_{2i}(x_1)h_{1j}(x_2)w^{ij}_{x_1x_1x_2} \;+\; h_{1i}(x_1)h_{2j}(x_2)w^{ij}_{x_1x_2x_2}\\ &+\; h_{2i}(x_1)h_{2j}(x_2)w^{ij}_{x_1x_1x_2x_2}\Big]\end{aligned} \tag{3.12}$$

where nodal values are indicated by superscript (ij) index pair (see Figure 3.1). Subscripts on w indicate spatial derivatives. Hermite interpolation polynomials are

$$\begin{aligned}h_{01}(x_1)&=\frac{1}{a^5}(a^5-10a^2x_1^3+15ax_1^4-6x_1^5)\\ h_{02}(x_1)&=\frac{1}{a^5}(10a^2x_1^3-15ax_1^4+6x_1^5)\\ h_{11}(x_1)&=\frac{1}{a^4}(a^4x_1-6a^2x_1^3+8ax_1^4-3x_1^5)\\ h_{12}(x_1)&=\frac{1}{a^4}(-4a^2x_1^3+7ax_1^4-3x_1^5)\\ h_{21}(x_1)&=\frac{1}{2a^3}(a^3x_1^2-3a^2x_1^3+3ax_1^4-x_1^5)\\ h_{22}(x_1)&=\frac{1}{2a^3}(a^2x_1^3-2ax_1^4+x_1^5)\end{aligned} \tag{3.13}$$

and similar expressions for $h_{01}(x_2)$, $h_{02}(x_2)$, $h_{11}(x_2)$, $h_{12}(x_2)$, $h_{21}(x_2)$ and $h_{22}(x_2)$ by replacing x_1 by x_2 and "a" by "b" in equation 3.13.

Nodal displacement vector is of the form

$$\mathbf{u}^{e} = [\mathbf{u}_1 \quad \mathbf{u}_2 \quad \mathbf{u}_3 \quad \mathbf{u}_4]^{T} \tag{3.14}$$

where each sub-vector $\mathbf{u}_k$ (k=1-4) at a node indicated by (ij) pair is

$$\mathbf{u}_k = [w^{ij} \quad w^{ij}_{x_1} \quad w^{ij}_{x_2} \quad w^{ij}_{x_1x_2} \quad w^{ij}_{x_1x_1} \quad w^{ij}_{x_2x_2} \quad w^{ij}_{x_1x_1x_2} \quad w^{ij}_{x_1x_2x_2} \quad w^{ij}_{x_1x_1x_2x_2}] \tag{3.15}$$

and the displacement interpolation matrix is, in view of equations 3.12 and 3.14,

$$\mathbf{N} = [\mathbf{N}_1 \quad \mathbf{N}_2 \quad \mathbf{N}_3 \quad \mathbf{N}_4] \tag{3.16}$$

where

$$\begin{aligned}
\mathbf{N}_1 &= [\ H^{01}_{01} \ H^{01}_{11} \ H^{11}_{01} \ H^{11}_{11} \ H^{01}_{21} \ H^{21}_{01} \ H^{11}_{21} \ H^{21}_{11} \ H^{21}_{21} \ ] \\
\mathbf{N}_2 &= [\ H^{02}_{01} \ H^{02}_{11} \ H^{12}_{01} \ H^{12}_{11} \ H^{02}_{21} \ H^{22}_{01} \ H^{12}_{21} \ H^{22}_{11} \ H^{22}_{21} \ ] \\
\mathbf{N}_3 &= [\ H^{02}_{02} \ H^{02}_{12} \ H^{12}_{02} \ H^{12}_{12} \ H^{02}_{22} \ H^{22}_{02} \ H^{12}_{22} \ H^{22}_{12} \ H^{22}_{22} \ ] \\
\mathbf{N}_4 &= [\ H^{01}_{02} \ H^{01}_{12} \ H^{11}_{02} \ H^{11}_{12} \ H^{01}_{22} \ H^{21}_{02} \ H^{11}_{22} \ H^{21}_{12} \ H^{21}_{22} \ ]
\end{aligned} \tag{3.17}$$

with the notation $H^{rs}_{pq} = h_{pq}(x_1)h_{rs}(x_2)$.

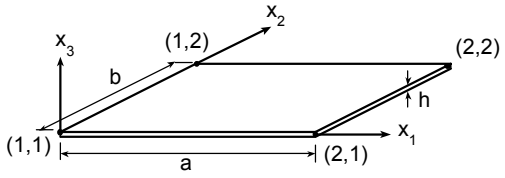

Figure 3.1 Rectangular plate element

From the classical thin-plate theory, the spatial differential operator $\mathbf{\Delta}$ and elasticity $\mathbf{D}$ matrices to be used in the element formulation are [19]

$$\mathbf{\Delta} = \begin{bmatrix} -x_3 \dfrac{\partial}{\partial x_1^2} \\ -x_3 \dfrac{\partial}{\partial x_2^2} \\ -2x_3 \dfrac{\partial^2}{\partial x_1 \partial x_2} \end{bmatrix} = -x_3 \begin{bmatrix} \dfrac{\partial}{\partial x_1^2} \\ \dfrac{\partial}{\partial x_2^2} \\ 2\dfrac{\partial^2}{\partial x_1 \partial x_2} \end{bmatrix} = -x_3 \mathbf{X} \tag{3.18}$$

and

$$\mathbf{D} = \frac{\mathrm{E}}{1-\nu^2}\begin{bmatrix} 1 & \nu & 0 \\ \nu & 1 & 0 \\ 0 & 0 & \dfrac{1-\nu}{2} \end{bmatrix} \tag{3.19}$$

where E is elasticity modulus and ν is Poisson's ratio.

Element mass and stiffness matrices can be obtained by substituting displacement interpolation, elasticity and spatial differential operator matrices into element mass and stiffness matrix expressions in equations 3.4 and 3.6, which yields

$$\mathbf{M}^{\mathrm{e}} = \int_{\mathrm{V}^{\mathrm{e}}} \rho \mathbf{N}^{\mathrm{T}} \mathbf{N} \mathrm{d}v = \int_{\mathrm{S}^{\mathrm{e}}} \rho \mathrm{h} \mathbf{N}^{\mathrm{T}} \mathbf{N} \mathrm{d}a \tag{3.20}$$

$$\mathbf{K}^{\mathrm{e}} = \int_{\mathrm{V}^{\mathrm{e}}} \mathbf{B}^{\mathrm{T}} \mathbf{D} \mathbf{B} \mathrm{d}v = \int_{\mathrm{S}^{\mathrm{e}}} \frac{\mathrm{h}^3}{12} \widetilde{\mathbf{B}}^{\mathrm{T}} \mathbf{D} \widetilde{\mathbf{B}} \mathrm{d}a, \qquad \widetilde{\mathbf{B}} = \mathbf{X}\mathbf{N} \tag{3.21}$$

Similarly, FE damping matrix can be obtained using equation 3.5 or 3.10 or 3.11, and load vector using equation 3.7.

Evaluation of element matrices and vectors can be carried out by analytical or numerical (e.g., Gaussian quadrature) integrations.

Boundary conditions for the two common plate configurations, namely, simply supported and clamped plate configurations are attained by specifying nodal displacement dof's as listed in Table 3.1 and 3.2 [86]. In these tables, restrained and free nodal dof are specified by 1 and by 0, respectively.

Table 3.1 Nodal boundary conditions for a simply supported plate

	w	w_{x_1}	w_{x_2}	$w_{x_1x_2}$	$w_{x_1x_1}$	$w_{x_2x_2}$	$w_{x_1x_1x_2}$	$w_{x_1x_2x_2}$	$w_{x_1x_1x_2x_2}$
Corner	1	1	1	0	1	1	0	0	0
x_1-edge	1	0	0	0	0	1	0	0	0
x_2-edge	1	0	0	0	1	0	0	0	0

Table 3.2 Nodal boundary conditions for a clamped plate

	w	w_{x_1}	w_{x_2}	$w_{x_1x_2}$	$w_{x_1x_1}$	$w_{x_2x_2}$	$w_{x_1x_1x_2}$	$w_{x_1x_2x_2}$	$w_{x_1x_1x_2x_2}$
Corner	1	1	1	1	1	1	1	1	0
x_1-edge	1	0	1	0	0	0	0	0	0
x_2-edge	1	1	0	0	0	0	0	0	0

3.2.2 A Flat Triangular Shell Element

A flat triangular element known as a facet triangular shell element is utilized to model bending and membrane vibrations of thin shells [87-92]. Facet shell element has six dof at each element node and the nodes are located at the three vertices of the element. This shell element is illustrated in Figure 3.2. In the figure, local Cartesian coordinate system (x_1, x_2, x_3) is at the centroid of the element, x_1-axis is in 31 direction and x_3-axis is perpendicular to the element surface.

The FE bending model is achieved through an implementation of a modified potential energy principle [87-92]. The FE formulation prevents the difficulties in achieving compatibility of bending rotations between contiguous elements and enables displacement interpolation functions to be assumed separately in the element interior and on the element boundary.

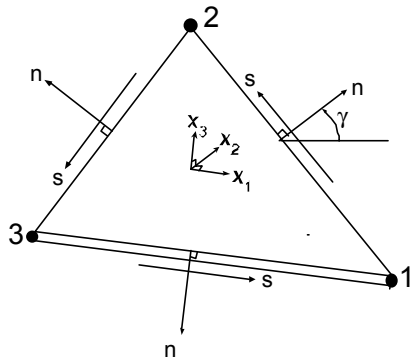

Figure 3.2 Triangular facet shell element

Bending action of the element is modeled by a nine term cubic polynomial to approximate the displacement field normal to the element plane, i.e,

$$\begin{aligned}\hat{w}(\xi_1,\xi_2,\xi_3) = {} & w_1\xi_1 + w_2\xi_2 + w_3\xi_3 + \alpha_1\xi_1\xi_2 + \alpha_2\xi_2\xi_3 + \alpha_3\xi_3\xi_1 \\ & + \alpha_4\xi_1\xi_2(\xi_2 - \xi_1) + \alpha_5\xi_2\xi_3(\xi_3 - \xi_2) + \alpha_6\xi_3\xi_1(\xi_1 - \xi_3)\end{aligned} \tag{3.22}$$

where w_1, w_2, w_3 are the nodal values of bending displacement, α_i (i=1-6) are the displacement coefficients that will be determined from known element bending dof's and ξ_1, ξ_2, ξ_3 are the triangular coordinates. These triangular coordinates are related to the local Cartesian coordinates by

$$\begin{bmatrix}\xi_1 \\ \xi_2 \\ \xi_3\end{bmatrix} = \frac{1}{2S^e}\begin{bmatrix}(x_1^2x_2^3 - x_1^3x_2^2) & (x_2^2 - x_2^3) & (x_1^3 - x_1^2) \\ (x_1^3x_2^1 - x_1^1x_2^3) & (x_2^3 - x_2^1) & (x_1^1 - x_1^3) \\ (x_1^1x_2^2 - x_1^2x_2^1) & (x_2^1 - x_2^2) & (x_1^2 - x_1^1)\end{bmatrix}\begin{bmatrix}1 \\ x_1 \\ x_2\end{bmatrix}$$

where the element area S^e is

$$S^e = \frac{1}{2}\begin{vmatrix}1 & x_1^1 & x_2^1 \\ 1 & x_1^2 & x_2^2 \\ 1 & x_1^3 & x_2^3\end{vmatrix}$$

On a typical element boundary between nodes i and j, separate fields of displacement $\hat{w}^*$ and normal rotation $\partial\hat{w}^*/\partial n$ are assumed to have respectively cubic and linear distributions as

$$\begin{aligned}\hat{w}^*(s) = {} & [1 - 3(\frac{s}{l_{ij}})^2 + 2(\frac{s}{l_{ij}})^3]w_i + l_{ij}[(\frac{s}{l_{ij}}) - 2(\frac{s}{l_{ij}})^2 + (\frac{s}{l_{ij}})^3]\frac{\partial w_i}{\partial s} \\ & + l_{ij}[3(\frac{s}{l_{ij}})^2 - 2(\frac{s}{l_{ij}})^3]w_j + [-(\frac{s}{l_{ij}})^2 + (\frac{s}{l_{ij}})^3]\frac{\partial w_j}{\partial s}\end{aligned} \tag{3.23}$$

$$\frac{\partial\hat{w}^*(s)}{\partial n} = [1 - (\frac{s}{l_{ij}})]\frac{\partial w_i}{\partial n} + (\frac{s}{l_{ij}})\frac{\partial w_j}{\partial n} \tag{3.24}$$

where l_{ij} is the element edge length between nodes i and j and coordinate "s" runs from node i to node j, and "n" is the outer normal of the edge (in the plane of the element) as illustrated in Figure 3.2, and w_k, $\partial w_k/\partial s$, $\partial w_k/\partial n$ (k = i, j) are the nodal values of displacement and its partial derivatives.

The partial derivatives with respect to coordinates "s" and "n" in equations 3.23 and 3.24 are related to the partial derivatives with respect to local Cartesian

coordinates x_1 and x_2 by

$$\frac{\partial(\,)}{\partial s} = -\sin(\gamma_{ij})\frac{\partial(\,)}{\partial x_1} + \cos(\gamma_{ij})\frac{\partial(\,)}{\partial x_2}$$

$$\frac{\partial(\,)}{\partial n} = \cos(\gamma_{ij})\frac{\partial(\,)}{\partial x_1} + \sin(\gamma_{ij})\frac{\partial(\,)}{\partial x_2}$$

where γ_{ij} is the angle measured from the x_1-axis to the outer normal "n" of the edge between nodes i and j. The partial derivatives with respect to local Cartesian coordinates are related to those of triangular coordinates by

$$\frac{\partial(\,)}{\partial x_i} = \sum_{j=1}^{3} \frac{\partial(\,)}{\partial \xi_j}\frac{\partial \xi_j}{\partial x_i} \quad , \quad (i = 1\text{-}3)$$

Implementation of the modified potential energy principle by using displacement fields of equations 3.22-3.24 yields [87-92]: the bending strain energy U_b associated with the interior displacement field of equation 3.22 is given by

$$U_b = \frac{1}{2}\boldsymbol{\alpha}^T \mathbf{H}_b \boldsymbol{\alpha}$$

The relation between generalized forces and displacement coefficients, and that between generalized displacements and nodal bending displacements are

$$\mathbf{Q} = \mathbf{B}^T \boldsymbol{\alpha}$$

and

$$\mathbf{q} = \mathbf{T}\mathbf{u}_b$$

where $\boldsymbol{\alpha}$ is the vector of displacement coefficients α_i (i=1-6); $\mathbf{H}_b$ is a positive definite symmetric matrix; **Q** and **q** are generalized force and displacement vectors, respectively; **B** is the matrix that relates the twelve generalized force components to six displacement coefficients α_i; and **T** is the matrix that relates the twelve generalized displacement components to nine nodal bending displacements ($\mathbf{u}_b$).

Generalized force vector **Q** is composed of the values of three concentrated forces (R_1, R_2, R_3) at the element nodes, three constant Kirchoff shear forces ($V_n^{12}, V_n^{23}, V_n^{31}$) along element edges and six components of normal bending moments ($M_n^{12}, M_n^{21}, M_n^{23}, M_n^{32}, M_n^{31}, M_n^{13}$) at the element nodes. The elements of the matrix **B** may be determined through relating the generalized forces **Q** to

displacement coefficients α_i by using the expressions

$$M_n = M_{x1}\cos^2(\gamma) + M_{x_2}\sin^2(\gamma) + M_{x_1x_2}\sin(2\gamma)$$

$$V_n = Q_n + \frac{\partial M_{ns}}{\partial s}$$

$$R_N = [M_{ns}]_{s^-}^{s^+} = M_{ns}\Big|^{s^+} - M_{ns}\Big|^{s^-} \quad , \quad N = 1\text{-}3$$

where

$$M_{ns} = \tfrac{1}{2}(M_{x_2} - M_{x_1})\sin(2\gamma) + M_{x_1x_2}$$

$$Q_n = \frac{\partial M_n}{\partial n} + \frac{\partial M_{ns}}{\partial s}$$

and M_{x_1}, M_{x_2} and $M_{x_1x_2}$ are related to $\hat{w}$ by

$$M_{x_1} = -D\left(\frac{\partial^2 \hat{w}}{\partial x_1^2} + v\frac{\partial^2 \hat{w}}{\partial x_2^2}\right)$$

$$M_{x_2} = -D\left(\frac{\partial^2 \hat{w}}{\partial x_2^2} + v\frac{\partial^2 \hat{w}}{\partial x_1^2}\right)$$

$$M_{x_1x_2} = -D(1-v)\frac{\partial^2 \hat{w}}{\partial x_1 \partial x_2}$$

where γ is the angle of inclination of an edge normal from the x_1-axis, v is Poisson's ratio and D is flexural rigidity.

The linear variation of normal bending moment and constant Kirchoff shear force in terms of the values of generalized forces on a typical side of the element between nodes i and j are

$$M_n = M_n^{ij}\left(1 - \frac{s}{l_{ij}}\right) + M_n^{ji}\frac{s}{l_{ij}}$$

$$V_n = V_n^{ij}$$

where M_n^{ij}, M_n^{ji} are the values of normal bending moment at each end of the edge and V_n^{ij} is the constant value of the Kirchoff shear force along the side.

Nodal bending displacements are defined by

$$\mathbf{u}_b = [\mathbf{u}_{b1} \quad \mathbf{u}_{b2} \quad \mathbf{u}_{b3}]^T \tag{3.25}$$

where $\mathbf{u}_{bi}$ (i = 1-3) is

$$\mathbf{u}_{bi} = [w_i \quad \theta_{x_1 i} \quad \theta_{x_2 i}] \tag{3.26}$$

with $\theta_{xi} = \partial w_i/\partial x_2$, $\theta_{yi} = -\partial w_i/\partial x_1$.

Through the implementation of the modified potential energy principle, the matrix **T** relating generalized displacements (associated with the generalized forces) to the element bending displacements may be obtained as [87-92]

$$\mathbf{T} = \begin{bmatrix}
1 & 0 & 0 & 0 & 0 & 0 & 0 & 0 & 0 \\
0 & 0 & 0 & 1 & 0 & 0 & 0 & 0 & 0 \\
0 & 0 & 0 & 0 & 0 & 0 & 1 & 0 & 0 \\
\frac{l_{12}}{2} & \frac{l_{12}^2}{12}c_{12} & \frac{l_{12}^2}{12}s_{12} & \frac{l_{12}}{2} & -\frac{l_{12}^2}{12}c_{12} & -\frac{l_{12}^2}{12}s_{12} & 0 & 0 & 0 \\
0 & 0 & 0 & \frac{l_{23}}{2} & \frac{l_{23}^2}{12}c_{23} & \frac{l_{23}^2}{12}s_{23} & \frac{l_{23}}{2} & -\frac{l_{23}^2}{12}c_{23} & -\frac{l_{23}^2}{12}s_{23} \\
\frac{l_{31}}{2} & \frac{l_{31}^2}{12}c_{31} & -\frac{l_{31}^2}{12}s_{31} & 0 & 0 & 0 & \frac{l_{31}}{2} & \frac{l_{31}^2}{12}c_{31} & \frac{l_{31}^2}{12}s_{31} \\
0 & -\frac{l_{12}}{3}s_{12} & \frac{l_{12}}{3}c_{12} & 0 & -\frac{l_{12}}{6}s_{12} & \frac{l_{12}}{6}c_{12} & 0 & 0 & 0 \\
0 & -\frac{l_{12}}{6}s_{12} & \frac{l_{12}}{6}c_{12} & 0 & -\frac{l_{12}}{3}s_{12} & \frac{l_{12}}{3}c_{12} & 0 & 0 & 0 \\
0 & 0 & 0 & 0 & -\frac{l_{23}}{3}s_{23} & \frac{l_{23}}{3}c_{23} & 0 & -\frac{l_{23}}{6}s_{23} & \frac{l_{23}}{6}c_{23} \\
0 & 0 & 0 & 0 & -\frac{l_{23}}{6}s_{23} & \frac{l_{23}}{6}c_{23} & 0 & -\frac{l_{23}}{3}s_{23} & \frac{l_{23}}{3}c_{23} \\
0 & -\frac{l_{31}}{6}s_{31} & \frac{l_{31}}{6}c_{31} & 0 & 0 & 0 & 0 & -\frac{l_{31}}{3}s_{31} & \frac{l_{31}}{3}c_{31} \\
0 & -\frac{l_{31}}{3}s_{31} & \frac{l_{31}}{3}c_{31} & 0 & 0 & 0 & 0 & -\frac{l_{31}}{6}s_{31} & \frac{l_{31}}{6}c_{31}
\end{bmatrix}$$

with notation $c_{ij} = \cos(\gamma_{ij})$ and $s_{ij} = \sin(\gamma_{ij})$.

The (9x9) element bending stiffness matrix $\mathbf{K}_b^e$ is given as [87-92]

$$\mathbf{K}_b^e = (\mathbf{BT})^T \mathbf{H}_b^{-1} (\mathbf{BT}) \tag{3.27}$$

The relations between displacement coefficients α_i (i=1-6) and element bending displacements are, in view of equation 3.22,

$$\begin{aligned}
\alpha_1 &= -\frac{1}{2} l_{12} \left(\frac{\partial w_2}{\partial s} - \frac{\partial w_1}{\partial s}\right) \\
\alpha_4 &= -l_{12} \left[\frac{1}{2}\left(\frac{\partial w_1}{\partial s} + \frac{\partial w_2}{\partial s}\right) - \Omega_{12}\right]
\end{aligned} \tag{3.28}$$

where Ω_{12} is the average rotation of the side between nodes 1 and 2 which is

$$\Omega_{12} = \frac{1}{l_{12}} \int_0^{l_{12}} \frac{\partial w}{\partial s} ds = w_2 - w_1 \tag{3.29}$$

The other pairs of coefficients (α_2, α_5) and (α_3, α_6) are obtained by cyclic permutation of the subscripts in equations 3.28 and 3.29.

The bending displacement field in equation 3.22 can be written as, in view of equation 3.25,

$$w = \mathbf{N}_w \mathbf{u}_b$$

where the bending displacement interpolation matrix $\mathbf{N}_w$ is, in view of equations 3.22 and 3.28,

$$\mathbf{N}_w = \mathbf{N}\mathbf{B}_w + \mathbf{N}_\alpha \mathbf{B}_{\alpha w} \tag{3.30}$$

with

$$\begin{aligned} &\mathbf{N} = [\xi_1 \quad \xi_2 \quad \xi_3] \\ &\mathbf{N}_\alpha = [\xi_1\xi_2 \quad \xi_2\xi_3 \quad \xi_3\xi_1 \quad \xi_1\xi_2(\xi_2 - \xi_1) \quad \xi_2\xi_3(\xi_3 - \xi_2) \quad \xi_3\xi_1(\xi_1 - \xi_3)] \end{aligned} \tag{3.31}$$

$$\mathbf{B}_w = \begin{bmatrix} 1 & 0 & 0 & 0 & 0 & 0 & 0 & 0 & 0 \\ 0 & 0 & 0 & 1 & 0 & 0 & 0 & 0 & 0 \\ 0 & 0 & 0 & 0 & 0 & 0 & 1 & 0 & 0 \end{bmatrix}$$

$$\mathbf{B}_{\alpha w} = \begin{bmatrix} 0 & \frac{1}{2}x_2^{21} & \frac{1}{2}x_1^{12} & 0 & -\frac{1}{2}x_2^{21} & -\frac{1}{2}x_1^{12} & 0 & 0 & 0 \\ 0 & 0 & 0 & 0 & \frac{1}{2}x_2^{32} & \frac{1}{2}x_1^{23} & 0 & -\frac{1}{2}x_2^{32} & -\frac{1}{2}x_1^{23} \\ 0 & -\frac{1}{2}x_2^{13} & -\frac{1}{2}x_1^{31} & 0 & 0 & 0 & 0 & -\frac{1}{2}x_2^{13} & \frac{1}{2}x_1^{31} \\ -1 & -\frac{1}{2}x_2^{21} & -\frac{1}{2}x_1^{12} & 1 & -\frac{1}{2}x_2^{21} & -\frac{1}{2}x_1^{12} & 0 & 0 & 0 \\ 0 & 0 & 0 & -1 & -\frac{1}{2}x_2^{32} & -\frac{1}{2}x_1^{23} & 1 & -\frac{1}{2}x_2^{32} & -\frac{1}{2}x_1^{23} \\ 1 & -\frac{1}{2}x_2^{13} & -\frac{1}{2}x_1^{31} & 0 & 0 & 0 & -1 & -\frac{1}{2}x_2^{13} & -\frac{1}{2}x_1^{31} \end{bmatrix}$$

with the notation $x_k^{ij} = x_k^i - x_k^j$ (i, j = 1-3; k = 1-2) and x_k^i representing the local Cartesian coordinates of i^{th} node.

The (9x9) element bending mass matrix $\mathbf{M}_b^e$ is, in view of equations 3.4 and 3.30,

$$\begin{aligned} \mathbf{M}_b^e &= \int_{S^e} \rho h \mathbf{N}_w^T \mathbf{N}_w \, da \\ &= \mathbf{B}_w^T [\int_{S^e} \rho h \mathbf{N}^T \mathbf{N} da] \mathbf{B}_w + \mathbf{B}_w^T [\int_{S^e} \rho h \mathbf{N}^T \mathbf{N}_\alpha da] \mathbf{B}_{\alpha w} \\ &+ \mathbf{B}_{\alpha w}^T [\int_{S^e} \rho h \mathbf{N}_\alpha^T \mathbf{N} da] \mathbf{B}_w + \mathbf{B}_{\alpha w}^T [\int_{S^e} \rho h \mathbf{N}_\alpha^T \mathbf{N}_\alpha da] \mathbf{B}_{\alpha w} \end{aligned} \tag{3.32}$$

Element load vector due to normal loading τ_n (acting on the element face) is, in view of equations 3.7 and 3.30,

$$\mathbf{f}_s^{eb} = \int_{S^e} \mathbf{N}_w^T \tau_n \, da = \int_{S^e} (\mathbf{B}_w^T \mathbf{N}^T + \mathbf{B}_{\alpha w}^T \mathbf{N}_\alpha^T) \tau_n \, da \tag{3.33}$$

The model for the membrane action of the element employs a nine term cubic polynomial to approximate each of the two membrane displacement components ($\hat{u}$, $\hat{v}$). The membrane displacement field component in x_1-direction is

$$\begin{aligned}\hat{u}(\xi_1,\xi_2,\xi_3) = {} & u_1\xi_1 + u_2\xi_2 + u_3\xi_3 + \alpha_1\xi_1\xi_2 + \alpha_2\xi_2\xi_3 + \alpha_3\xi_3\xi_1 \\ & + \alpha_4\xi_1\xi_2(\xi_2 - \xi_1) + \alpha_5\xi_2\xi_3(\xi_3 - \xi_2) + \alpha_6\xi_3\xi_1(\xi_1 - \xi_3)\end{aligned} \tag{3.34}$$

where u_1, u_2 and u_3 are the nodal values of the membrane displacement component $\hat{u}$, and the coefficients α_1 and α_4 are

$$\begin{aligned}\alpha_1 &= \frac{1}{2} l_{12}(\theta_{x_3 2} - \theta_{x_3 1})\cos(\gamma_{12}) \\ \alpha_4 &= l_{12}[\frac{1}{2}(\theta_{x_3 1} + \theta_{x_3 2}) - \Omega_o]\cos(\gamma_{12})\end{aligned} \tag{3.35}$$

with $\theta_{x_3 i}$ denoting the so-called drilling dof's associated with x_3-direction, and Ω_o representing the average rotation of the element in its plane as

$$\Omega_o = \frac{1}{2S^e} \int_{S^e} (\frac{\partial \hat{v}}{\partial x_1} - \frac{\partial \hat{u}}{\partial x_2}) da \tag{3.36}$$

Similarly, other remaining pairs of coefficients (α_2, α_5) and (α_3, α_6) are obtained by cyclic permutation of the subscripts in equations 3.35 and 3.36.

The membrane displacement field component in x_2- direction is defined as

$$\begin{aligned}\hat{v}(\xi_1,\xi_2,\xi_3) = {} & v_1\xi_1 + v_2\xi_2 + v_3\xi_3 + \alpha_1\xi_1\xi_2 + \alpha_2\xi_2\xi_3 + \alpha_3\xi_3\xi_1 \\ & + \alpha_4\xi_1\xi_2(\xi_2 - \xi_1) + \alpha_5\xi_2\xi_3(\xi_3 - \xi_2) + \alpha_6\xi_3\xi_1(\xi_1 - \xi_3)\end{aligned} \tag{3.37}$$

where v_1, v_2 and v_3 are the nodal values of the membrane displacement component $\hat{v}$ and the coefficients α_1 and α_4 are

$$\begin{aligned}\alpha_1 &= \frac{1}{2} l_{12}(\theta_{x_3 2} - \theta_{x_3 1})\sin(\gamma_{12}) \\ \alpha_4 &= l_{12}[\frac{1}{2}(\theta_{x_3 1} + \theta_{x_3 2}) - \Omega_o]\sin(\gamma_{12})\end{aligned} \tag{3.38}$$

and remaining pairs of coefficients can be determined again by cyclic permutation of the subscripts of equation 3.38.

The nodal displacement vector is

$$\mathbf{u}_m = [\mathbf{u}_{m1} \quad \mathbf{u}_{m2} \quad \mathbf{u}_{m3}]^T \tag{3.39}$$

where $\mathbf{u}_{mi}$ (i = 1-3) is

$$\mathbf{u}_{mi} = [u_i \quad v_i \quad \theta_{x_3 i}] \tag{3.40}$$

The membrane displacement field components in equations 3.34 and 3.37 can be written as, in view of equation 3.39,

$$u = \mathbf{N}_u \mathbf{u}_m$$
$$v = \mathbf{N}_v \mathbf{u}_m$$

with the displacement interpolation matrices $\mathbf{N}_u$, $\mathbf{N}_v$ defined as

$$\begin{aligned} \mathbf{N}_u &= \mathbf{N}\mathbf{B}_u + \mathbf{N}_\alpha \mathbf{B}_{\alpha u} \\ \mathbf{N}_v &= \mathbf{N}\mathbf{B}_v + \mathbf{N}_\alpha \mathbf{B}_{\alpha v} \end{aligned} \tag{3.41}$$

where the matrices $\mathbf{N}$, $\mathbf{N}_\alpha$ are the same as those in equation 3.31 and the matrices $\mathbf{B}_u$, $\mathbf{B}_v$, $\mathbf{B}_{\alpha u}$ and $\mathbf{B}_{\alpha v}$ are, in view of equations 3.34-3.38,

$$\mathbf{B}_u = \begin{bmatrix} 1 & 0 & 0 & 0 & 0 & 0 & 0 & 0 & 0 \\ 0 & 0 & 0 & 1 & 0 & 0 & 0 & 0 & 0 \\ 0 & 0 & 0 & 0 & 0 & 0 & 1 & 0 & 0 \end{bmatrix}$$

$$\mathbf{B}_v = \begin{bmatrix} 0 & 1 & 0 & 0 & 0 & 0 & 0 & 0 & 0 \\ 0 & 0 & 0 & 0 & 1 & 0 & 0 & 0 & 0 \\ 0 & 0 & 0 & 0 & 0 & 0 & 0 & 1 & 0 \end{bmatrix}$$

$$\mathbf{B}_{\alpha u}^T = \begin{bmatrix} 0 & 0 & 0 & X_1^{23} x_2^{21} & X_1^{23} x_2^{32} & X_1^{23} x_2^{13} \\ 0 & 0 & 0 & X_2^{23} x_2^{21} & X_2^{23} x_2^{32} & X_2^{23} x_2^{13} \\ -\frac{1}{2} x_2^{21} & 0 & \frac{1}{2} x_2^{13} & \frac{1}{2} x_2^{21} & 0 & \frac{1}{2} x_2^{13} \\ 0 & 0 & 0 & X_1^{31} x_2^{21} & X_1^{31} x_2^{32} & X_1^{31} x_2^{13} \\ 0 & 0 & 0 & X_2^{31} x_2^{21} & X_2^{31} x_2^{32} & X_2^{31} x_2^{13} \\ \frac{1}{2} x_2^{21} & -\frac{1}{2} x_2^{32} & 0 & \frac{1}{2} x_2^{21} & \frac{1}{2} x_2^{32} & 0 \\ 0 & 0 & 0 & X_1^{12} x_2^{21} & X_1^{12} x_2^{32} & X_1^{12} x_2^{13} \\ 0 & 0 & 0 & X_2^{12} x_2^{21} & X_2^{12} x_2^{32} & X_2^{12} x_2^{13} \\ 0 & \frac{1}{2} x_2^{32} & -\frac{1}{2} x_2^{13} & 0 & \frac{1}{2} x_2^{32} & \frac{1}{2} x_2^{13} \end{bmatrix}$$

$$\mathbf{B}_{\alpha v}^{T} = \begin{bmatrix} 0 & 0 & 0 & X_1^{23}x_1^{21} & X_1^{23}x_1^{32} & X_1^{23}x_1^{13} \\ 0 & 0 & 0 & X_2^{23}x_1^{21} & X_2^{23}x_1^{32} & X_2^{23}x_1^{13} \\ -\frac{1}{2}x_1^{21} & 0 & \frac{1}{2}x_1^{13} & \frac{1}{2}x_1^{21} & 0 & \frac{1}{2}x_1^{13} \\ 0 & 0 & 0 & X_1^{31}x_1^{21} & X_1^{31}x_1^{32} & X_1^{31}x_1^{13} \\ 0 & 0 & 0 & X_2^{31}x_1^{21} & X_2^{31}x_1^{32} & X_2^{31}x_1^{13} \\ \frac{1}{2}x_1^{21} & -\frac{1}{2}x_1^{32} & 0 & \frac{1}{2}x_1^{21} & \frac{1}{2}x_1^{32} & 0 \\ 0 & 0 & 0 & X_1^{12}x_1^{21} & X_1^{12}x_1^{32} & X_1^{12}x_1^{13} \\ 0 & 0 & 0 & X_2^{12}x_1^{21} & X_2^{12}x_1^{32} & X_2^{12}x_1^{13} \\ 0 & \frac{1}{2}x_1^{32} & -\frac{1}{2}x_1^{13} & 0 & \frac{1}{2}x_1^{32} & \frac{1}{2}x_1^{13} \end{bmatrix}$$

with the notation $x_k^{ij} = x_k^i - x_k^j$, $X_k^{ij} = -(x_k^i - x_k^j)/4S^e$ (i, j = 1-3; k = 1-2) and x_k^i representing the local Cartesian coordinates of i^{th} node.

The (9x9) element membrane stiffness matrix is, in view of equation 3.6,

$$\mathbf{K}_m^e = \int_{S^e} h\tilde{\mathbf{B}}^T \mathbf{D}\tilde{\mathbf{B}} da \tag{3.42}$$

where

$$\tilde{\mathbf{B}} = \mathbf{\Delta}\begin{bmatrix} \mathbf{N}_u \\ \mathbf{N}_v \end{bmatrix}$$

and the spatial differential operator $\mathbf{\Delta}$ is

$$\mathbf{\Delta} = \begin{bmatrix} \frac{\partial}{\partial x_1} & 0 \\ 0 & \frac{\partial}{\partial x_2} \\ \frac{\partial}{\partial x_1} & \frac{\partial}{\partial x_2} \end{bmatrix}$$

The (9x9) element membrane mass matrix $\mathbf{M}_m^e$ is

$$\mathbf{M}_m^e = \mathbf{M}_u + \mathbf{M}_v \tag{3.43}$$

where in view of equations 3.4 and 3.41,

$$\mathbf{M}_u = \int_{S^e} \rho h \mathbf{N}_u^T \mathbf{N}_u \, da$$
$$= \mathbf{B}_u^T [\int_{S^e} \rho h \mathbf{N}^T \mathbf{N} da] \mathbf{B}_u + \mathbf{B}_u^T [\int_{S^e} \rho h \mathbf{N}^T \mathbf{N}_\alpha da] \mathbf{B}_{\alpha u}$$
$$+ \mathbf{B}_{\alpha u}^T [\int_{S^e} \rho h \mathbf{N}_\alpha^T \mathbf{N} da] \mathbf{B}_u + \mathbf{B}_{\alpha u}^T [\int_{S^e} \rho h \mathbf{N}_\alpha^T \mathbf{N}_\alpha da] \mathbf{B}_{\alpha u}$$

$$\mathbf{M}_v = \int_{S^e} \rho h \mathbf{N}_v^T \mathbf{N}_v \, da$$
$$= \mathbf{B}_v^T [\int_{S^e} \rho h \mathbf{N}^T \mathbf{N} da] \mathbf{B}_v + \mathbf{B}_v^T [\int_{S^e} \rho h \mathbf{N}^T \mathbf{N}_\alpha da] \mathbf{B}_{\alpha v}$$
$$+ \mathbf{B}_{\alpha v}^T [\int_{S^e} \rho h \mathbf{N}_\alpha^T \mathbf{N} da] \mathbf{B}_v + \mathbf{B}_{\alpha v}^T [\int_{S^e} \rho h \mathbf{N}_\alpha^T \mathbf{N}_\alpha da] \mathbf{B}_{\alpha v}$$

Element load vector due to in-plane loading τ_m with components τ_{mu}, τ_{mv} is, in view of equations 3.7 and 3.41,

$$\mathbf{f}_s^{em} = \int_{S^e} (\mathbf{N}_u^T \tau_{mu} + \mathbf{N}_v^T \tau_{mv}) da$$
$$= \int_{S^e} [(B_u^T N^T + B_{\alpha u}^T N_\alpha^T) \tau_{mu} + (B_v^T N^T + B_{\alpha v}^T N_\alpha^T) \tau_{mv}] da \qquad (3.44)$$

Final forms of element mass and stiffness matrices are obtained by combining bending and membrane models of the element matrices in accordance with element total nodal displacement vector $\mathbf{u}^e$ arranged as

$$\mathbf{u}^e = [\mathbf{u}_1^e \quad \mathbf{u}_2^e \quad \mathbf{u}_3^e]^T \qquad (3.45)$$

where, in view of equations 3.26 and 3.40,

$$\mathbf{u}_i^e = \begin{bmatrix} u_i & v_i & w_i & \theta_{xi} & \theta_{yi} & \theta_{zi} \end{bmatrix} \quad , \quad i = 1\text{-}3$$

Therefore, element (18x18) mass and stiffness matrices are

$$\mathbf{M}^e = \mathbf{M}_b^e \oplus \mathbf{M}_m^e$$
$$\mathbf{K}^e = \mathbf{K}_b^e \oplus \mathbf{K}_m^e$$

and element (18x1) load vector is

$$\mathbf{f}_s^e = \mathbf{f}_s^{eb} \oplus \mathbf{f}_s^{em}$$

where the symbol $\oplus$ denotes arrangement of element matrices in equations 3.27, 3.32, 3.33, 3.42, 3.43 and 3.44 according to the order of dof's indicated in equation 3.45.

CHAPTER 4

SOUND-STRUCTURE INTERACTION

Sound-structure interaction analysis studies the coupled dynamic motion of fluid-solid media, and requires formulation of the dynamics of each medium separately and combining them by using interaction mechanism.

In this study, the interaction problem considered is due to coupling of interior acoustic domain to its bounding thin-walled elastic structure. Interaction of the elastic boundary to the rest of outer domain is not considered.

The chapter has two main sections that present a general numerical approach for the interaction analysis, and an analytical formulation for a specific interaction study, respectively.

First section introduces the BE-FE approach to analyze sound-structure interaction problem mentioned above, where BEM is used for acoustic domain and FEM for enclosing thin-walled elastic structure. Hence this section is based on the formulations of both BEM given in Chapter 2 and FEM introduced in Chapter 3. After presenting formulation for the interaction mechanism, three available approaches to obtain coupled system behavior are given.

In the second section, a fundamental interaction problem in acoustic studies is considered. Utilizing the works of other researchers on this interaction problem [63-73], admittance boundary condition is included on interaction surface, resulting in a reformulation of the analytical solution and extension of the method to allow modeling of sound absorptive treatments.

Analytical solution derived in this chapter will be assessed in Chapter 5. Later, both of the BE-FE approach and the analytical solution will be used in the computational sound-structure interaction studies to be presented in Chapter 6.

4.1 Boundary Element-Finite Element Interaction Analysis

Dynamics of acoustic medium enclosed by an elastic thin-walled structure is an interaction problem of fluid and solid media. Response of each medium is coupled to each other. This interaction problem will be analyzed by the BE-FE approach in which BEM is used to model the acoustic medium and FEM is used to model structure. Therefore, the interface region between the acoustic medium and structure is modeled by both BEM and FEM.

It is assumed that the acoustic fluid is inviscid; hence, it can exert only normal loads to its bounding structure and only normal components of structure response at the interface between two media can excite the acoustic domain.

The governing matrix form BE equation of acoustic medium is given in equation 2.25, i.e.,

$$\mathbf{Hp} = \mathbf{Gv} + \mathbf{f} \tag{4.1}$$

The governing matrix form FE structural equation 3.9 can be rewritten in a more compact form as

$$\mathbf{D}_s\mathbf{u} = \mathbf{f}_s \tag{4.2}$$

where the structural dynamic matrix $\mathbf{D}_s$ is

$$\mathbf{D}_s = -\omega^2\mathbf{M} + i\omega\mathbf{C} + \mathbf{K}$$

with displacement and loading notation simplified by omitting the sign (^) over the variables here and later in formulations.

Structural load $\mathbf{f}_s$ in equation 4.2 is considered to be composed of two parts as

$$\mathbf{f}_s = \mathbf{f}_a + \mathbf{f}_e \tag{4.3}$$

where $\mathbf{f}_a$ represents load on the structure due to the internal acoustic pressure and $\mathbf{f}_e$ represents load due to external excitation.

Structural equation 4.2 becomes, in view of equation 4.3,

$$\mathbf{D}_s\mathbf{u} = \mathbf{f}_a + \mathbf{f}_e \tag{4.4}$$

In this study, the positive direction of unit norma of interface will be taken from fluid to solid region. It is obvious that the traction τ acting on fluid region, at a point of interface, would be $\underline{\tau}$=-p$\underline{n}$, where p denotes the fluid pressure. Thus, the traction acting on the solid region (at a point of interface) is

$$\boldsymbol{\tau} = p\mathbf{n} \tag{4.5}$$

It may be noted that, for an interface element, $\underline{n}$ would be the same in acoustic and structural regions if geometric description of the interface element is identical in BE and FE models.

Acoustic pressure can be expressed as, in view of equation 2.17,

$$p = \mathbf{N}_a \mathbf{p}^e \tag{4.6}$$

where $\mathbf{N}_a$ and $\mathbf{p}^e$ represent acoustic pressure interpolation matrix and nodal acoustic pressure vector used in BE formulation, respectively.

Hence, acoustic load on structure can be written in local coordinates as, in view of equations 3.7, 4.5 and 4.6,

$$\mathbf{f}_a^e = \int_{S^e} \mathbf{N}_s^T \mathbf{n} \mathbf{N}_a \mathbf{p}^e \, da \tag{4.7}$$

where $\mathbf{N}_s$ represents the matrix formed by structural displacement interpolation functions used in FE formulation by considering displacements in three orthogonal directions.

Acoustic load to the whole structure is, in view of equation 3.7,

$$\mathbf{f}_a = \sum_e \mathbf{A}^{e\,T} \mathbf{f}_a^e = \sum_e \mathbf{A}^{e\,T} \mathbf{T}^e \mathbf{p}^e = \mathbf{T}\mathbf{p} \tag{4.8}$$

with element coupling matrix $\mathbf{T}^e$ defined as, in view of equation 4.7,

$$\mathbf{T}^e = \int_{S^e} \mathbf{N}_s^T \mathbf{n} \mathbf{N}_a \, da \tag{4.9}$$

Continuity of displacement at the interface requires that normal velocity of acoustic fluid and structure are equal. At an interface point, one can write

$$v_n = i\omega \mathbf{n}^T \mathbf{w} \tag{4.10}$$

where v_n is the normal component of acoustic particle velocity and $\mathbf{w}$ is the vector whose components are the displacements in the three-orthogonal directions.

Equation 4.10 can be rewritten for an interface element as, in view of equation 3.2,

$$v_n = i\omega \mathbf{n}^T \mathbf{N}_s \mathbf{u}^e = i\omega \mathbf{n}^T \mathbf{N}_s \mathbf{A}^e \hat{\mathbf{u}}^e \tag{4.11}$$

Due to the discrete nature of BE and FE methods, displacement continuity requirement can be imposed at nodes of interface elements. Continuity relation for

each BE can be expressed as, in view of equation 4.11,

$$\mathbf{v}_n^e = \mathbf{L}^e \mathbf{u}^{\hat{e}} \tag{4.12}$$

where $\mathbf{v}_n^e$ is the nodal acoustic normal velocity vector and $\mathbf{L}^e$ is the coupling matrix which has row vectors of the form, in view of equation 4.11,

$$\mathbf{l}^{eT} = i\omega \mathbf{n}^T \mathbf{N}_s A^e \tag{4.13}$$

with each row of $\mathbf{L}^e$ formed by evaluating expression for $\mathbf{l}^{eT}$ at an acoustic node used in BE formulation.

Velocity continuity for the whole interface surface can be expressed as

$$\mathbf{v} = \sum_e \mathbf{L}^e \mathbf{u}^{\hat{e}} = \mathbf{L}\mathbf{u} \tag{4.14}$$

In summary, interface conditions to coupled BE and FE equations are imposed as: displacement continuity which is satisfied by matching of acoustic normal velocity to structure normal velocity at the nodes of BE; force equilibrium which is attained by means of acoustic pressure loading to FE equations.

Using interface conditions, coupled equations of acoustic medium and structure can be expressed in three distinct ways. These are called mixed variable, fluid variable and structural variable approaches [53].

In the mixed variable approach, governing equations of each medium is directly coupled to each other, which can be described as: first, BE equation 4.1 is rewritten using interface conditions expressed in equation 4.14 as

$$\mathbf{H}\mathbf{p} = \mathbf{G}\mathbf{L}\mathbf{u} + \mathbf{f} \tag{4.15}$$

Then, FE equation 4.4 is rewritten as, in view of interface conditions expressed in equation 4.8,

$$\mathbf{D}_s \mathbf{u} = \mathbf{T}\mathbf{p} + \mathbf{f}_e \tag{4.16}$$

Finally, equations 4.15 and 4.16 are written together as

$$\begin{bmatrix} \mathbf{H} & -\mathbf{G}\mathbf{L} \\ -\mathbf{T} & \mathbf{D}_s \end{bmatrix} \begin{bmatrix} \mathbf{p} \\ \mathbf{u} \end{bmatrix} = \begin{bmatrix} \mathbf{f} \\ \mathbf{f}_e \end{bmatrix} \tag{4.17}$$

Solution of coupled equation 4.17 yields both acoustic pressure and structural displacements at once.

In the fluid variable approach: first, structural displacement vector is obtained

from equation 4.16 as

$$\mathbf{u} = \mathbf{D}_s^{-1}(\mathbf{T}\mathbf{p} + \mathbf{f}_e) \tag{4.18}$$

Then, substituting structural displacement using equation 4.18 into equation 4.15 yields

$$(\mathbf{H} - \mathbf{G}\mathbf{L}\mathbf{D}_s^{-1}\mathbf{T})\mathbf{p} = \mathbf{G}\mathbf{L}\mathbf{D}_s^{-1}\mathbf{f}_e + \mathbf{f} \tag{4.19}$$

where solution of equation 4.19 yields the acoustic pressure only. The structural displacements may then be calculated using equation 4.18.

In the structural variable approach: first, acoustic pressure vector is obtained from equation 4.15 as

$$\mathbf{p} = \mathbf{H}^{-1}(\mathbf{G}\mathbf{L}\mathbf{u} + \mathbf{f}) \tag{4.20}$$

Then, substituting acoustic pressure using equation 4.20 into equation 4.16 results

$$(\mathbf{D}_s - \mathbf{T}\mathbf{H}^{-1}\mathbf{G}\mathbf{L})\mathbf{u} = \mathbf{T}\mathbf{H}^{-1}\mathbf{f} + \mathbf{f}_e \tag{4.21}$$

where solution of equation 4.21 yields structural displacements only, after which acoustic pressure may be calculated using equation 4.20.

Sound-structure interaction formulation presented above can be extended to include more complicated boundary conditions. For example, only some part of the bounding structure may be elastic or acoustical absorptive treatment may be taken into consideration. These situations can be modeled by partitioning BE and FE matrices according to boundary conditions in consideration and proceeding thereafter as described in this section. Formulations for the stated complex boundary conditions and others including modal models are available in literature [14, 43].

4.2 Analytical Solution of a Cavity-Backed-Plate Problem

A fundamental case study in sound-structure interaction analyses is called the cavity-backed-plate problem. The formulation given below is prepared with view of previous work on the topic by other researchers [63-73]. Configuration for this fundamental study is illustrated in Figure 4.1. The cavity is a small rectangular parallelepiped room and all the walls except one are rigid. The elastic wall of the cavity is exposed to uniform external pressure and to cavity internal pressure.

Analytical formulation for the cavity-backed-plate problem is extended to include

admittance boundary condition to model absorptive acoustic treatment on the interface surface. The interface surface is modeled as a simply supported elastic plate interacting with the enclosed acoustic domain. Structural damping is also taken into consideration. Acoustic fluid and structure behave in accordance with the assumptions of linear acoustics and elasticity, respectively.

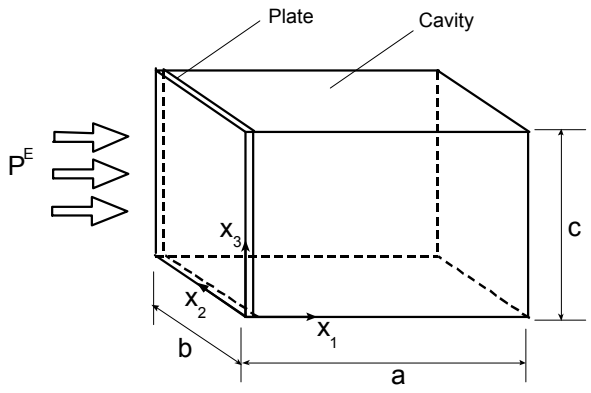

Figure 4.1 Cavity-backed-plate configuration

Acoustic velocity potential Ψ inside the cavity satisfies linearized homogenous wave equation, that is

$$\nabla^2\Psi(\underline{x},t)-\frac{1}{c_o^2}\frac{\partial^2}{\partial t^2}\Psi(\underline{x},t)=0 \tag{4.22}$$

where ∇^2 is the Laplacian operator and c_o is the speed of sound.

Initial and boundary conditions are

$$\Psi\big|_{t=0}=0, \qquad \left.\frac{\partial\Psi}{\partial t}\right|_{t=0}=0 \tag{4.23}$$

$$\left.\frac{\partial\Psi}{\partial x_1}\right|_{x_1=0}=-v_a(x_2,x_3,t), \qquad \left.\frac{\partial\Psi}{\partial x_1}\right|_{x_1=a}=0 \tag{4.24}$$

$$\left.\frac{\partial\Psi}{\partial x_2}\right|_{x_2=0}=0, \qquad \left.\frac{\partial\Psi}{\partial x_2}\right|_{x_2=b}=0 \tag{4.25}$$

$$\left.\frac{\partial \Psi}{\partial x_3}\right|_{x_3=0} = 0, \qquad \left.\frac{\partial \Psi}{\partial z}\right|_{x_3=c} = 0 \tag{4.26}$$

where a, b and c are the dimensions of the cavity in x_1, x_2 and x_3-axis directions respectively, v_a is the component of acoustic particle velocity in the outer normal direction at the vibrating interface plate surface.

In the case of non-absorbing plate surface, normal component of acoustic particle velocity is equal to plate transverse velocity. On the other hand, when sound absorptive treatment is considered, normal component of acoustical and structural velocities differ [14, 43, 93]. Hence, relative acoustic particle normal velocity v_r may be defined as the acoustic particle normal velocity v_a with respect to the structural normal velocity v_s as

$$v_r = v_a - v_s \tag{4.27}$$

On this sound-absorbing boundary, relative acoustic particle normal velocity and acoustic pressure p are related by

$$v_r = Yp \tag{4.28}$$

where Y represents the boundary admittance and is equal to the reciprocal value of the boundary impedance.

Admittance boundary condition is illustrated in Figure 4.2, which is adapted from literature [43]. In this figure, components of acoustic particle and structural velocities in the direction of outer normal vector $\underline{n}$ are shown. Acoustic pressure within cavity, external uniform excitation to the plate and absorptive treatment on the interior plate surface as the admittance boundary are illustrated. In the formulations, locally reacting admittance boundary condition is considered to model sound absorptive treatment. Admittance value is restricted to a frequency dependent parameter and is uniform over the plate surface.

Using the relationship between relative acoustic particle velocity and acoustic pressure given in equation 4.28, acoustic particle normal velocity can be obtained from equation 4.27 as

$$v_a = v_s + Yp \tag{4.29}$$

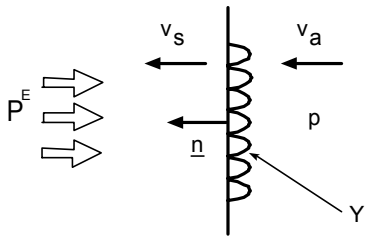

Figure 4.2 Admittance boundary condition on the plate surface

Using the separation of variables method, solution of equation 4.22 in Laplace domain may be written as

$$\overline{\Psi}(\underline{x},s) = \sum_{m,n=0}^{\infty} [A_{mn}\cosh(\alpha(s)x_1) + B_{mn}\sinh(\alpha(s)x_1)]\cos(\frac{m\pi}{b}x_2)\ \cos(\frac{n\pi}{c}x_3) \tag{4.30}$$

where A_{mn} and B_{mn} are some constants and

$$\alpha(s) = \frac{1}{c_o}\sqrt{\omega_{mn}^2 + s^2}$$

$$\omega_{mn}^2 = c_o^2\left[(\frac{m\pi}{b})^2 + (\frac{n\pi}{c})^2\right]$$

$$\overline{\Psi}(\underline{x},s) = \int_0^{\infty} \Psi(\underline{x},t)\, e^{-st} dt$$

Acoustic pressure and velocity potential are related by

$$\overline{P}(\underline{x},s) = -\rho_o s\overline{\Psi}(\underline{x},s) \tag{4.31}$$

where ρ_o is the acoustic fluid equilibrium density.

Laplace transforming the boundary conditions in equation 4.24, one obtains

$$\left.\frac{\partial\overline{\Psi}}{\partial x_1}\right|_{x_1=0} = -\overline{v}_a(x_2,x_3,s) \tag{4.32}$$

$$\left.\frac{\partial\overline{\Psi}}{\partial x_1}\right|_{x_1=a} = 0 \tag{4.33}$$

Simply supported plate transverse deflection in Laplace domain, using Navier double sine series solution is

$$\overline{w}(x_2, x_3, s) = \sum_{q,r=1}^{\infty} \overline{C}_{qr} \sin(\frac{q\pi}{b} x_2) \sin(\frac{r\pi}{c} x_3) \tag{4.34}$$

where $\overline{C}_{qr}$ are some constants and transformed plate deflection is defined as

$$\overline{w}(x_2, x_3, s) = \int_0^{\infty} w(x_2, x_3, t)\, e^{-st} dt$$

Hence, plate velocity can be expressed in terms of plate deflection as

$$\overline{v}_s(x_2, x_3, s) = s\overline{w}(x_2, x_3, s) \tag{4.35}$$

Coefficients A_{mn} and B_{mn} in equation 4.30 are obtained by using boundary conditions given in equations 4.32 and 4.33. Substituting acoustic particle velocity from equation 4.29 and velocity potential solution from equation 4.30, in view of equations 4.31, 4.34 and 4.35, into equation 4.32 and multiplying both sides of resulting expression by $\cos(m\pi x_2/b)\cos(n\pi x_3/c)$ then integrating over the plate surface area and similarly substituting velocity potential given in equation 4.30 into equation 4.33 and multiplying by $\cos(m\pi x_2/b)\cos(n\pi\, x_3/c)$ and integrating over the plate surface area yield expressions from which the coefficients A_{mn} and B_{mn} can be obtained as

$$A_{mn} = \sum_{q,r=1}^{\infty} KK' \overline{C}_{qr} B_{\substack{mn \\ qr}} \frac{s}{\alpha(s)\tanh(a\alpha(s)) + \rho_o sY} \tag{4.36}$$

$$B_{mn} = -\sum_{q,r=1}^{\infty} KK' \overline{C}_{qr} B_{\substack{mn \\ qr}} \frac{s\tanh(a\alpha(s))}{\alpha(s)\tanh(a\alpha(s)) + \rho_o sY} \tag{4.37}$$

where the modal coupling coefficient $B_{\substack{mn \\ qr}}$ is given by

$$B_{\substack{mn \\ qr}} = \frac{4}{bc} \int_0^b \int_0^c \sin(\frac{q\pi}{b} x_2) \sin(\frac{r\pi}{c} x_3) \cos(\frac{m\pi}{b} x_2) \cos(\frac{n\pi}{c} x_3) dx_2 dx_3 \tag{4.38}$$

and K and K′ equal to 0.5 for m and n equal to zero, respectively, and equal to 1 for m and n greater than zero, respectively.

Substituting explicit expressions for the coefficients A_{mn} and B_{mn} given in equations 4.36 and 4.37 into equation 4.30, velocity potential can be found as

$$\overline{\Psi}(\underline{x},s) = s\sum_{m,n=0}^{\infty}\sum_{q,r=1}^{\infty} KK'\overline{C}_{qr}B_{mn}^{qr}\overline{Z}\cos(\frac{m\pi}{b}x_2)\cos(\frac{n\pi}{c}x_3) \tag{4.39}$$

where

$$\overline{Z} = \frac{\cosh((a-x_1)\alpha(s))}{\alpha(s)\sinh(a\alpha(s)) + \rho_o sY\cosh(a\alpha(s))}$$

Pressure within cavity can be written using equations 4.31 and 4.39 as

$$\overline{P}(\underline{x},s) = -\rho_o s^2\sum_{m,n=0}^{\infty}\sum_{q,r=1}^{\infty} KK'\overline{C}_{qr}B_{mn}^{qr}\overline{Z}\cos(\frac{m\pi}{b}x_2)\cos(\frac{n\pi}{c}x_3) \tag{4.40}$$

Laplace transformed governing equation for the simply supported plate is

$$D\nabla^4\overline{w} + s^2\rho h\overline{w} = \overline{P}^C(x_2,x_3,s) - \overline{P}^E(x_2,x_3,s) \tag{4.41}$$

where ∇^4 is the biharmonic Laplacian operator and ρ is the plate mass density, h is the plate thickness, P^E and P^C are loading on the plate surface due to externally applied excitation and interior cavity acoustic pressure, respectively, and plate flexural rigidity D is, by denoting elastic modulus by E, structural loss factor by η and Poisson's ratio by *v*,

$$D = \frac{E(1+i\eta)h^3}{12(1-v^2)}$$

Subtituting plate deflection given in equation 4.34 into equation 4.41 yields

$$\sum_{q,r=1}^{\infty}\rho h(\omega_{qr}^2 + s^2)\overline{C}_{qr}\sin(\frac{q\pi}{b}x_2)\sin(\frac{r\pi}{c}x_3) = \overline{P}^C(x_2,x_3,s) - \overline{P}^E(x_2,x_3,s) \tag{4.42}$$

where

$$\omega_{qr}^2 = \pi^4\frac{D}{\rho h}\left[(\frac{q}{b})^2 + (\frac{r}{c})^2\right]^2$$

Cavity acoustic pressure load on plate can be found by evaluating equation 4.40 at $x_1 = 0$. Hence, using cavity pressure loading on plate as described and multiplying both sides of equation 4.42 by $\sin(q\pi x_2/b)\sin(r\pi x_3/c)$ and integrating over the plate surface yields

$$\rho h(\omega_{qr}^2 + s^2)\overline{C}_{qr} + \rho_o s^2\sum_{m,n=0}^{\infty}\sum_{k,l=1}^{\infty} KK'\overline{C}_{kl}B_{mn}^{kl}B_{mn}^{qr}\overline{Z} = \overline{P}_{qr}^E \quad , \quad q,r = 1,2,... \tag{4.43}$$

where

$$\overline{P}_{qr}^{E} = -\frac{4}{qr\pi^2}\overline{P}^{E}(\cos(q\pi)-1)(\cos(r\pi)-1) \tag{4.44}$$

Matrix form of equation 4.43 may be written as

$$\mathbf{Dc} = \mathbf{f} \tag{4.45}$$

Truncating q at Q, r at R and letting N_{QR} = Q x R, the vectors **c** and **f**, and the matrix **D** in equation 4.45 are defined as

$$\mathbf{c}^{T} = \left[\overline{C}_{11} \quad \ldots \quad \overline{C}_{qr} \quad \ldots \quad \overline{C}_{QR}\right]_{1xN_{QR}}$$

$$\mathbf{f}^{T} = \left[f_{11} \quad \ldots \quad f_{qr} \quad \ldots \quad f_{QR}\right]_{1xN_{QR}}$$

with

$$f_{qr} = -\frac{4\overline{P}_{1}^{E}}{qr\pi^2}\cos((q\pi)-1)\cos((r\pi)-1)$$

$$\mathbf{D} = \rho h\mathbf{\Lambda}(s) + \rho_o s^2 \sum_{m,n=0}^{M,N} KK'\overline{Z}\,\mathbf{b}\mathbf{b}^{T}$$

$$\mathbf{\Lambda}(s) = \begin{bmatrix} \omega_{11}^2 + s^2 & & & \\ & \ddots & & \\ & & \omega_{qr}^2 + s^2 & \\ & & & \ddots \\ & & & \omega_{QR}^2 + s^2 \end{bmatrix}_{N_{QR}xN_{QR}}$$

where row vector $\mathbf{b}^{T}$ is formed using modal coupling coefficients $B_{\substack{mn \\ qr}}$ as

$$\mathbf{b}^{T} = \left[B_{\substack{mn \\ 11}} \quad \ldots \quad B_{\substack{mn \\ qr}} \quad \ldots \quad B_{\substack{mn \\ QR}}\right]_{1xN_{QR}}$$

Solution for the unknown coefficients C_{qr} may be obtained from equation 4.45 as

$$\mathbf{c} = \mathbf{D}^{-1}\mathbf{f} \tag{4.46}$$

Therefore, equation 4.40 may be rewritten using vector products as

$$\overline{P}(\underline{x},s) = -\rho_o s^2 \sum_{m,n=0}^{\infty} KK'\mathbf{b}^{T}\mathbf{c}\overline{Z}\cos(\frac{m\pi}{b}x_2)\cos(\frac{n\pi}{c}x_3) \tag{4.47}$$

Substituting equation 4.46 into equation 4.47 yields Laplace transformed pressure within cavity as

$$\bar{P}(\underline{x},s) = -\rho_o s^2 \sum_{m,n=0}^{\infty} KK' \mathbf{b}^T \mathbf{D}^{-1} \mathbf{f} \bar{Z} \cos(\frac{m\pi}{b} x_2) \cos(\frac{n\pi}{c} x_3) \qquad (4.48)$$

Steady-state harmonic response due to harmonic excitation $P^E e^{i\omega t}$ can be obtained by evaluating equation 4.48 at $s = i\omega$.

When both of two opposing walls of the cavity are flexible and simply supported plates then analytical formulation for this case can be derived similarly as presented in this section by including related boundary conditions for the second plate. In the case of acoustically perfect reflective surface conditions, in other words, for zero acoustic admittance value, analytical solutions for the mentioned case of two-flexible wall problem is available in literature [73, 79].

CHAPTER 5

ASSESMENT OF THE ANALYTICAL SOLUTION TO THE CAVITY-BACKED-PLATE PROBLEM

This chapter assesses the analytical solution of a sound-structure interaction problem known as the cavity-backed-plate problem. This analytical solution, which enhances the formulations available in literature, is derived in Chapter 4.

Interest in dynamic behavior of plates in relation to their aeroelastic stability and excitation by noise in aerospace applications led to studies involving model response of a cavity-backed-plate problem [63]. This problem is a particular example that was studied in several research studies [63-73]. Most of the major studies cited in literature either investigate this problem for different configurations or use published data for verification [23, 40, 43, 54, 55, 80]. Hence, it is practically a benchmark problem in sound-structure interaction studies.

Since its first introduction into literature in early 1960's [63], analytical solutions to the cavity-backed-plate problem have been improved, and in late 1970's, a research study provided a set of experimental results [70]. A rather recent analytical solution was published in late 1970's by one of the pioneers on the subject [72]. After 1980's, cavity-backed-plate problem became one of the subjects in computational acoustic studies [23, 40, 43, 54, 55, 80].

In this chapter, the analytical solution to the cavity-backed-plate problem as developed in Chapter 4 is investigated. First, some convergence studies of the solution are presented when acoustically perfect reflective boundary conditions are considered. Then, case studies illustrating the effects of sound absorptive conditions on cavity acoustic field are given. Absorptive treatment is considered on full interaction boundary. Next, structural damping is taken into consideration to investigate its effects on the problem.

5.1 Cavity-Backed-Plate Convergence Study

In the following, inquiry and verification of the analytical solution to the cavity-backed-plate study are presented. Configuration for this study is shown in Figure 5.1. This figure illustrates that uniform external pressure (P^E) excites the elastic wall of the cavity. The elastic wall is a simply-supported plate where full interaction is considered while the other walls of the cavity are rigid. Cavity is referred to in a Cartesian coordinate system $\underline{x} = (x_1, x_2, x_3)$ located at the corner shown in the figure. Cavity dimensions, acoustic field and plate properties are given in Table 5.1.

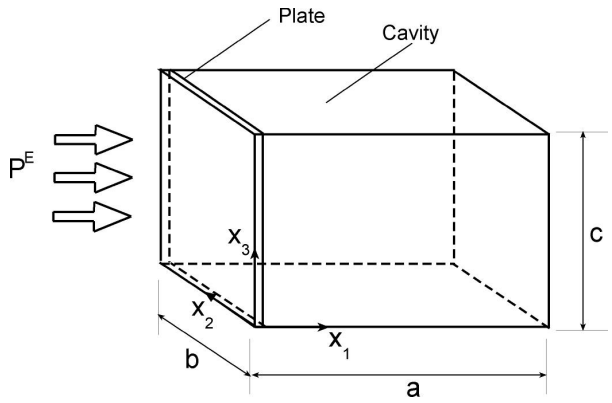

Figure 5.1 Cavity-backed-plate configuration

Table 5.1 Properties of cavity-backed-plate configuration

Cavity	Acoustic field	Plate
a = 0.2 m b = 0.2 m c = 0.2 m	fluid: air equilibrium density: $\rho_o = 1.21$ kg/m^3 speed of sound: $c_o = 340$ m/s	material: brass density: $\rho = 8500$ kg/m^3 elasticity modulus: E = 104 GPa Poisson's ratio: $\nu = 0.37$ loss factor: $\eta = 0$ thickness: h = 0.9144 mm lateral dimensions: 0.2 m by 0.2 m

For this study, frequency range of interest is between 0 Hz and 1000 Hz [70]. Uncoupled plate (f_{qr}) and cavity (f_{lmn}) modes are [2, 3]

$$f_{qr} = \frac{1}{2}\sqrt{\frac{D}{\rho h}}\left(\left(\frac{q}{b}\right)^2 + \left(\frac{r}{c}\right)^2\right)$$
$$f_{lmn} = \frac{c_o}{2}\sqrt{\left(\frac{l}{a}\right)^2 + \left(\frac{m}{b}\right)^2 + \left(\frac{n}{c}\right)^2} \quad (5.1)$$

where D is the plate flexural rigidity, and q, r, l, m and n represent modal indices. Table 5.2 lists uncoupled plate and cavity modes found from equation 5.1.

Table 5.2 Uncoupled plate and cavity modes

Uncoupled plate mode		Uncoupled cavity mode	
(q, r)	f_{qr} (Hz)	(l, m, n)	f_{lmn} (Hz)
(1,1)	78.06		
(1,2), (2,1)	195.14		
(2,2)	312.23		
(1,3), (3,1)	390.29		
(2,3), (3,2)	507.37		
(1,4), (4,1)	663.48		
(3,3)	702.51		
(2,4), (4,2)	780.57		
		(0,1,0), (0,0,1)	850.00
(3,4), (4,3)	975.71		

Acoustic pressure at interior surface point $\underline{x}$ = (a, b/2, c/2) is obtained using equation 4.48. Figure 5.2 illustrates the results for the sound pressure level (SPL) (SPL = 20 log (P^E/P)) and phase at the response location for acoustically perfect reflective surface conditions. The SPL results are illustrated in the same way as available in literature [70, 72].

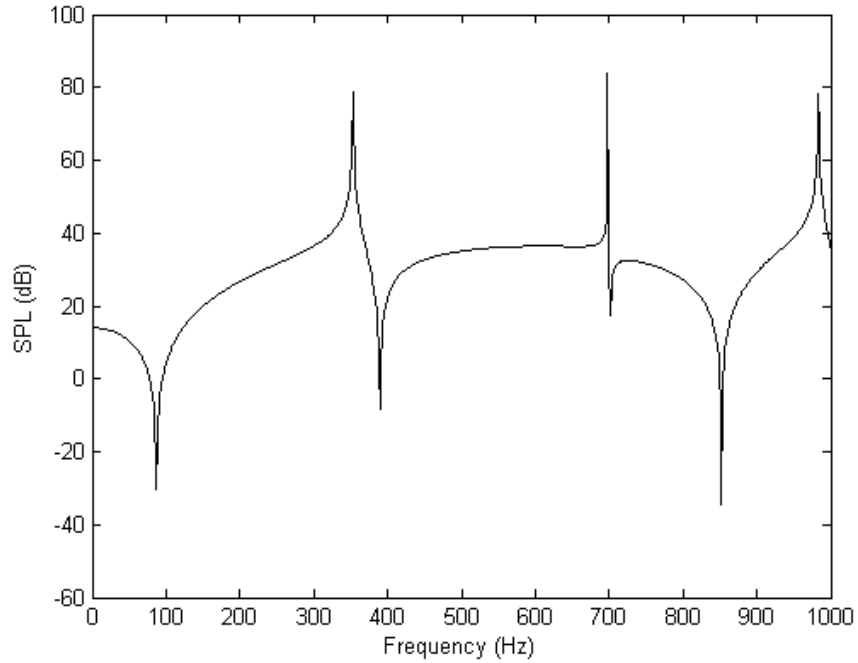

(a)

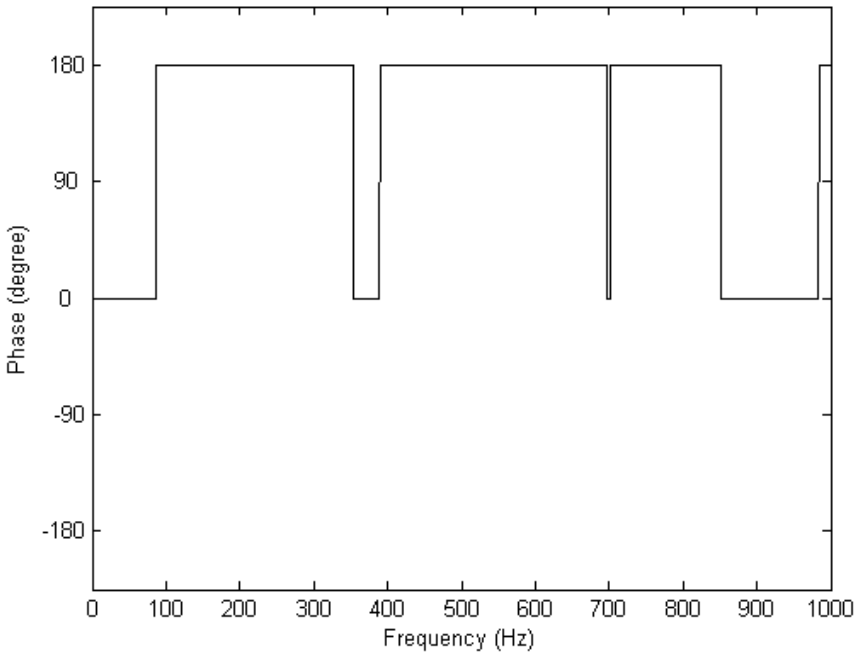

(b)

Figure 5.2 Response of cavity-backed-plate: (a) SPL, (b) Phase

In Figure 5.2, a dip in SPL response indicates a coupled system resonance. In this figure, SPL at a coupled system mode is truncated due to frequency resolution used in the calculations. Furthermore, although there exists a high modal density of uncoupled plate and acoustic modes (see Table 5.2), interaction of the acoustic field with its bounding structure yields only four coupled system modes due to selective coupling [63-73].

Convergence study for the derived equation 4.48 is carried out as follows. Maximum number of plate and acoustic modes retained in the formulation is gradually increased and their effects on coupled system modes are observed. Both SPL and phase information, using a frequency resolution of 0.01 Hz in calculations, are used to estimate a resonance frequency. At a coupled mode, corresponding resonance frequency is obtained by arithmetically evaluating the mid-point between two frequencies where a 180 degree phase change occurrs (see Figure 5.2).

There exist four coupled system modes; convergence for each of these modes is analyzed as described above and results of these analyses are illustrated in Tables 5.3-5.6. In these tables, M, N and Q, R represent maximum number of acoustic and plate modes retained in formulation (see Chapter 4, section 4.2)

Table 5.3 First coupled system mode convergence (Hz)

M, N / Q, R	0	1	2	3	4	5	6
1	86.82	86.82	86.76	86.76	86.76	86.76	86.76
2	86.82	86.82	86.76	86.76	86.76	86.76	86.76
3	86.80	86.80	86.74	86.74	86.74	86.74	86.74
4	86.80	86.80	86.74	86.74	86.74	86.74	86.74
5	86.80	86.80	86.74	86.74	86.74	86.74	86.74
6	86.80	86.80	86.74	86.74	86.74	86.74	86.74
7	86.80	86.80	86.74	86.74	86.74	86.74	86.74
8	86.80	86.80	86.74	86.74	86.74	86.74	86.74

Table 5.4 Second coupled system mode convergence (Hz)

M, N / Q, R	0	1	2	3	4	5	6
1	-	-	-	-	-	-	-
2	-	-	-	-	-	-	-
3	390.37	390.37	389.91	389.91	389.76	389.76	389.76
4	390.37	390.37	389.91	389.91	389.76	389.76	389.76
5	390.37	390.37	389.91	389.91	389.76	389.76	389.76
6	390.37	390.37	389.91	389.91	389.76	389.76	389.76
7	390.37	390.37	389.91	389.91	389.76	389.76	389.76
8	390.37	390.37	389.90	389.90	389.76	389.76	389.76

Table 5.5 Third coupled system mode convergence (Hz)

M, N / Q, R	0	1	2	3	4	5	6
1	-	-	-	-	-	-	-
2	-	-	-	-	-	-	-
3	702.46	702.46	701.82	701.82	701.45	701.45	701.42
4	702.46	702.46	701.82	701.82	701.45	701.45	701.42
5	702.46	702.46	701.82	701.82	701.45	701.45	701.42
6	702.46	702.46	701.82	701.82	701.45	701.45	701.42
7	702.46	702.46	701.82	701.82	701.45	701.45	701.42
8	702.46	702.46	701.82	701.82	701.45	701.45	701.42

Table 5.6 Fourth coupled system mode convergence (Hz)

M, N / Q, R	0	1	2	3	4	5	6
1	851.77	851.77	851.76	851.76	851.76	851.76	851.76
2	851.77	851.77	851.76	851.76	851.76	851.76	851.76
3	852.34	852.34	852.34	852.34	852.34	852.34	852.34
4	852.34	852.34	852.34	852.34	852.34	852.34	852.34
5	851.99	851.99	851.99	851.99	851.99	851.99	851.99
6	851.99	851.99	851.99	851.99	851.99	851.99	851.99
7	851.97	851.97	851.97	851.97	851.97	851.97	851.97
8	851.97	851.97	851.97	851.97	851.97	851.97	851.97

In Tables 5.4 and 5.5 a result listed as "-" indicates that a coupled system mode could not be determined. This situation occurs when maximum number of modes used in the calculations is not enough to model system behavior adequately. In order to properly model coupled system behavior, the maximum number of modes retained in calculations should not be less than those necessary to model uncoupled modes in the frequency range of analysis. Besides, analytical solution is an approximate modal solution involving summation of trigonometric series. Hence, a further increase for the number of modes to be retained in formulations should be preferred. Furthermore, nearby modes that lie outside the analysis region may affect coupled system behavior. Therefore, possible effects of these modes may need to be considered in determining the number modes to be retained in formulations.

As already stated, this case study is the subject of previous research studies. Two sets of comparative results obtained using equation 4.48 and published data in literature are illustrated in Tables 5.7 and 5.8. In the first set (Table 5.7) the value

used for speed of sound is c_o = 340 m/s, and in the second set (Table 5.8), all listed results indicated as "calculated " are for the case of c_o = 343 m/s.

Table 5.7 First set of comparative results for cavity-backed-plate study

Uncoupled modes (Hz)	Coupled system modes (Hz)	Coupled system modes (Hz) [72]
78.06	86.74	86.88
390.29	389.76	389.76
702.51	701.42	701.36
850.00	851.97	851.91

Table 5.8 Second set of comparative results for cavity-backed-plate study

Plate, cavity modes (Hz) Calculated		Plate, cavity modes (Hz) Calculated [23]		Plate, cavity modes (Hz) Measured [70]	
Uncoupled	Coupled	Uncoupled	Coupled	Uncoupled	Coupled
78.06	86.88	78	87	78	91
390.29	389.76	390	390.4	392	397
702.51	701.42	702	702.5	706	730
857.50	859.46	857	860	Not reported	864

Table 5.7 reveals that computations using equation 4.48 are in good agreement to the data available obtained from literature. In this table, compared results for coupled system modes are calculated using similar analytical solutions. However, Table 5.8 illustrates the coupled system modes that are determined using three different approaches. Tables 5.7 and 5.8 indicate that the most noticeable effect of interaction is on the first uncoupled plate mode. Also, an increase of 3 m/s in the speed of sound yielded a noticeable shift of uncoupled and coupled cavity-originated

modes towards higher frequencies, while only minor effects are observed for the uncoupled and coupled plate-originated modes.

5.2 Effects of Sound Absorptive Treatment

In this section, sound absorptive treatment on the full interaction surface of the cavity-backed-plate problem is considered. Sound absorptive treatment is applied only on the interior plate surface. Effect of this treatment on the coupled system modes and acoustic field response of the cavity are presented.

Configuration properties are given in Table 5.1. In addition to these data, sound absorptive treatment is introduced using a locally reacting admittance Y, which is modeled by, in view of published data in literature [94, 95],

$$Y = \frac{f}{\rho_o c_o}\overline{Y} \quad , \quad \overline{Y} = \alpha e^{i\theta}$$

where α and θ are sound absorbing material dependent constant and phase angle, respectively, f is cyclic frequency, and admittance is uniform on the plate surface.

Table 5.9 illustrates the effect of this treatment on the coupled system modes for admittance parameters (α, θ) selected from available data in literature [94]. Each coupled mode is calculated using 0.01 Hz frequency of resolution, and maximum number of acoustic (M, N) and plate (Q, R) modes that are used in the calculations are indicated in this table. For a non-zero admittance value, a coupled mode is indicated by the frequency where a peak in acoustic pressure response is observed.

Table 5.9 Coupled modes due to sound absorptive treatment

Admittance parameters (α, θ)	Coupled system modes (Hz) (M, N = 6; Q, R = 8)
(0, 0°)	86.74, 389.76, 701.42, 851.97
(2/10000, 80°)	86.33, 389.75, 701.36, 809.16
(4/10000, 80°)	85.96, 389.74, 701.29, 771.56

When sound absorptive treatment is considered, SPL (SPL = 20 log (P^E/P)) at an interior surface point $\underline{x}$ = (a, b/2, c/2) is obtained using the developed analytical solution. Results are illustrated in Figure 5.3 for different levels of treatment. This figure illustrates the effect of absorptive treatment on the coupled modes. In the figure, an expected amount of acoustic pressure attenuation is indicated with an increase of SPL (a resonance is shown by a dip). It is observed that, increasing values of admittance is effective in attenuating acoustic pressure in the neighborhood of coupled cavity-originated modes, while only small level of changes are observed in the vicinity of coupled plate-originated modes.

No published data in literature is available to make comparison with for the studied sound absorptive treatment on the plate interior surface. However, results of the analytical solution with and without considering sound absorptive treatment will be compared to BE-FE analysis results in Chapter 6.

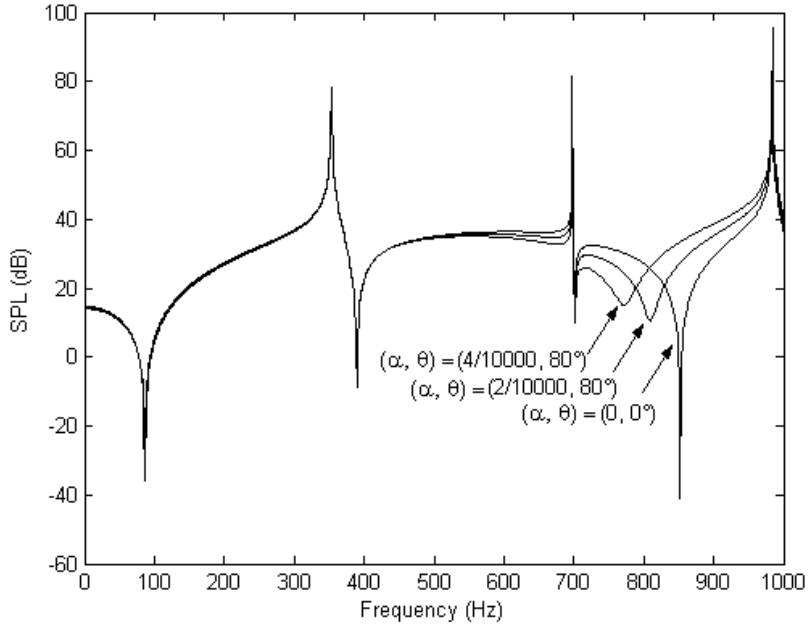

Figure 5.3 Effect of sound absorptive treatment to cavity-backed-plate study

5.3 Effects of Structural Damping

In the following, effect of structural damping on acoustic response of the cavity-backed-plate problem is illustrated. Structural damping is considered as an alternative mean in attenuating coupled system response.

Configuration properties are kept same as in Table 5.1 except with the addition of structural damping for the plate. Since structural loss factor for the plate material (brass) is very small ($\eta < 0.001$) [8], SPL acoustic response at an interior surface point $\underline{x} = (a, b/2, c/2)$ is obtained using loss values even larger than those found in literature. Structural damping effect on the coupled system behavior is illustrated in Figure 5.4. It is observed that structural damping effects are local to regions near coupled mode frequencies. In this figure, SPL changes are indicated at coupled system modes. As before, response level at coupled system modes are truncated due to frequency resolution used in calculations.

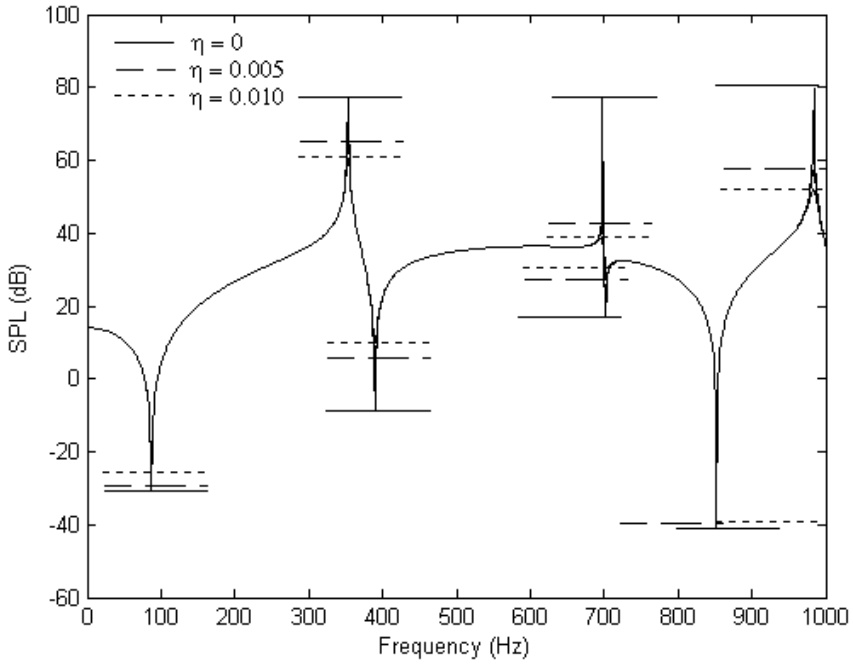

Figure 5.4 Effect of structural damping to cavity-backed-plate study

CHAPTER 6

COMPUTATIONAL ACOUSTIC ANALYSES

This chapter presents some computer implementation and case study applications of the analysis methods presented in previous chapters. The contents are organized in two sections.

In the first section, the main steps in computer implementations of BE and BE-FE methods are given. Additional analysis details in view of BE and FE formulations are also described.

Second section is devoted to the analysis of some case studies using the implemented methods. Most of the case studies presented in this section involve a fundamental geometric shape for analysis domain. Analytical solutions for acoustic field variables within this analysis domain are available in literature [5, 8]. Verification of BE implementation is illustrated with two case studies. A sound-structure interaction study known as cavity-backed-plate problem is analyzed by BE-FE method and analysis results are compared to the results using analytical solution developed in Chapter 4. Case studies involving sound absorptive treatment on the full interaction boundary in the cavity-backed-plate problem and modified configurations with additional full interaction surfaces are presented. Next, a more complicated problem is analyzed. Here, interaction effects are studied by BEM and by a modal method known as acoustoelasticity, in the presence of a Helmholtz resonator tuned to cavity acoustic mode. Section continues with a multi-domain BE analysis of a cavity-resonator configuration and with an investigation of positioning effectiveness of resonators. Section ends by summarizing the case studies and discussing, in view of presented material, contributions of the thesis to computational acoustic studies.

6.1 Computer Implementation of BE and BE-FE Methods

Numerical acoustic analyses using BE and BE-FE methods are performed through computer implementation of these techniques. In this study, several simple computer programs have been coded in Fortran and in Matlab ® platform to analyze some special acoustic problems considered in the following sections.

BE and BE-FE analyses are performed in frequency domain by solving system of equations at each frequency point in the analysis range. The two flow charts in Figure 6.1 illustrate the main steps of BE and BE-FE analyses. Some details are described below.

Input data for a typical analysis are the acoustic fluid properties (i.e., equilibrium density, speed of sound) and structure properties (i.e., density, elasticity modulus, Poisson's ratio, structural loss factor), geometric information of acoustical domain and structure, boundary conditions, excitations (i.e., acoustical and mechanical loads), number of numerical integration points and error tolerance in the solutions.

BE matrices can be computed in two separate sections, which involve computation for regular and singular integrals, respectively. These matrices have non-linear frequency dependence hence need to be re-evaluated at each frequency point of analysis. Furthermore, BE influence matrices are densely populated, complex valued and non-symmetric.

FE matrices, namely mass, damping and stiffness matrices are symmetric and sparse. These matrices need to be evaluated only once unless input data (geometric description and/or material properties of structure) is altered.

After imposing boundary conditions, BE or BE-FE system equations can be solved for unknown field variables on the boundary surface using Gaussian elimination technique with complex solution algorithms. Solution within domain of analysis can be calculated using already obtained boundary surface solution.

Convergence of results can be determined by observing the resulting effect of refining geometric mesh, increasing number of numerical integration points and adjusting error tolerance; or by comparing the results to other solutions (analytical, numerical or experimental) if available.

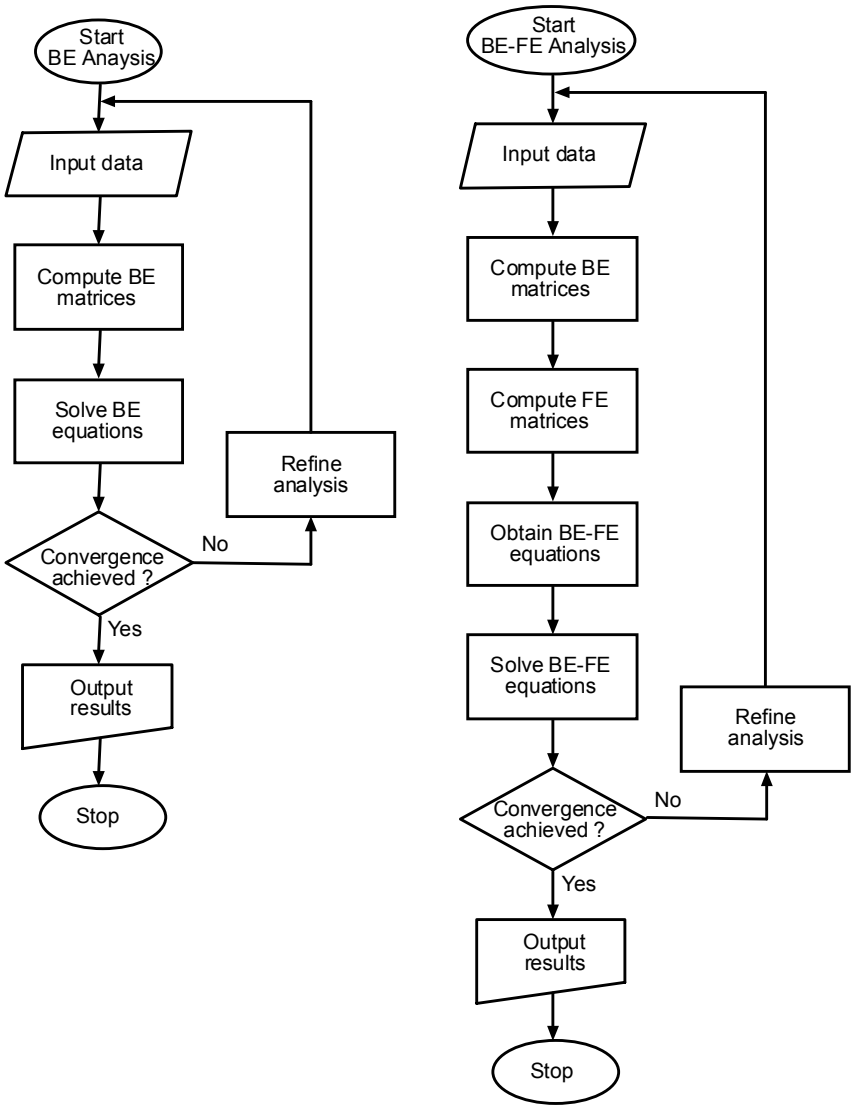

Figure 6.1 Flow charts for BE and BE-FE analyses

6.2 Computational Studies

In the following sections a selection of acoustic case studies are given to illustrate application of computer implementations of the BE and BE-FE methods. These studies involve use of the formulations introduced in Chapters 2, 3, 4 and 5. Case studies are selected to verify the implemented numerical and/or analytical solutions, to illustrate some details of acoustic analysis and to present some new applications with comparisons of analysis results obtained by different techniques.

6.2.1 BE Acoustic Field Analysis

In most of the case studies, acoustic domain of interest is mainly a rectangular parallelepiped cavity. This main geometric configuration is chosen due to availability of related analytical or experimental solutions found in literature. It should be noted that, as described in the previous chapters, BE and BE-FE methods are general tools to analyze various configurations.

Parallelepiped cavity used in the following acoustic analyses is illustrated in Figure 6.2. The cavity is referred to the Cartesian coordinate system $\underline{x} = (x_1, x_2, x_3)$ located at a corner shown in the figure and has dimensions of a, b and c in x_1-, x_2- and x_3-directions, respectively.

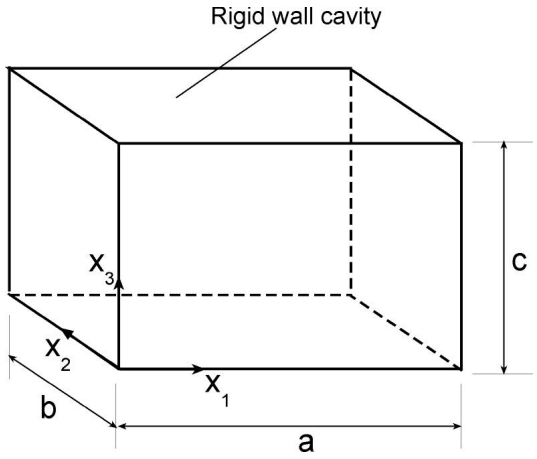

Figure 6.2 Parallelepiped cavity

In the case of rigid wall cavity with perfectly reflective boundaries and excited by a compact acoustic source, steady-state harmonic acoustic pressure solution is [5, 8]

$$\hat{p}(\underline{x}) = -i\omega\rho_o \frac{\hat{Q}}{V} \sum_{n=1}^{N} \frac{\psi_n(\underline{x})\psi_n(\underline{x}_o)}{\Lambda_n(k^2 - k_n^2)} \tag{6.1}$$

where $\hat{p}$ is the amplitude of sound pressure, i is the imaginary constant, ω is angular frequency, ρ_o is equilibrium fluid density, V is cavity volume, $\hat{Q}$ is the source strength of the compact source located at $\underline{x}_o$, k is wave number, n indicates acoustic modes, N is the maximum number of modes, ψ_n are mode shapes and Λ_n are modal coefficients.

Acoustic particle velocity is, in view of equations 6.1 and 2.3,

$$\hat{v}_j(\underline{x}) = \frac{\hat{Q}}{V} \sum_{n=1}^{N} \frac{\partial\psi_n(\underline{x})}{\partial x_j} \frac{\psi_n(\underline{x}_o)}{\Lambda_n(k^2 - k_n^2)} \tag{6.2}$$

Acoustic modes (eigenfunctions) of the rigid-walled cavity satisfy [5, 8],

$$\nabla^2\psi_n(\underline{x}) + k_n^2\psi_n(\underline{x}) = 0$$

where eigenfunctions and eigenvalues are

$$\psi_n(\underline{x}) = A_n \cos(\frac{n_1\pi}{a}x_1)\cos(\frac{n_2\pi}{b}x_2)\cos(\frac{n_3\pi}{c}x_3)$$

and

$$k_n^2 = (\frac{n_1\pi}{a})^2 + (\frac{n_2\pi}{b})^2(\frac{n_3\pi}{c})^2$$

with n_i indicating an acoustic mode represented by three non-negative integer numbers (n_1, n_2, n_3), and A_n representing modal scaling constants.

The orthogonality condition relating eigenfunctions to modal coefficients Λ_n is

$$\frac{1}{V}\int_V \psi_n(\underline{x})\psi_m(\underline{x})\, dv = \Lambda_n\delta_{nm}$$

where δ_{nm} is the Kronecker delta.

The normal component of acoustic particle velocity is equal to zero on the rigid boundary surface of the acoustic domain.

6.2.1.1 Case Study 1: Rigid Wall Cavity Response

In this case study, acoustic response of a rigid walled enclosure (see Figure 6.2) due to excitation by a compact acoustic source is analyzed by BEM. Cavity dimensions and acoustic field properties for this study are given in Table 6.1. A purpose of this case study is to verify the implementation of the quadrilateral elements. So, boundary surface is modeled separately by four quadrilateral BE patches, namely, QLC, QLL, QLQ and QQQ elements. Walls of the cavity are modeled using a uniform surface mesh and for each quadrilateral element type, there are 864 total acoustic variable nodes. Figure 6.3 illustrates a typical boundary surface mesh used in the BE analysis.

For this case study, enclosure geometry involves only planar surfaces. Therefore, boundary surface can be modeled accurately using linear geometric interpolation functions. In other words quadratic geometric interpolation functions (used in QQQ elements) is unnecessary and increases computational cost in the BE analysis.

Acoustic pressure and its phase at the interior response point are calculated between frequencies 100 Hz and 275 Hz. BE analysis results for sound pressure level SPL, (SPL = 20 log (P/P_{ref}) dB, P_{ref}=20 μPa) and phase response are illustrated in Figure 6.4. In this figure, analytical solutions using equation 6.1 are also illustrated.

Table 6.1 Properties of rigid wall parallelepiped cavity configuration

Cavity dimensions	Acoustic field properties, excitation and response locations
a = 1.36 m b = 1.13 m c = 0.97 m	fluid: air equilibrium density: ρ_o = 1.21 kg/m^3 speed of sound: c_o = 340 m/s source strength: $\hat{Q}=10^{-6}$ 1/s source location: $\underline{x}_o$ = (0.01, 0.01, 0.01) response location: $\underline{x}$ = (a-0.01, b-0.01, 0.01)

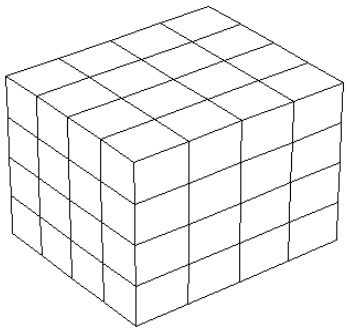

Figure 6.3 Typical surface mesh of rigid wall cavity

In the illustrations, both the analytical and the BE SPL responses at cavity modes are truncated because of the frequency resolution used in the calculations and due to numerical integration orders and error tolerances used in BE evaluations.

Comparison of analytical and BE solutions in Figure 6.4 reveals that, both analyses results are in good agreement over the whole frequency range. Deviations are more noticeable at higher frequencies. The deviations could be minimized by increasing number of modes used in analytical solution and by using a refined BE analysis involving a finer mesh, increased numerical integration orders and reduced error tolerances. It is observed that performances of all quadrilateral elements are good. Due their higher order acoustic variable interpolation functions, QLQ and QQQ elements perform better than QLC and QLL elements.

Calculated acoustic modes of the rigid wall cavity are given in Table 6.2. An acoustic mode is estimated using SPL and phase response data. At an acoustic mode, as it can be observed from Figure 6.4, a peak SPL response and a zero degree phase pair occur. BE results in Table 6.2 are obtained using 0.1 Hz frequency resolutions in computations.

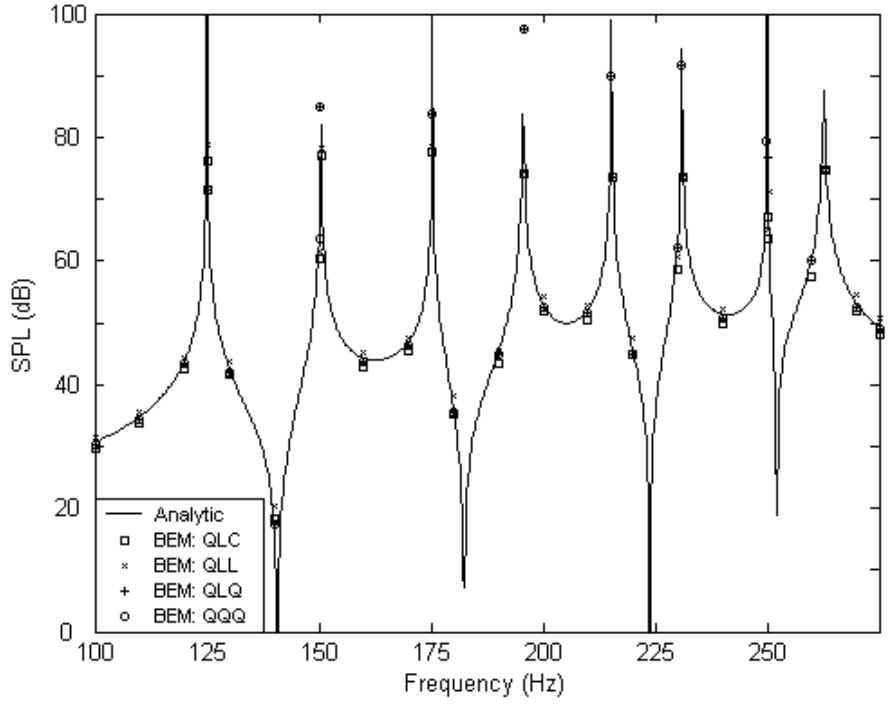

(a)

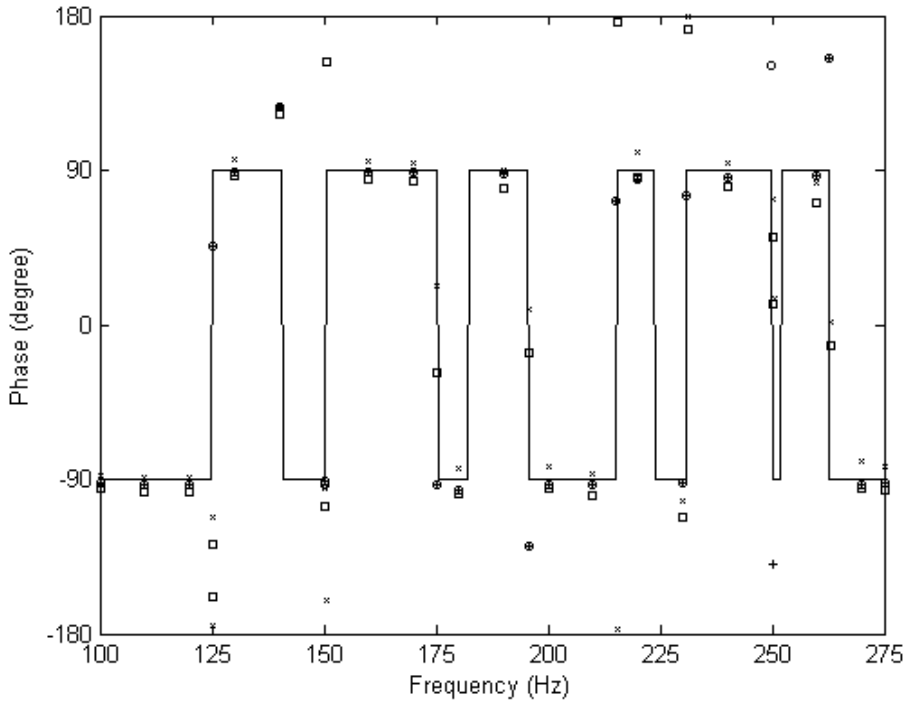

(b)

Figure 6.4 Rigid wall enclosure response: (a) SPL, (b) Phase

Table 6.2 Rigid wall cavity modes

Mode (n)	Analytical modes (Hz)	BE modes (Hz)			
		QLC	QLL	QLQ	QQQ
1	125.0	125.2	125.2	125.0	125.0
2	150.4	150.6	150.6	150.4	150.4
3	175.3	175.4	175.4	175.2	175.2
4	195.6	195.8	196.0	195.6	195.6
5	215.3	215.4	215.6	215.2	215.2
6	231.0	231.2	231.2	231.0	231.0
7	250.0	250.4	250.6	250.0	250.0
8	262.6	263.0	263.2	262.6	262.6

For this case study, interior acoustic pressure and particle velocity solutions at the cavity cross-section $x_3 = c/2$ are also monitored. Results of BE analysis, using a refined surface mesh with QLQ BE patches yielding a total of 1944 acoustic variable nodes, are compared to the analytical results using equations 6.1 and 6.2. Figure 6.5 illustrates the interior acoustic pressure contours and projection of normalized particle velocity vectors at 195 Hz which is a frequency point close to the fourth acoustic mode (195.6 Hz).

Illustrated results of BE analysis and analytical solutions reveal that at the frequency point close to the cavity acoustic resonance, analyses are in moderate agreement. Differences are noticeable in the illustrated pressure contours shown in Figure 6.5. However, in this figure, directional information of illustrated velocity vectors is in good agreement since projection of the normalized acoustic particle velocity vectors at the cavity cross-section are plotted. BE analysis results could be further improved by using a refined analysis with increased number of numerical integration points and reduced error tolerance for the solutions.

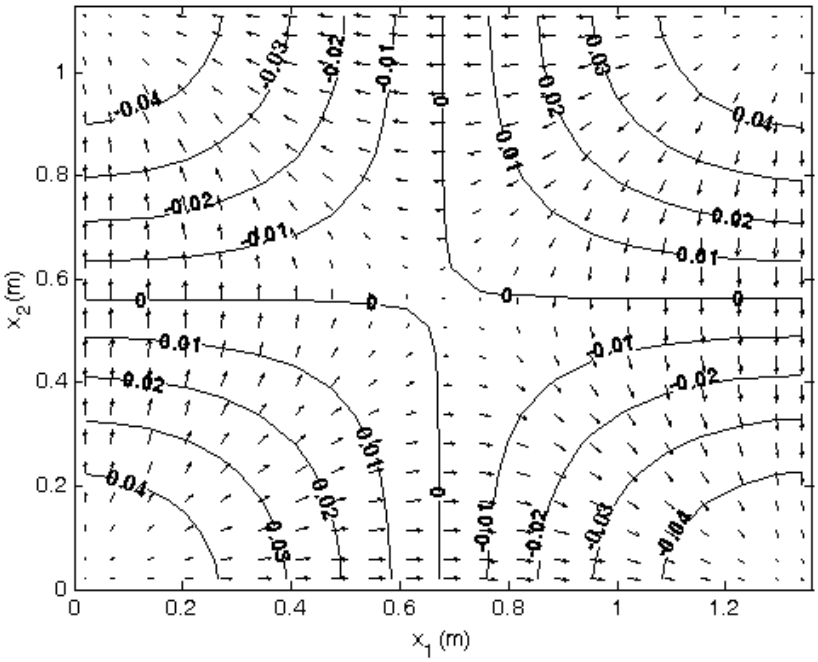

(a)

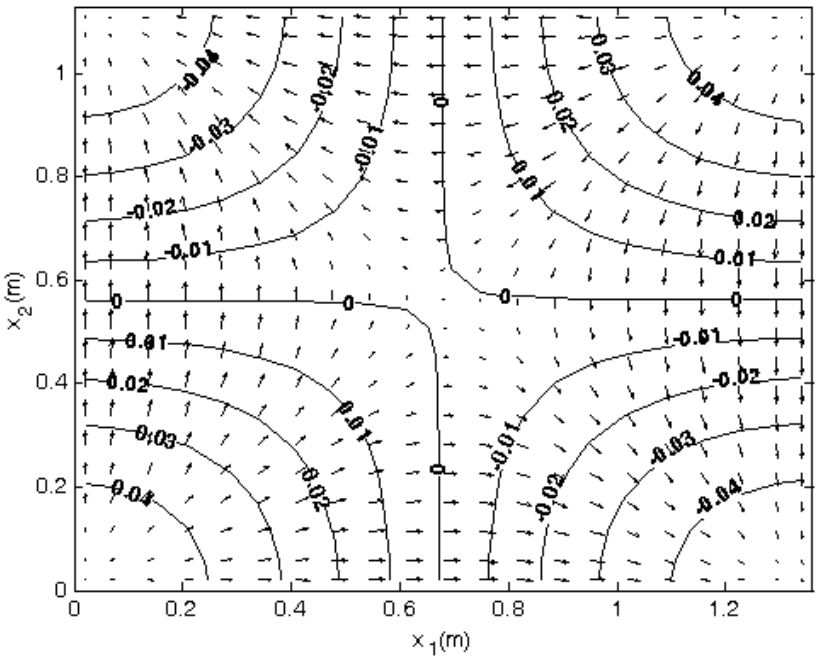

(b)

Figure 6.5 Interior acoustic field (pressure contours and particle velocity vectors) at cross-section $x_3 = c/2$ and at frequency 195 Hz: (a) analytical, (b) BEM

6.2.1.2 Case Study 2: Pulsating Sphere

In the second case study, a pulsating sphere is considered. The elastic surface of the sphere pulsates harmonically with a uniform radial velocity. The analytical solution for acoustic pressure is [14, 62]

$$\hat{p}(r) = \rho_o c_o \hat{v}\left(\frac{a}{r}\right)\left(\frac{ika}{1+ika}\right)e^{-ik(r-a)} \tag{6.3}$$

where r is the radial distance measured from the center of the sphere, a is the radius of the sphere and $\hat{v}$ is the amplitude of surface velocity.

The surface of the sphere is modeled by triangular BE patches, namely, TLC, TLL, TLQ and TQQ elements. Although this case study posseses geometric and acoustic field symmetry, total sphere surface is considered in the BE analysis. A sphere with 1 m radius is chosen. Figure 6.6 illustrates surface mesh for the case of 200 TLL elements. Acoustic pressure on the pulsating boundary surface is obtained by BE analysis and compared to the analytical solution given in equation 6.3. Comparative results are listed in Table 6.3 for five wave numbers. BE results are obtained by evaluating arithmetic average of surface nodal solutions. Results indicate good performance of the triangular elements. For this case study, use of quadratic geometric interpolation functions is advantageous in modeling the curved boundary surface.

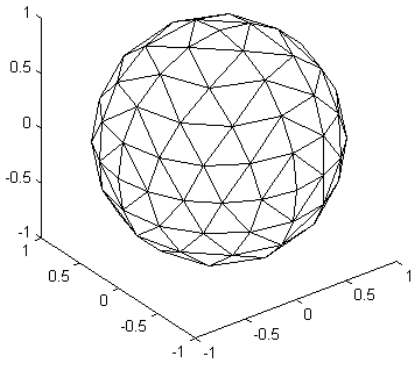

Figure 6.6 A typical surface mesh used in the pulsating sphere study

Table 6.3 Comparative results for pulsating sphere study

k	Analytical solution $\hat{p}(a)/(\rho_o c_o \hat{v})$	BEM solution			
		512 TLC elements	200 TLL elements	200 TLQ elements	72 TQQ elements
1	0.5000+0.5000i	0.4974+0.5022i	0.4936+0.5049i	0.4935+0.5076i	0.4997+0.5004i
2	0.8000+0.4000i	0.7981+0.4043i	0.7967+0.4097i	0.7994+0.4168i	0.7997+0.4005i
3	0.9000+0.3000i	0.8820+0.3012i	0.8756+0.3067i	0.9043+0.3222i	0.8960+0.2963i
4	0.9412+0.2353i	0.9465+0.2424i	0.9532+0.2486i	0.9495+0.2596i	0.9421+0.2373i
5	0.9615+0.1923i	0.9620+0.1997i	0.9652+0.2065i	0.9739+0.2203i	0.9607+0.1937i

6.2.2 BE-FE Acoustic Field Analysis

This section presents applications of the BE-FE method to analyze sound-structure interaction problems. Presented case studies include a selection from those cases analyzed analytically in Chapter 5. Furthermore, additional case studies involving more complex interaction mechanisms are presented.

6.2.2.1 Case Study 3: Cavity Backed by One Plate

First, computational analysis of the cavity-backed-plate case study presented in Chapters 4 and 5 is given. The configuration for the cavity backed by one plate study is illustrated in Figure 6.7. Table 6.4 lists the properties of the analysis domain. Figure 6.7 illustrates that uniform external pressure (P^E) excites the elastic wall of the cavity. This elastic wall is modeled as a simply-supported plate where full acoustic-structure interaction is considered while rest of the walls of the cavity are assumed to be rigid. Cavity is referred to a Cartesian coordinate system $\underline{x} = (x_1, x_2, x_3)$ located at a corner as shown in the Figure 6.7.

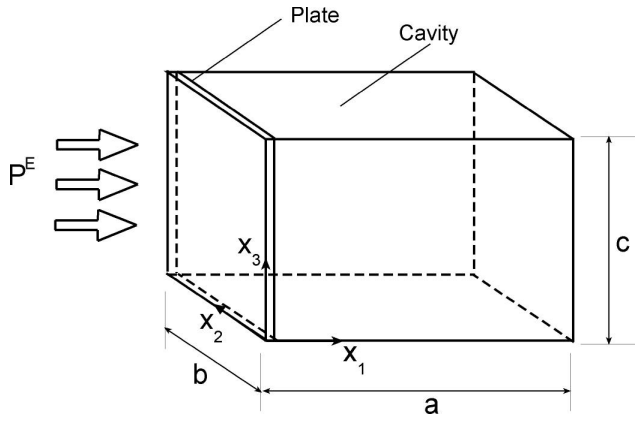

Figure 6.7 Cavity backed by one plate configuration

Table 6.4 Properties of cavity backed by one plate configuration

Cavity	Acoustic field	Plate
a = 0.2 m b = 0.2 m c = 0.2 m	fluid: air equilibrium density: $\rho_o = 1.21$ kg/m^3 speed of sound: $c_o = 340$ m/s response location: $\underline{x} = (a, b/2, c/2)$	material: brass density: $\rho = 8500$ kg/m^3 elasticity modulus: E = 104 GPa Poisson's ratio: $\nu = 0.37$ loss factor: $\eta = 0$ thickness: h = 0.9144 mm lateral dimensions: 0.2 m by 0.2 m

Boundary surface is modeled by BEM using 150 QLQ elements and plate is modeled by FEM using 25 rectangular plate elements. As described in Chapter 2, boundary surface is considered to be composed of two regions. One is the rigid part and the other is the remaining elastic boundary. BE equations can be written as

$$\begin{bmatrix}\mathbf{H}^0 & \mathbf{H}^1\end{bmatrix}\begin{bmatrix}\mathbf{p}^0 \\ \mathbf{p}^1\end{bmatrix} = \begin{bmatrix}\mathbf{G}^0 & \mathbf{G}^1\end{bmatrix}\begin{bmatrix}\mathbf{v}^0 \\ \mathbf{v}^1\end{bmatrix} + \mathbf{f} \tag{6.4}$$

where nodal variables associated with the rigid and elastic regions are indicated by superscripts 0 and 1, respectively. The BE matrices are partitioned according to this nodal classification. **H** and **G** are the acoustic pressure and the velocity influence matrices, respectively, and **f** is the excitation vector due to compact acoustic sources.

On the boundary surface, the acoustic particle normal velocity (**v**) related to the surface normal velocity ($\mathbf{v}_s$) and the acoustic pressure (**p**) through

$$\begin{bmatrix}\mathbf{v}^0 \\ \mathbf{v}^1\end{bmatrix} = \begin{bmatrix}\mathbf{v}_s^0 \\ \mathbf{v}_s^1\end{bmatrix} + \begin{bmatrix}\mathbf{Y}^0 & \mathbf{0} \\ \mathbf{0} & \mathbf{Y}^1\end{bmatrix}\begin{bmatrix}\mathbf{p}^0 \\ \mathbf{p}^1\end{bmatrix} \tag{6.5}$$

where **Y** denotes the diagonal admittance matrix.

FE equations for the elastic plate are

$$\mathbf{D}_s\mathbf{u} = \mathbf{f}_a + \mathbf{f}_e \tag{6.6}$$

where $\mathbf{D}_s$ is the structure dynamic matrix, $\mathbf{u}$ is the plate normal displacement vector, $\mathbf{f}_a$ is the load vector on the plate due to interior acoustic pressure $\mathbf{p}^1$ and $\mathbf{f}_e$ is the load vector on the plate due to external excitation.

On the elastic plate, interface conditions relating load on the plate to interior acoustic pressure, and acoustic normal velocity $\mathbf{v}_s^1$ to plate normal displacement are

$$\mathbf{f}_a = \mathbf{T}\mathbf{p}^1 \tag{6.7}$$

and

$$\mathbf{v}_s^1 = \mathbf{L}\mathbf{u} \tag{6.8}$$

where $\mathbf{T}$ and $\mathbf{L}$ are the coupling matrices.

Combining equations 6.4 and 6.6 in view of equations 6.5, 6.7 and 6.8,

$$\begin{bmatrix} \mathbf{H}^0 - \mathbf{G}^0\mathbf{Y}^0 & \mathbf{H}^1 - \mathbf{G}^1\mathbf{Y}^1 & -\mathbf{G}^1\mathbf{L} \\ \mathbf{0} & -\mathbf{T} & \mathbf{D}_s \end{bmatrix} \begin{bmatrix} \mathbf{p}^0 \\ \mathbf{p}^1 \\ \mathbf{u} \end{bmatrix} = \begin{bmatrix} \mathbf{G}^0\mathbf{v}_s^0 + \mathbf{f} \\ \mathbf{f}_e \end{bmatrix} \tag{6.9}$$

For this case study, there is no compact acoustic source, hence, $\mathbf{f} = \mathbf{0}$. With no sound absorptive treatment, admittance matrices are $\mathbf{Y}^0 = \mathbf{0}$ and $\mathbf{Y}^1 = \mathbf{0}$. On rigid surfaces, the boundary conditions are $\mathbf{v}^0 = \mathbf{0}$ and $\mathbf{v}_s^0 = \mathbf{0}$.

Equation 6.9 is the mixed-variable formulation of this study. Structural-variable-formulation might be preferred due to reduced sizes of system matrices. Due to reasonable matrix sizes, solution of equation 6.9 is preferred in the BE-FE analysis.

Figure 6.8 comparatively illustrates the SPL (SPL = 20 log (P^E/P)) and phase at response location obtained by BE-FE analysis and the developed analytical solution presented in Chapter 4. Results of the BE-FE analysis and analytical solution are in good agreement.

Next, the same cavity-backed-plate configuration but with sound absorptive treatment on the interior plate surface is considered. Properties of this modified configuration are given in Table 6.4. The absorptive treatment is modeled by taking the locally reacting admittance condition as $Y = (\alpha f/\rho_o c_o)e^{i\theta}$ [94, 95]. Figure 6.9 illustrates the results for SPL (SPL = 20 log (P^E/P)) and phase at response location using admittance parameter values of $\alpha = 4/10000$ and $\theta = 80°$. The results obtained by BE-FE analysis and analytical solutions are in good agreement.

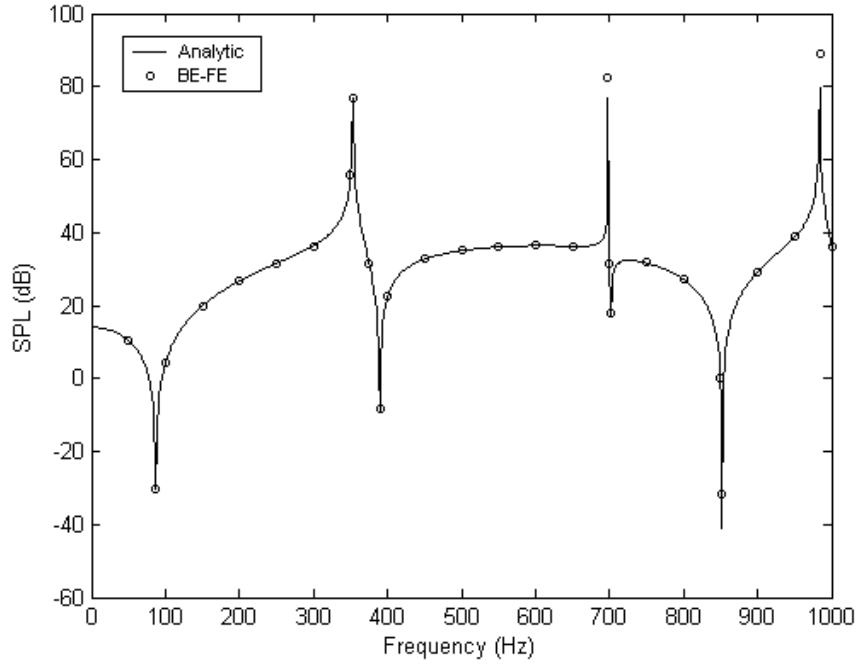

(a)

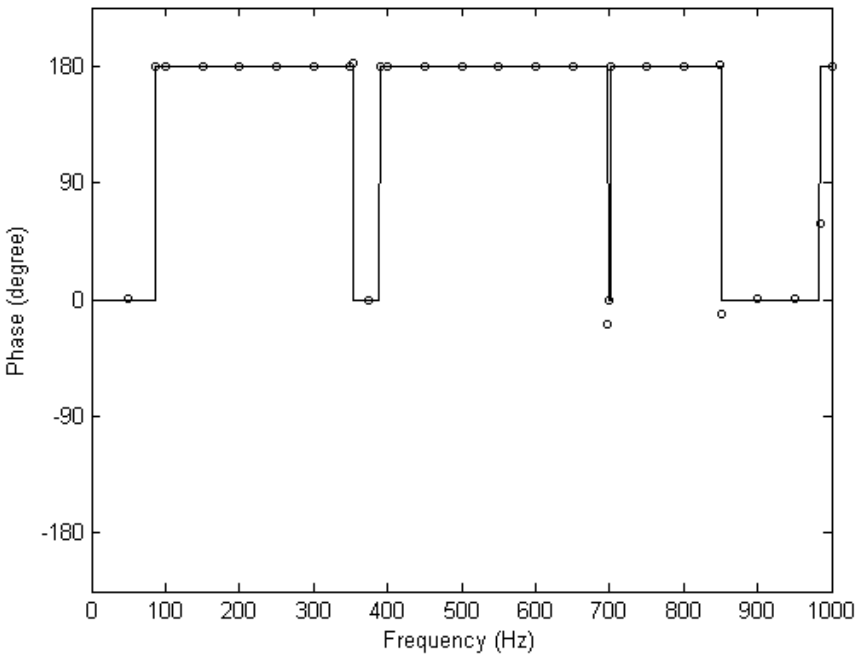

(b)

Figure 6.8 Cavity-backed-plate response: (a) SPL, (b) Phase

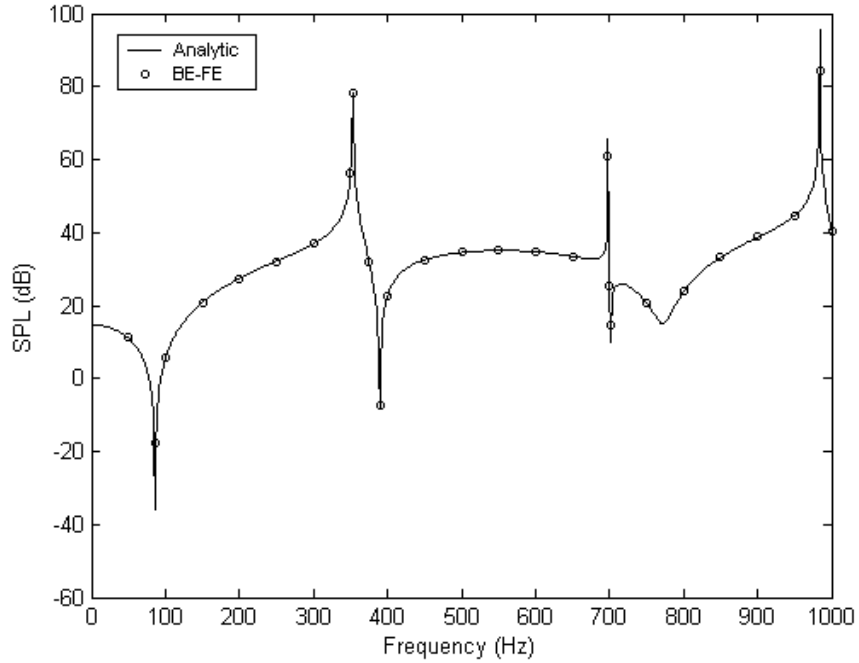

(a)

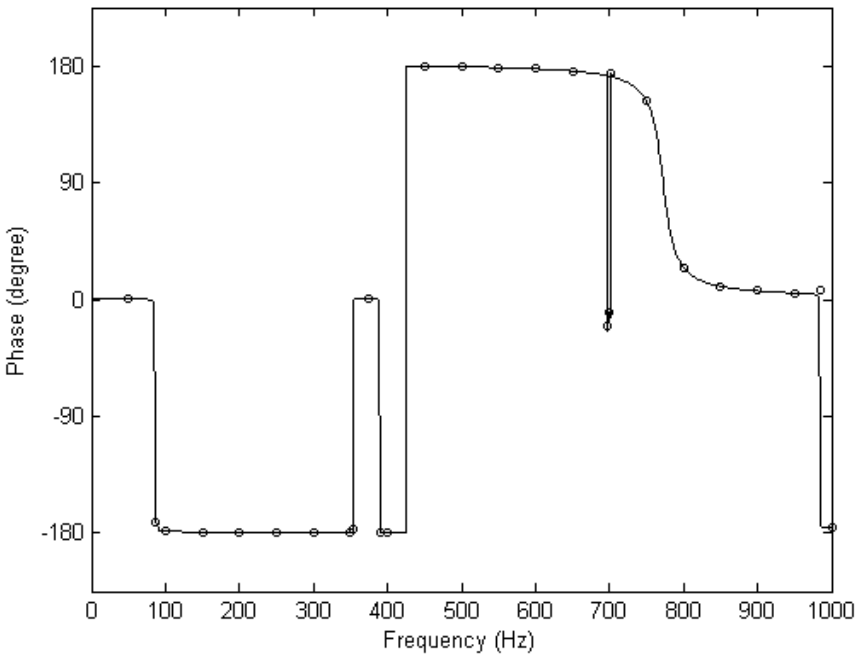

(b)

Figure 6.9 Cavity-backed-plate response with sound absorptive treatment: (a) SPL, (b) Phase

6.2.2.2 Case Study 4: Cavity Backed by Two Plates

This case study illustrates the effect of introducing another elastic plate to the cavity backed by one plate configuration. This second plate is also simply-supported and located parallel to the first plate constitutes the wall opposing to the first plate. Figure 6.10 illustrates this modified configuration.

BE-FE equations for the two interacting plate case is similar to the cavity backed by a single plate study. However, addition of the second plate needs to be accounted in the formulation. Using previous notations of the cavity backed by one plate study, BE equations can be written as

$$\begin{bmatrix}\mathbf{H}^0 & \mathbf{H}^1 & \mathbf{H}^2\end{bmatrix}\begin{bmatrix}\mathbf{p}^0\\ \mathbf{p}^1\\ \mathbf{p}^2\end{bmatrix}=\begin{bmatrix}\mathbf{G}^0 & \mathbf{G}^1 & \mathbf{G}^2\end{bmatrix}\begin{bmatrix}\mathbf{v}^0\\ \mathbf{v}^1\\ \mathbf{v}^2\end{bmatrix}+\mathbf{f} \tag{6.10}$$

where superscript 2 is used to indicate the association of related variables with the second plate.

FE equations for the two plates are

$$\begin{aligned}\mathbf{D}_s^1\mathbf{u}^1&=\mathbf{f}_a^1+\mathbf{f}_e^1\\ \mathbf{D}_s^2\mathbf{u}^2&=\mathbf{f}_a^2+\mathbf{f}_e^2\end{aligned} \tag{6.11}$$

and interface conditions are

$$\begin{aligned}\mathbf{f}_a^1&=\mathbf{T}^1\mathbf{p}^1\\ \mathbf{f}_a^2&=\mathbf{T}^2\mathbf{p}^2\end{aligned} \tag{6.12}$$

and

$$\begin{aligned}\mathbf{v}^1\mathbf{L}^1&=\mathbf{u}^1\\ \mathbf{v}^2\mathbf{L}^2&=\mathbf{u}^2\end{aligned} \tag{6.13}$$

When BE and FE equations 6.10 and 6.11 are written together, in view of equations 6.12 and 6.13,

$$\begin{bmatrix}\mathbf{H}^0 & \mathbf{H}^1 & \mathbf{H}^2 & -\mathbf{G}^1\mathbf{L}^1 & -\mathbf{G}^2\mathbf{L}^2\\ \mathbf{0} & -\mathbf{T}^1 & \mathbf{0} & \mathbf{D}_s^1 & \mathbf{0}\\ \mathbf{0} & \mathbf{0} & -\mathbf{T}^2 & \mathbf{0} & \mathbf{D}_s^2\end{bmatrix}\begin{bmatrix}\mathbf{p}^0\\ \mathbf{p}^1\\ \mathbf{p}^2\\ \mathbf{u}^1\\ \mathbf{u}^2\end{bmatrix}=\begin{bmatrix}\mathbf{G}^0\mathbf{v}^0+\mathbf{f}\\ \mathbf{f}_e^1\\ \mathbf{f}_e^2\end{bmatrix} \tag{6.14}$$

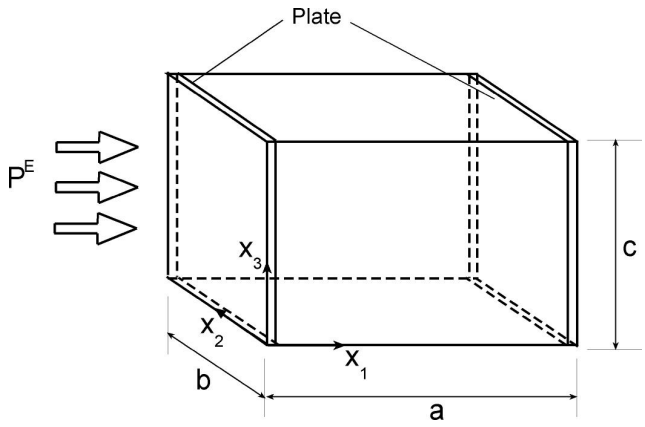

Figure 6.10 Cavity-backed by two plates configuration

For this case study, configuration properties are as listed in Table 6.4, both plates have identical properties, and $\mathbf{f} = \mathbf{0}$, $\mathbf{f}_e^2 = \mathbf{0}$, $\mathbf{v}^0 = \mathbf{0}$ in equation 6.14. Figure 6.11 shows results for SPL (SPL = 20 log (P^E/P)) and phase at response location. BE-FE analysis results are obtained by solving equation 6.14. Analytical solution for this case study is available in literature [73, 79]. The illustrated analytical results are obtained as described in Chapter 4. Results of BE-FE analysis and analytical solution are in good agreement. Furthermore, it is observed that introduction of the second plate produced a noticeable effect only near the first coupled mode of the cavity backed by a single plate study. For this study coupled modes are found at frequencies 77 Hz, 95 Hz, 390 Hz, 701 Hz, 854 Hz.

It should be noted that in cavity-backed by plate(s) case study configurations only out-of-plane (normal to plate surface) structure displacements need to be considered. In the next case study both in-plane and out-of-plane motion of an elastic structure interacting with interior acoustic field of a cavity is considered. This type of structural behavior may be found in many practical engineering applications.

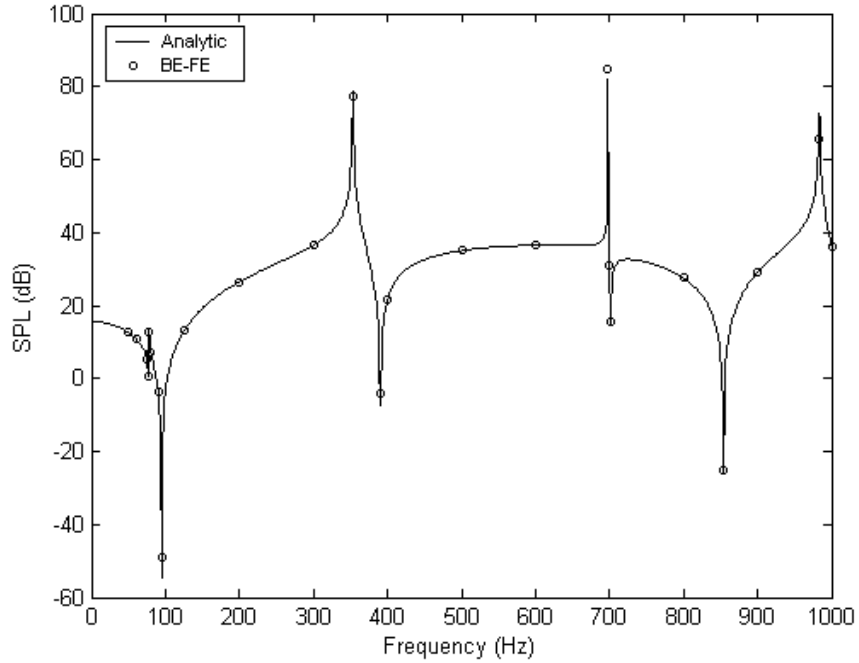

(a)

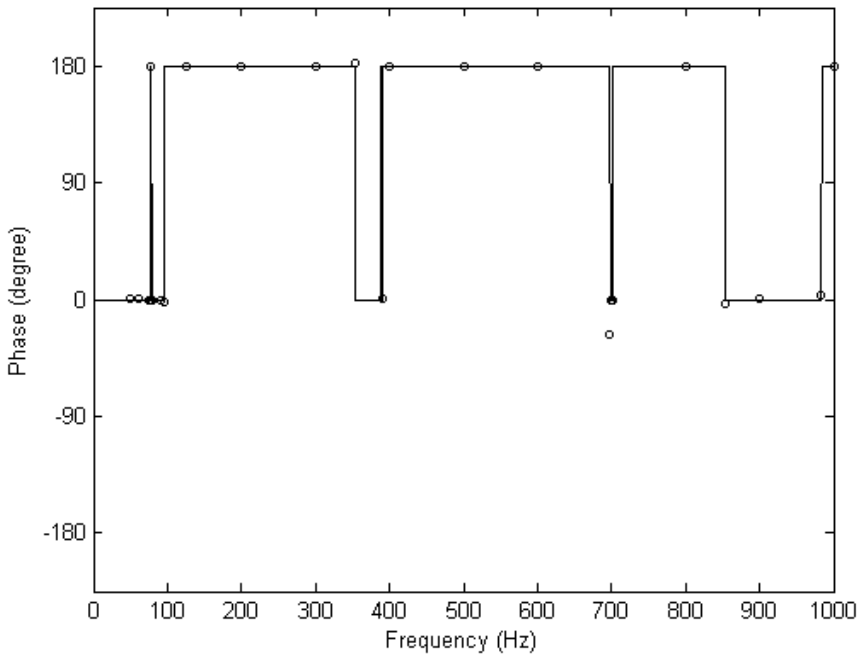

Figure 6.11 Cavity-backed by two plates response: (a) SPL, (b) Phase

6.2.2.3 Case Study 5: Cavity with L-shaped Folded Plate

The configuration used in this study involves a parallelepiped cavity with rigid wall boundary surface except an L-shaped elastic region as illustrated in Figure 6.12. A compact acoustic source in the cavity excites the coupled system. Configuration properties for this study is given in Table 6.1 except addition of an L-shaped folded steel plate structure with properties: $\rho = 7850$ kg/m^3, h = 1.21 mm, E = 207 GPa, ν = 0.3 and $\eta = 0$ and response location is $\underline{x}$ = (a-0.15, b/2, c-0.15). The dimensions of the L-shaped folded plate are: width is 215 mm and segment lengths from 90° fold line are 280 mm and 428 mm. Short side of the L-shaped structure forms the elastic boundary of the cavity wall at $x_1 = 1.36$ m and long side lies on the $x_3 = 0.97$ m face of the cavity. The folded plate is centered on the symmetry line $x_2 = 0.565$ m. Nodal displacements along the peripheral boundary of the L-shaped plate are set to zero (fixed boundary condition). Uncoupled modes of L-shaped plate with free and fixed boundary conditions are listed in Table 6.5. For comparison, Table 6.5 includes modes for the free boundary condition case found in literature [92].

Table 6.5 Uncoupled L-shaped folded plate modes

Calculated plate modes (Hz)		Free plate modes (Hz) [92]	
Fixed	Free	Measured	Calculated
161.92	10.70	10.49	10.73
186.45	24.76	25.24	24.85
209.45	32.70	32.24	32.99
286.08	38.28	36.44	38.80

This case study is analyzed by the BE-FE method. Boundary surface is modeled with 968 TLC BE patches and the elastic plate is modeled with 168 triangular shell FE patches as illustrated in Figure 6.13. Figure 6.14 illustrates BE-FE analysis results for SPL (SPL = 20 log (P/P_{ref}) dB, Pref=20 μPa) and phase response together

with rigid wall analytical solutions. The coupled modes at frequencies 160.5 Hz, 187.0 Hz and 208.8 Hz are originated by the folded plate. It is observed that, introduction of the folded plate structure modifies rigid wall acoustic cavity modes slightly. First plate mode yielded the most noticeable effect on the acoustic field.

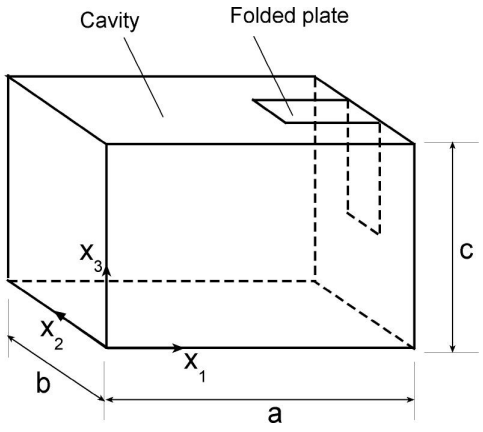

Figure 6.12 Configuration of a cavity with a L-shaped elastic region

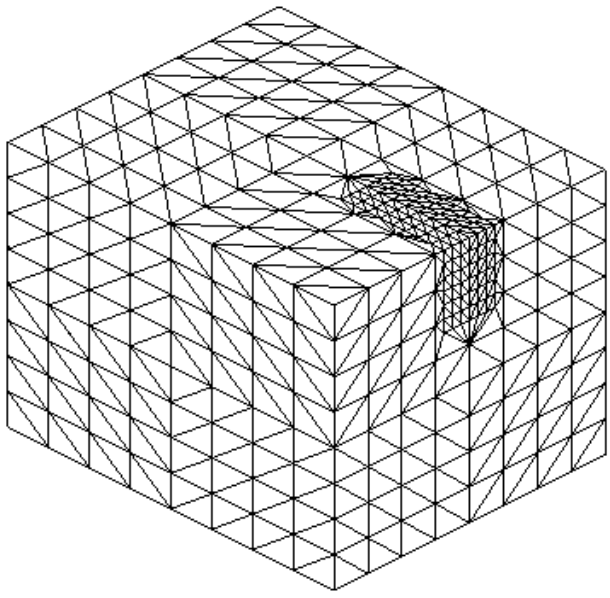

Figure 6.13 Mesh used for the cavity with a L-shaped elastic region

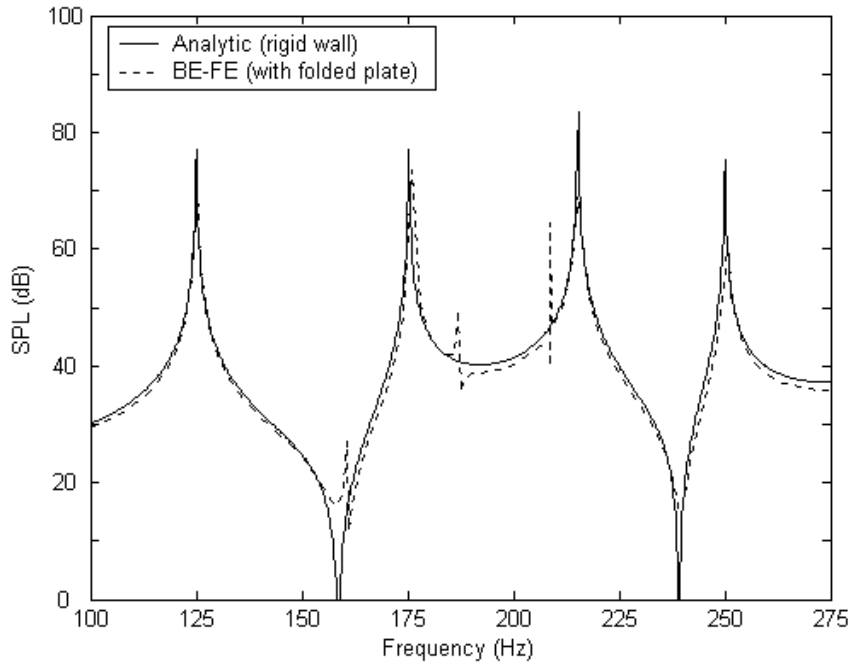

(a)

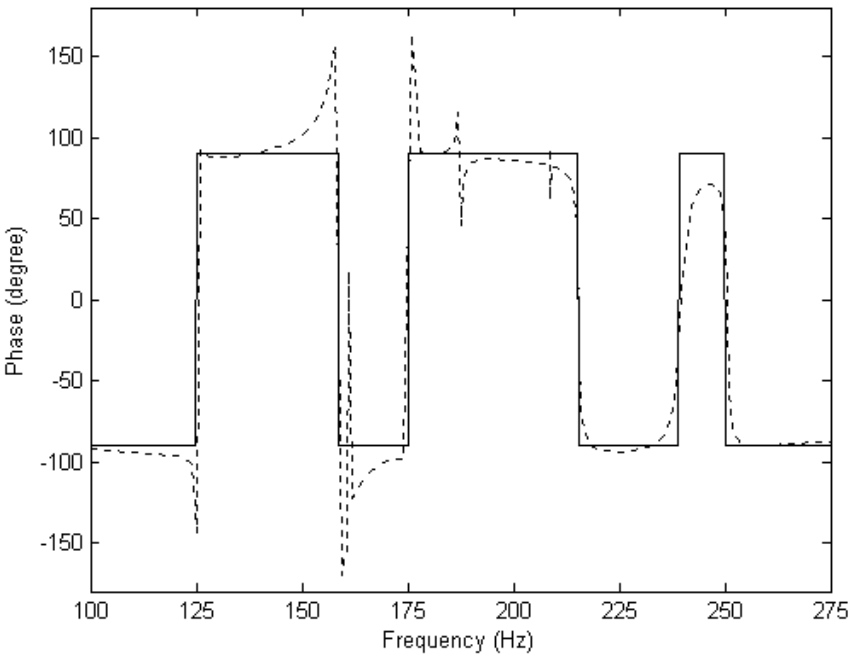

(b)

Figure 6.14 Response of the cavity with folded plate region: (a) SPL, (b) Phase

6.2.3 Cavity-Helmholtz Resonator Interaction Analysis

In this section modification of acoustic response of a rigid-walled parallelepiped cavity by Helmholtz resonators is analyzed.

6.2.3.1 Case Study 6: Single-Domain BE Analysis

The configuration for cavity and resonator coupling is illustrated in Figure 6.15. The cavity and acoustic field properties are same as those given in Table 6.1. The uncoupled acoustic modes of the rigid wall cavity are listed in Table 6.6.

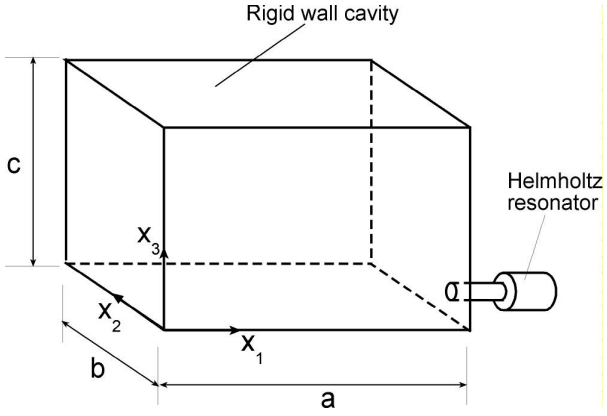

Figure 6.15 Cavity and Helmholtz resonator coupling

Table 6.6 Acoustic modes of rigid wall cavity

Mode	Modal index			Frequency (Hz) (analytical)	Mode type
n	n_1	n_2	n_3		
1	1	0	0	125.0	axial
2	0	1	0	150.4	axial
3	0	0	1	175.3	axial
4	1	1	0	195.6	tangential
5	1	0	1	215.3	tangential
6	0	1	1	231.0	tangential
7	2	0	0	250.0	axial
8	1	1	1	262.6	oblique

Helmholtz resonator considered in this study has a hollow cylindrical geometric shape as illustrated in Figure 6.16. In this figure, resonator volume (V), resonator cavity height (h), neck cross-section area (S), neck length (L), neck radius (r) and cavity radius (R) are indicated. Denoting acoustic wavelength by λ, when $\lambda >> L$, $\lambda >> V^{1/3}$ and $\lambda >> S^{1/2}$, the resonator behaves as a lumped single degree of freedom acoustic element. Mass of this lumped element is provided by the fluid in the neck, its stiffness is provided by the acoustic pressure in the resonator cavity, and its resistance is provided by resonator aperture [4]. The resonator frequency is [4]

$$f_o = \frac{c_o}{2\pi}\sqrt{\frac{S}{L_{eff}V}} \tag{6.15}$$

where L_{eff} is the effective neck length of the resonator. For the type of placement as shown in Figure 5.16, the effective neck length is approximated by [4]

$$L_{eff} = L + 1.7r$$

A set of Helmholtz resonators, tuned to uncoupled cavity modes as listed in Table 6.7, are used in this study. The dimensions of the resonators are selected in view of cavity modes listed in Table 6.6 and equation 6.15.

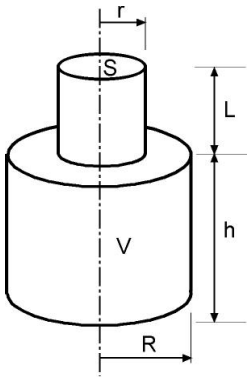

Figure 6.16 Helmholtz resonator geometry

Table 6.7 Properties of resonators

Helmholtz resonator	Resonator dimensions (m) (L: neck length, r: neck radius, R: cavity radius, h: cavity height)				Resonator frequency f_o (Hz)
	L	r	R	h	
HR1	0.05	0.01	0.03	0.31080	125.0
HR2	0.05	0.01	0.03	0.21468	150.4
HR3	0.05	0.01	0.03	0.15802	175.3
HR4	0.05	0.01	0.03	0.12692	195.6
HR5	0.05	0.01	0.03	0.10476	215.3
HR6	0.05	0.01	0.03	0.09100	231.0
HR7	0.05	0.01	0.03	0.07770	250.0
HR8	0.05	0.01	0.03	0.07040	262.6

The cavity and Helmholtz resonators are modeled using QQQ type BE patches. A typical mesh used in BE analysis is illustrated in Figure 6.17. In this figure resonator dimensions are exaggerated to show details.

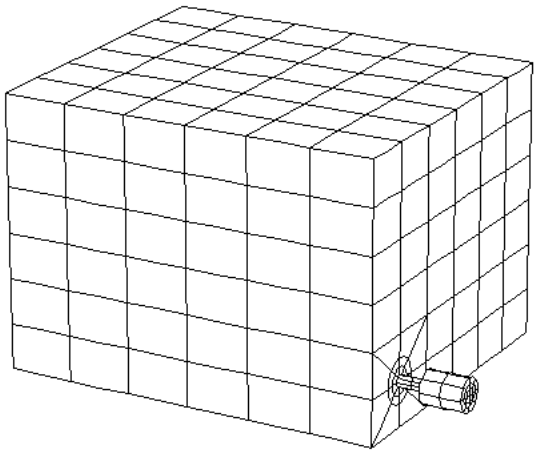

Figure 6.17 Typical mesh used in cavity-resonator interaction study

Interaction of the cavity with each Helmholtz resonator listed in Table 6.7 is analyzed by BEM. Results from the BE analyses are compared to results obtained by a modal method known as method of acoustoelasticity.

Acoustoelasticity is a general theory used to analyze interaction between acoustic pressure field and elastic boundary surface of enclosures [22]. Analysis of cavity and Helmholtz resonator interaction by acoustoelasticity method is also available in literature [83], where lumped idealization of resonator behavior is coupled to cavity modes that are expressed in terms of rigid wall uncoupled acoustic modes. In other words, in modal method of acoustoelasticity a Helmholtz resonator is considered as an acoustic point source.

When a Helmholtz resonator, tuned to an acoustic cavity mode, interacts with cavity, original mode disappears and two new modes arise. These new modes lie on either side of the original uncoupled mode. The separation between the new modes is proportional to the square root of resonator volume to cavity volume ratio. The separation is maximum for oblique modes and minimum for axial modes, and proportional to modal pressure amplitude at the position of the resonator location [81, 82].

In case studies illustrated below, each Helmholtz resonator is positioned individually at location $\underline{x}$ = (a, b/6, c/6) as indicated in Figures 6.15 and 6.17. Resulting modification of the acoustic field due to cavity and resonator interaction is examined by evaluating SPL's, (SPL = 20 log (P/P_{ref}) dB, Pref=20 μPa) at the interior response point.

Comparative SPL results obtained by BE and acoustoelasticity methods are illustrated in Figure 6.18. In this figure, BE results are plotted over a frequency range where rigid wall cavity acoustic field is effectively modified due to cavity and Helmholtz resonator interaction. Analysis results obtained by the modal method of acoustoelasticity are given over the whole frequency range of interest. As can be observed from Figure 6.18, analysis results of each method are in good agreement for each cavity-resonator configuration except those involving HR1 and HR2. Refined BE analyses for these two configurations did not yield noticeable improvements.

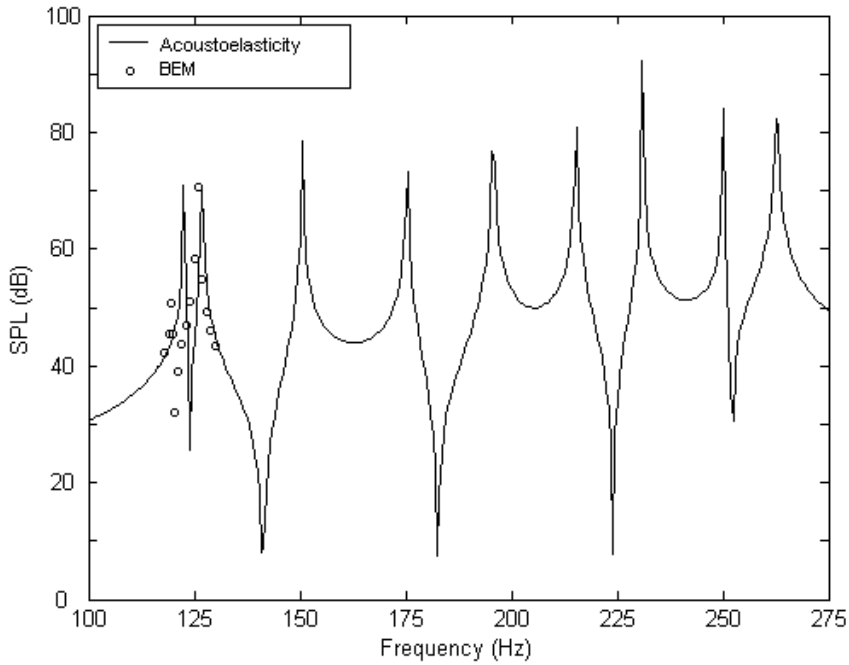

(a)

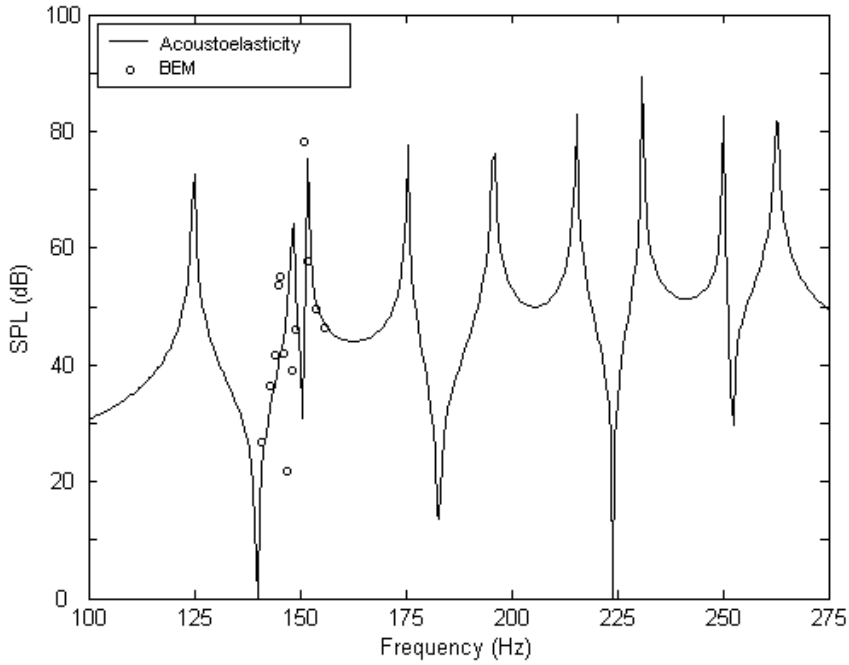

(b)

Figure 6.18 SPL response of cavity coupled to Helmholtz resonator:
(a) HR1, (b) HR2, (c) HR3, (d) HR4, (e) HR5, (f) HR6, (g) HR7, (h) HR8

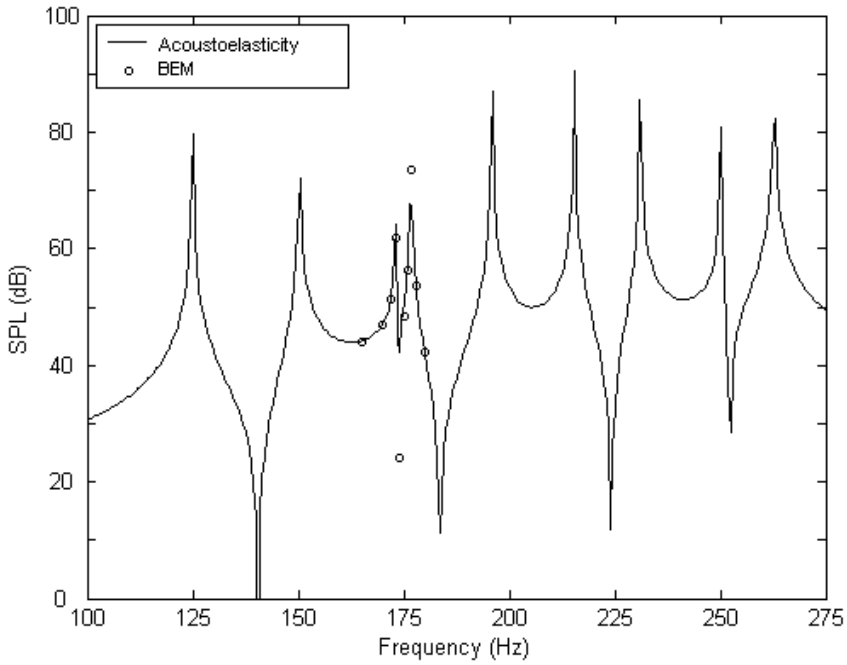

(c)

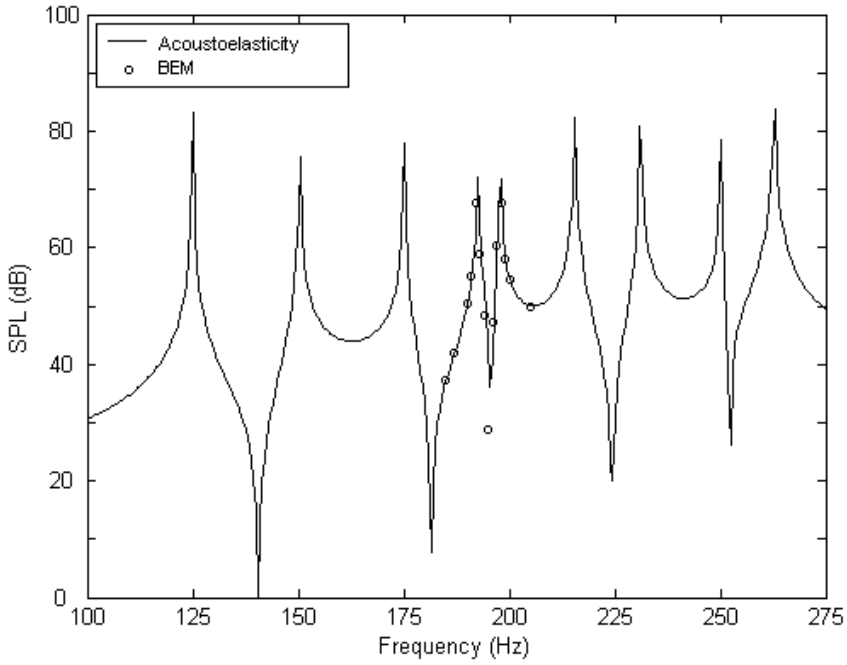

(d)

Figure 6.18 (Continued)

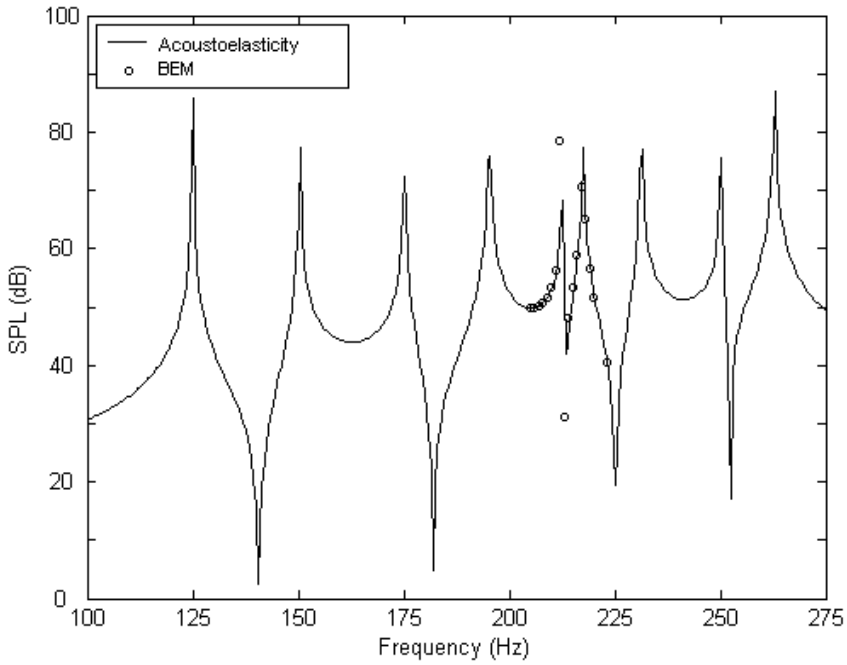

(e)

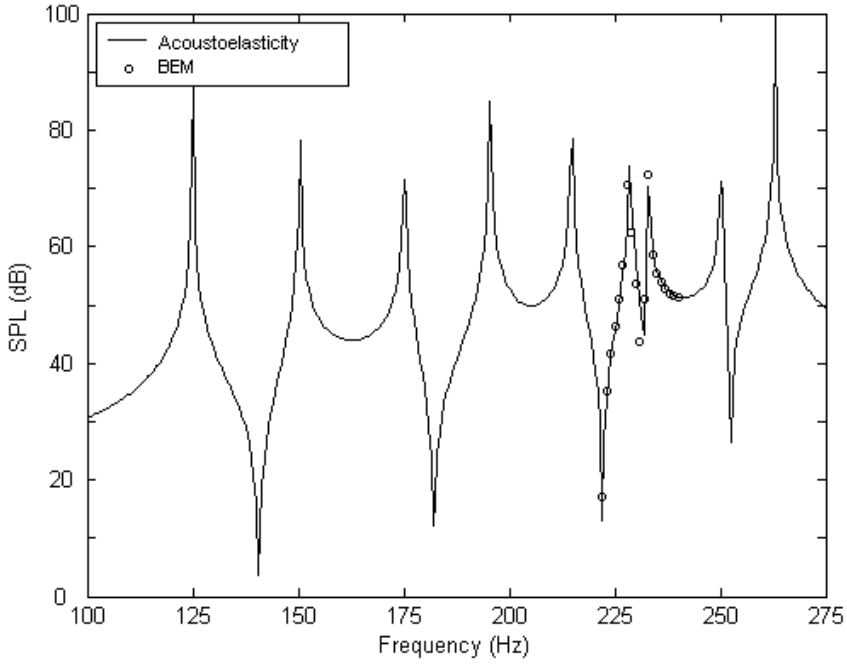

(f)

Figure 6.18 (Continued)

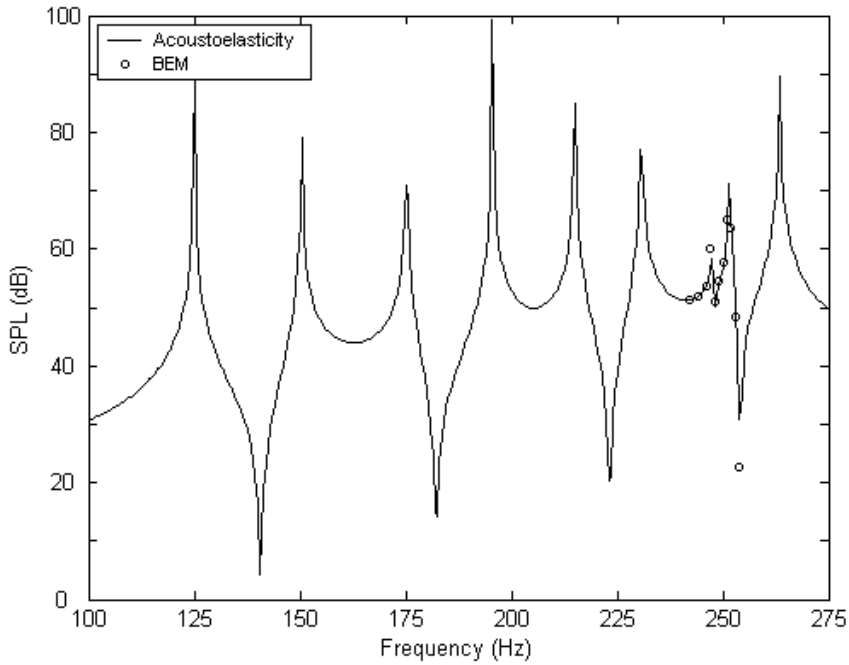

(g)

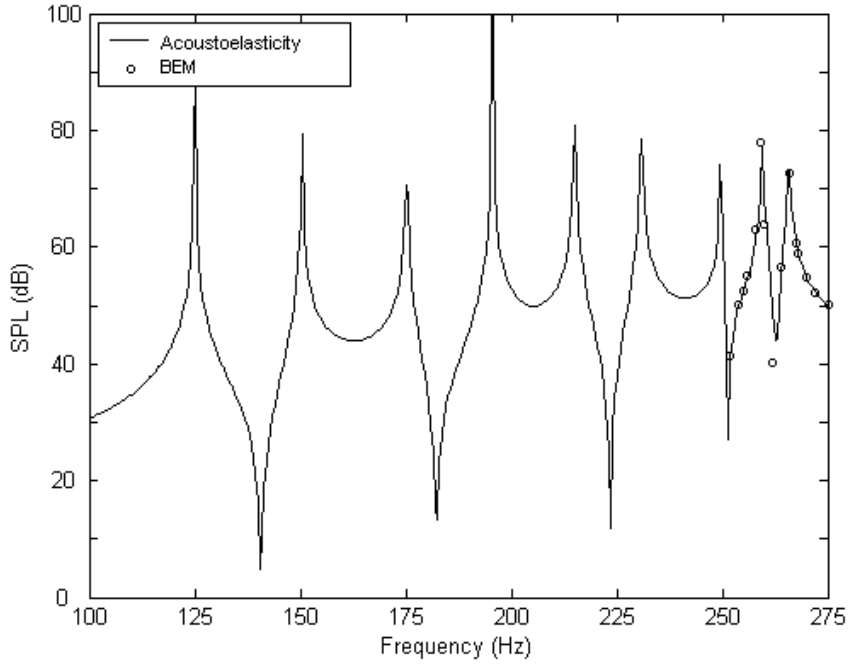

(h)

Figure 6.18 (Continued)

Table 6.8 lists the new modes appearing in the vicinity of original uncoupled acoustic modes due to resonator-cavity interactions (see Figure 6.18).

Table 6.8 Cavity-resonator coupled modes

Original mode (Hz)		New modes (Hz)	
n	Analytical	BEM	Acoustoelasticity
1	125.0	(120, 126)	(122, 127)
2	150.4	(146, 151)	(148, 152)
3	175.3	(173, 177)	(173, 176)
4	195.6	(192, 198)	(192, 198)
5	215.3	(212, 217)	(212, 218)
6	231.0	(228, 233)	(228, 233)
7	250.0	(247, 251)	(248, 252)
8	262.6	(259, 266)	(260, 266)

6.2.3.2 Case Study 7: Multi-Domain BE Analysis

In this case study, a multi-domain BE analysis is utilized in order to investigate the disagreement of analysis results observed in the previous cavity-resonator interaction study. In particular, the case involving HR1 is chosen. Figure 6.19 illustrates the cavity and resonator configuration. In multi-domain BE analysis, initially, cavity and Helmholtz resonator are considered as two separate acoustic domains and then the BE formulations of these two domains are coupled to each other. Addition of interface region between cavity and resonator in multi-domain BE analysis might yield a better computational model for the interaction study.

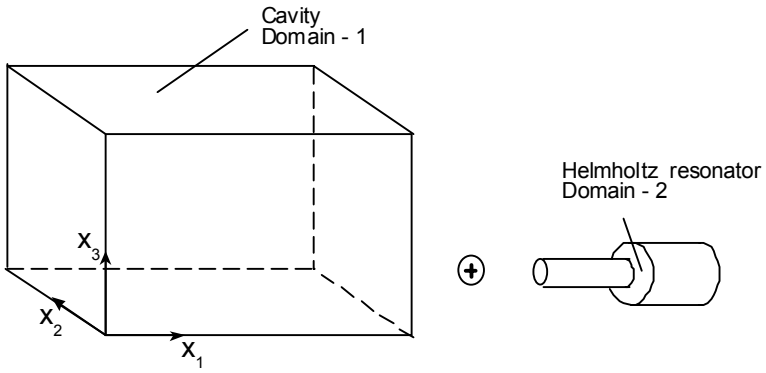

Figure 6.19 Configuration used in multi-domain BE analysis

Results obtained by single-domain and multi-domain BE analyses are illustrated in Figure 6.20. Single-domain and multi-domain analyses yielded similar results. The two new mode pairs, due to cavity-resonator interaction, obtained by single- and multi-domain BE analyses are (120 Hz, 126 Hz) and (119 Hz, 126 Hz), respectively.

Possible reasons for the discrepancy between BE and acoustoelasticity solutions could include the following. In acoustoelasticity method, Helmholtz resonators are approximated as point sources. On the other hand, BE analysis is carried out by modeling the physical geometry of the resonators. Besides, as noted by other researchers [22, 24], in acoustoelasticity method, particle velocity calculations on flexible interaction surfaces are slow in convergence and suffer in accuracy. Furhermore, when Helmholtz resonator cavity height is long compared to neck length, as in the HR1 case, equation 6.15 used in the acoustoelasticity method yields overestimated results [84]. Therefore, lumped parameter idealization used in acoustoelasticity method might not properly model the behavior of the resonator. It should be noted that in all methods modeling errors could be more pronounced at the lower frequency region due to increase in inertial effects compared to those in higher frequency region.

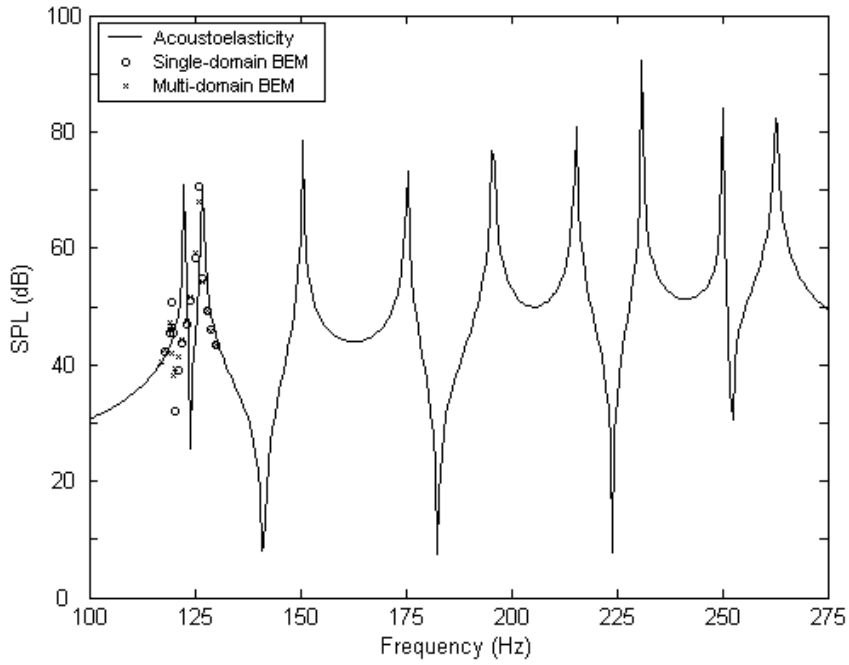

Figure 6.20 SPL response using single-domain and multi-domain BE analysis

6.2.3.3 Case Study 8: Resonator Positioning Effects

The effect of Helmholtz resonator location is investigated as the last case study. Figure 6.21 illustrates three locations where HR3 is positioned. These locations are A = (a, b/6, c/6), B = (a, b/3, c/3) and C = (a, b/2, c/2). Effects of resonator coupling to cavity by changing resonator position are illustrated in Figure 6.22. As can be seen in this figure, both BE and acoustoelasticity analyses are in good agreement, and response of acoustic field is as expected. In other words, when the resonator is positioned at or near an acoustic pressure anti-node of the cavity (i.e., at A or B) cavity-resonator interaction may modify original acoustic field effectively and when it is positioned at or near a pressure node of the cavity (i.e., at C), the effect of the resonator diminishes.

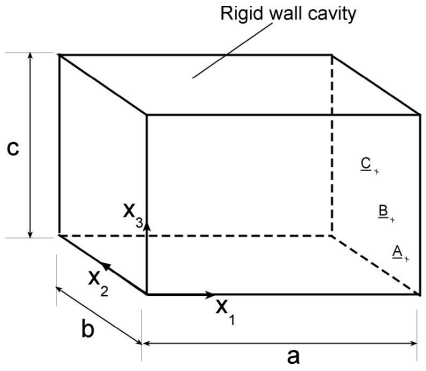

Figure 6.21 Configurations used in resonator position analyses

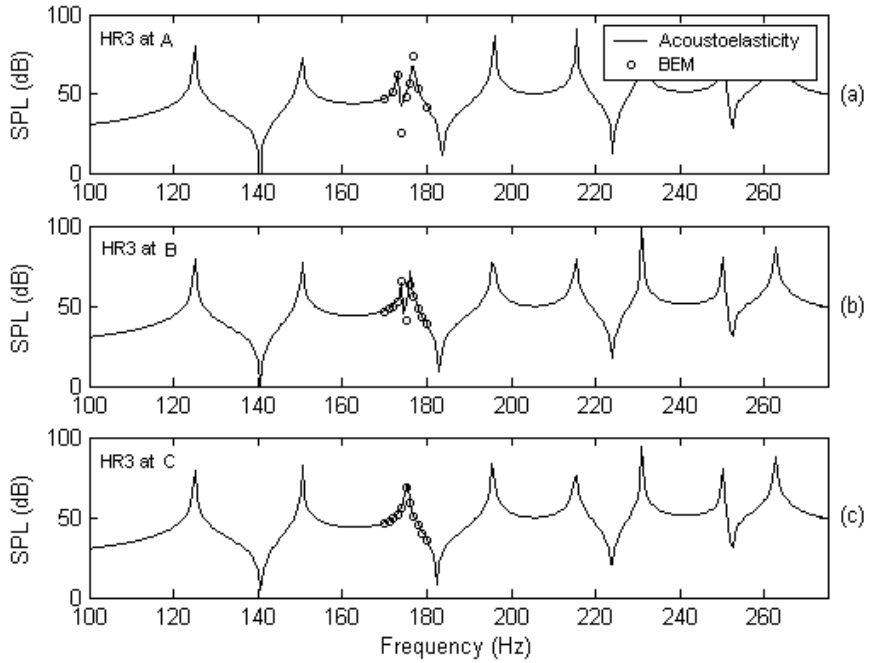

Figure 6.22 Positioning effect of resonator HR3; (a) at A, (b) at B, (c) at C

6.2.4 Overview of Case Studies

Flexibility provided with the BE and the BE-FE methods as given in Chapters 2, 3 and 4 can be utilized to analyze several sound-structure interaction configurations [98-100]. In this section, computational acoustic analyses of a selected set of case studies are given. Presented case studies illustrate acoustic analyses in enclosures

where partial and/or full interaction between acoustic domain(s) and enclosing boundary is considered.

Verification of BE implementation is provided through comparisons of analysis results and analytical solutions for the case studies. In these case studies, it is observed that higher order elements involving quadratic variable interpolation functions used in BE formulation perform better in terms of modeling accuracy. This observation is in agreement with published data about the convergence of BE formulation [96, 97]. A case study was used to illustrate computation of acoustic pressure field and particle velocity within analysis domain using BE acoustic particle velocity formulation [16]. This formulation may be utilized in research studies involving acoustic intensity analysis.

BE-FE analysis of a cavity-backed-plate study with and without sound absorptive treatments are presented. Comparisons of BE-FE analysis results to those obtained by the derived analytical formulation are given. Both analyses yielded good agreement. A case study that involved a rather more complicated sound-structure interaction due to an additional fully interacting boundary to the cavity-backed-plate problem is given. Last case study for BE-FE acoustic analysis involved a more general structural behavior that may be found in many practical applications. Case studies for which BE-FE and developed analytical solutions have been used for acoustic analysis may provide a basis for analytical and experimental research studies in acoustics. BE-FE analysis of the cavity-backed-plate study involving sound absorptive treatment, which is also verified by the derived analytical solution, is a new and unique study that may be utilized in related research studies.

Case studies are given to illustrate acoustic field modification of a rigid wall cavity due to its interaction with a modally tuned Helmholtz resonator. Both BEM and acoustoelasticity methods are utilized to analyze cavity-resonator interaction. In the studied cases, it is observed that results from these methods are in good agreement in most of the frequency range of analysis. Deviations, which are more noticeable at lower frequency region, are quite negligible for most practical engineering applications. Analysis of cavity-resonator interaction by BEM provided an alternative approach to existing modal based approaches [81, 82, 83]. These case

studies can also be utilized as a basis for research studies.

Sound-structure analysis is an active research area with numerous engineering applications. However, essential experimental studies are rare in literature. To this end, the presented fundamental case studies along with the derived analytical, BE and BE-FE formulations could provide a basis for further research in acoustics with special emphasis on sound-structure interaction.

Computation time for acoustic analysis in a sound-structure interaction study depends on several factors that vary with the order of BE or BE-FE system matrices, number of quadrature points used in the numerical evaluation of integrals and error tolerance used in solutions. Computationally most expensive parts of analyses are the construction of the BE matrices at each frequency point of analysis and solution of final BE or BE-FE equations.

CHAPTER 7

DISCUSSION, CONCLUSIONS AND FUTURE WORK

In this thesis, steady-state dynamic sound-structure interaction between coupled acoustic domain(s) with enclosing rigid or elastic boundary is studied. Linear acoustic (inviscid) and elasticity theories are assumed in modeling interactions in frequency domain.

Single- and multi-domain direct BE formulations for acoustic analysis within enclosures are presented. For the enclosing thin plate or shell-like structure, FE formulation is used. Combining these BE and FE formulations, BE-FE method is used to analyze sound-structure interaction problems. Mixed-, structural- and fluid-variable approaches to combine BE and FE equations are considered to model BE-FE sound-structure coupling.

Existing analytical formulations for a fundamental sound-structure interaction problem (cavity-backed-plate problem) are considered to develop an enhanced analytical formulation to include locally reacting sound absorptive treatment on fully coupled interaction surface. Modal and frequency response acoustic analyses of cavity-backed-plate problem with and without sound absorptive treatment are given. Convergence observed in these analyses indicates accurate modeling by this new formulation. In addition, independent BE-FE analyses of cavity-backed-plate problems also supported the accuracy of the developed analytical solution. Coupled modal frequencies obtained by a reduced form of the developed solution (i.e., without sound absorptive treatment) and available experimental data as well as analytical and acoustoelasticity solutions are generally in good agreement. However, discrepancies between experimental data and all other solutions indicate the need for more reliable experimental investigations to the interaction problem. Modifications of interior acoustic field of the coupled cavity-plate system due to sound absorptive treatment and structural damping illustrate that absorptive treatment is more

effective in attenuating acoustic pressure than structural damping.

Acoustic field analysis using BEM can be interpreted as computational acoustic analysis using discrete form of BE integral equations. In this thesis, two families of discontinuous BE patches, namely, triangular and quadrilateral elements, are utilized. These elements provide flexibility in modeling the acoustic domain. A treatment of regular and singular integrals in BE formulation for these elements are given. Rectangular plate and triangular shell elements are used to develop FE models for thin plate or shell-like structures. Consequently, provided BE and BE-FE methods have the flexibility to analyze various interaction configurations.

Acoustic analyses of a wide spectrum of configurations using the derived analytical solution and implemented BE and BE-FE methods are presented comparatively. These configurations involve cavity-boundary and cavity-Helmholtz resonator interactions. Presented case studies illustrate the details of analytical and computational acoustic analyses.

In view of this thesis, a range of analytical, computational and experimental topics can be considered for future research.

The analytical solution developed in this thesis is a contribution to the limited number of analytical solutions to sound-structure interaction problems available in literature. An extension of the derived solution could include double-plate configurations involving sound absorptive treatment.

Regarding computational topics, the following could be investigated: cavity-Helmholtz resonator configurations including multiple coupled resonators with and without sound absorptive treatment; BE acoustic particle velocity computations that might involve acoustic intensity analyses; implementation of axisymmetric BE patches; and, adaptive algorithms considering weak or strong interaction conditions.

The case studies provided in thesis involve basic and widely applicable configurations. It is believed that experimental investigation of these cases would complement the presented analytical and computational studies. Such a combination of theoretical, numerical and experimental work can provide an invaluable basis for benchmark case development in the field of acoustics.

REFERENCES

1. D.T. Blackstock, Fundamentals of Physical Acoustics, J. Wiley & Sons, Inc., USA, 2000.

2. F. Fahy, Sound and Structural Vibration: Radiation, Transmission and Response, Academic Press, G.B, 1985.

3. M. C. Junger, D. Feit, Sound Structures and Their Interaction, MIT Press, USA, 1972.

4. L.E. Kinsler, A.R. Frey, A.B. Coppens, J.V. Sanders, Fundamentals of Acoustics, J. Wiley & Sons, Inc., USA, 1982.

5. P.M. Morse, K.U. Ingard, Theoretical Acoustics, McGraw-Hill, Inc., USA, 1968.

6. P.M. Morse, H. Feshbach, Methods of Theoretical Physics, McGraw-Hill, Inc., USA, 1953.

7. R. Ohayon, C. Soize, Structural Acoustics and Vibration, Academic Press, G.B., 1998.

8. A.D. Pierce, Acoustics: an Introduction to Its Physical Principles and Applications, Acoustical Society of America, USA, 1991.

9. E. Skudrzyk, Foundations of Acoustics: Basic Mathematics and Basic Acoustics, Springer-Verlag, Austria, 1971.

10. L.C. Wrobel, The Boundary Element Method: Vol. 1, Applications in Thermo-Fluids and Acoustics, J. Wiley & Sons, Ltd., G.B, 2002.

11. M.H. Aliabadi, The Boundary Element Method: Vol. 2, Applications in Solids and Structures, J. Wiley & Sons, Ltd., G.B, 2002.

12. C.A. Brebbia, J. Dominguez, Boundary Elements: an Introductory Course, Computational Mechanics Publications, G.B., 1992.

13. M. Bonnet, Boundary Integral Equation Methods for Solids and Fluids, J. Wiley & Sons, Ltd., G.B., 1995.

14. R.D. Ciskowski, C.A. Brebia, Boundary Element Methods in Acoustics, Computatinal Mechanics Publications, U.K., 1991.

15. L. Gaul, M. Kogl, M. Wagner, Boundary Element Methods for Engineers and Scientists: an Introductory Course with Advanced Topics, Springer-Verlag, Germany, 2003.

16. Y. Mengi, Boundary Element Method: Lecture Notes, ES-507, Middle East Technical University, 2003-04.

17. K.J. Bathe, Finite Element Procedures, Prentice Hall, USA, 1996.

18. R.D. Cook, D.S. Malkus, M.E. Plesha, Concepts and Applications of Finite Element Analysis, J. Wiley & Sons, Inc., USA, 1989.

19. M. Petyt, Introduction to Finite Element Vibration Analysis, Cambridge University Press, U.K., 1998.

20. W. Weaver Jr., P.R. Johnston, Structural Dynamics by Finite Elements, Prentice-Hall, Inc., USA, 1987.

21. O.C. Zienkiewicz, The Finite Element Method, McGraw-Hill, Inc., G.B, 1977.

22. E.H. Dowell, G.F. Gorman, D.A. Smith, "Acoustoelasticity: general theory, acoustic natural modes and forced response to sinusoidal excitation, including comparisons with experiment", Journal of Sound and Vibration, Vol. 52, pp. 519-542, 1977.

23. V.B. Bokil, U.S. Shirahatti, “A technique for the modal analysis of sound-structure interaction problems”, Journal of Sound and Vibration, Vol. 210, pp. 243-254, 1998.

24. V. Jayachandran, S.M. Hirsch, J.Q. Sun, “On the numerical modeling of interior sound fields by the modal function expansion approach”, Journal of Sound and Vibration, Vol. 210, pp. 243-254, 1998.

25. G.M.L. Gladwell, G. Zimmermann, “On energy and complementary energy formulations of acoustic and structural vibration problems”, Journal of Sound and Vibration, Vol. 3, pp. 233-241, 1966.

26. G.M.L. Gladwell, “A variational formulation of damped acouto-structural vibration problems”, Journal of Sound and Vibration, Vol. 4, pp. 172-186, 1966.

27. A. Craggs, “The transient response of a coupled plate-acoustic system using plate and acoustic finite elements”, Journal of Sound and Vibration, Vol. 15, pp. 509-528, 1971.

28. T. Shuku, K. Ishihara, “The analysis of the acoustic field in irregularly shaped rooms by the finite element method”, Journal of Sound and Vibration, Vol. 29, pp. 67-76, 1973.

29. M. Petyt, J. Lea, G.H. Koopmann, “A finite element method for determining the acoustic modes of irregular shaped cavities”, Journal of Sound and Vibration, Vol. 45, pp. 495-502, 1976.

30. A. Craggs, G. Stead, “Sound transmission between enclosures – a study using plate and acoustic finite elements”, Acustica, Vol. 55, pp. 89-98, 1976.

31. M. Petyt, S.P. Lim, “Finite element analysis of the noise inside a mechanically excited cylinder”, International Journal for Numerical Methods in Engineering, Vol. 13, pp. 109-122, 1978.

32. T.L. Richards, S.K. Jha, “A simplified finite element method for studying acoustic characteristics inside a car cavity”, Journal of Sound and Vibration, Vol. 63, pp. 61-72, 1979.

33. D.J. Nefske, J.A. Wolf Jr., L.J. Howell, “Structural-acoustic finite element analysis of the automobile passenger compartment: a review of current practice”, Journal of Sound and Vibration, Vol. 80, pp. 247-266, 1982.

34. J. Mackerle, “Some remarks on progress with finite elements”, Computers and Structures, Vol. 55, pp. 1101-1106, 1995.

35. G.C. Everstine, “Finite element formulations of structural acoustic problems”, Computers and Structures, Vol. 65, pp. 307-321, 1997.

36. J. Mackerle, “Fluid-structure interaction problems, finite element and boundary element approaches: a bibliography (1995-1998)”, Finite Elements in Analysis and Design, Vol. 31, pp. 231-240, 1999.

37. W.A. Bell, W.L. Meyer, B.T. Zinn, “Predicting the acoustics of arbitrarily shaped bodies using an integral approach”, American Institute of Aeronautics and Astronautics Journal, Vol. 15, pp. 813-820, 1977.

38. R.J. Bernhard, B.K. Gardner, C.G. Mollo, C.R. Kipp, “Prediction of sound fields in cavities using boundary-element methods”, American Institute of Aeronautics and Astronautics Journal, Vol. 25, pp. 1176-1183, 1987.

39. A. Sestieri, D.D. Vescovo, P. Lucibello, “Structural-acoustic coupling in complex shaped cavities”, Journal of Sound and Vibration, Vol. 96, pp. 219-233, 1984.

40. J.B. Mariem, M.A. Hamdi, “A new boundary finite element method for fluid-structure interaction problems”, International Journal for Numerical Methods in Engineering, Vol. 24, pp. 1251-1267, 1987.

41. R.D. Ciskowski, L.H. Royster, “Boundary element solution to predict steady-state response of a 3-D coupled fluid cavity-elastic structure system”, Noise-Con 88 Proceedings, pp. 579-584, 1988.

42. M. Tanaka, Y. Masuda, “Boundary element method applied to certain structural-acoustic coupling problems”, Computer Methods in Applied Mechanics and Engineering, Vol. 71, pp. 225-234, 1988.

43. S. Suzuki, S. Maruyama, H. Ido, “Boundary element analysis of cavity noise

problems with complicated boundary conditions", Journal of Sound and Vibration, Vol. 130, pp. 79-91, 1989.

44. I.C. Mathews, "Numerical techniques for three-dimensional steady-state fluid –structure interaction", Journal of Acoustical Society of America, Vol. 79, pp. 1317-1325, 1986.

45. R.A. Jeans, I.C. Mathews, "Solution of fluid-structure interaction problems using a coupled finite element and variational boundary element technique", Journal of Acoustical Society of America, Vol. 88, pp. 2459-2466, 1990.

46. C. Rajakumar, A.Ali, S.M. Yunus, "A new acoustic interface element for fluid-structure interaction problems", International Journal for Numerical Methods in Engineering, Vol. 33, pp. 369-386, 1992.

47. G.C. Everstine, F.M. Henderson, "Coupled finite element / boundary element approach for fluid-structure interaction", Journal of Acoustical Society of America, Vol. 87, pp. 1938-1947, 1990.

48. S. Kopuz, N. Lalor, "Analysis of interior acoustic field using the finite element method and the boundary element method", Applied Acoustics, Vol. 45, pp. 193-210, 1995.

49. S. Kopuz, Y.S. Unlusoy, M. Caliskan, "Integrated FEM/BEM approach to the dynamic and acoustic analysis of plate structures", Engineering Analysis with Boundary Elements, Vol. 17, pp. 269-277, 1996.

50. A.F. Seybert, T.W. Wu, W.L. Li, "A coupled FEM/BEM for fluid structure interaction using Ritz vectors and eigenvectors", Transactions of ASME, Vol. 115, pp. 152-158, 1993.

51. C.Y.R. Cheng, A.F. Seybert, T.W. Wu, "A multidomain boundary element solution for silencer and muffler performance prediction", Journal of Sound and Vibration, Vol. 151, pp. 119-129, 1991.

52. T.W. Wu, A. Dandapani, "A boundary element solution for sound transmission through thin panels", Journal of Sound and Vibration, Vol. 171, pp. 145-157, 1994.

53. M.R. Bai, K. Wu, “Free vibration of a thin spherical shell containing a compressible fluid”, Journal of Acoustical Society of America, Vol. 95, pp. 3300-3310, 1995.

54. C.M. Lee, L.H. Royster, R.D. Ciskowski, “Formulation for an FE and BE coupled problem and its application to the earmuff-earcanal system”, Engineering Analysis with Boundary Elements, Vol. 16, pp. 305-315, 1995.

55. C.S. Pates, U.S. Shirahatti, C. Mei, “Sound-structure interaction analysis of composite panels using coupled boundary and finite element methods”, Journal of Acoustical Society of America, Vol. 98, pp. 1216-1221, 1995.

56. A.G. Niyogi, M.K. Laha, P.K. Sinha, “A coupled FE-BE analysis of acoustic cavities confined inside laminated composite enclosures”, International Journal of Aircraft Engineering and Aerospace Technology, Vol. 72, pp. 345-357, 2000.

57. L. Gaul, W. Wenzel, “A coupled symmetric BE-FE method for acoustic fluid-structure interaction”, Engineering Analysis with Boundary Elements, Vol. 26, pp. 629-636, 2002.

58. Q. Huang, T.A. Cruse, “Some notes on singular integral techniques in boundary element analysis”, International Journal for Numerical Methods in Engineering, Vol. 36, pp. 2643-2659, 1993.

59. M. Guiggiani and A. Gigante, “A general algorithm for multidimensional Cauchy principal value integrals in the boundary element method”, Transactions of ASME, Vol. 57, pp. 906-915, 1990.

60. M. Guiggiani, G. Krishnasamy, T.J. Rudolphi, F.J. Rizzo, “A general algorithm for the numerical solution of hypersingular boundary integral equations”, Transactions of ASME, Vol. 59, pp. 604-614, 1992.

61. J.C.F. Telles, “A self-adaptive co-ordinate transformatioin for efficient numerical evaluation of general boundary element integrals”, International Journal for Numerical Methods in Engineering, Vol. 24, pp. 959-973, 1987.

62. J.J. R. Silva, L.C. Wrobel, J.C.F. Telles, “A new family of continuous / discontinous three-dimensional boundary elements with application to acoustic wave propagation”, International Journal for Numerical Methods in

Engineering, Vol. 36, pp. 1661-1679, 1993.

63. E.H. Dowell, H.M. Voss, "The effect of a cavity on panel vibration" American Institute of Aeronautics and Astronautics Journal, Vol. 1, 476-477, 1963.

64. R.H. Lyon, "Noise reduction of rectangular enclosures with one flexible wall", Journal of the Acoustical Society of America, Vol. 35, pp.1791-1797, 1963.

65. A.J. Pretlove, "Free vibrations of a rectangular panel backed by a closed rectangular cavity", Journal of Sound and Vibration, Vol. 2, pp.197-209, 1965.

66. A.J. Pretlove, "Forced vibrations of a rectangular panel backed by a closed rectangular cavity", Journal of Sound and Vibration, Vol. 3, pp. 252-261, 1966.

67. D.J. Ketter, "Coupled cavity/panel vibrations", American Institute of Aeronautics and Astronautics Journal, Vol. 3, pp. 2162-2164, 1965.

68. T. Kihlman," Sound radiation into a rectangular room. Applications to airborne sound transmission in buildings", Acustica, Vol. 18, pp. 11-20, 1967.

69. M.C. Bhattacharya, M.J. Crocker, "Forced vibration of a panel and radiation of sound into a room", Acustica, Vol. 22, pp. 275-294, 1969/70.

70. R.W. Guy, M.C. Bhattacharya, "The transmission of sound through a cavity-backed finite plate", Journal of Sound and Vibration, Vol. 27, pp. 207-223, 1973.

71. R.W. Guy, "The response of a cavity backed panel to external airborne excitation: A general analysis", Journal of the Acoustical Society of America Vol. 65, pp. 719-731, 1979.

72. R.W. Guy, "The steady state transmission of sound at normal and oblique incidence through a thin panel backed by a rectangular room – a multi modal

analysis", Acustica, Vol. 43, pp. 295-304, 1979.

73. R.W. Guy, "The transmission of airborne sound through a finite panel, air gap, panel and cavity configuration – a steady state analysis", Acustica, Vol. 49, pp. 323-333, 1981.

74. J. Pan, D.A. Bies, "An experimental investigation into the interaction between a sound field and its boundaries", Journal of the Acoustical Society of America, Vol. 83, pp. 1436-1444, 1988.

75. J. Pan, D.A. Bies, "The effect of fluid-structural coupling on sound waves in an enclosure-Theoretical part", Journal of the Acoustical Society of America, Vol. 87, pp. 691-707, 1990.

76. J. Pan, D.A. Bies, "The effect of fluid-structural coupling on sound waves in an enclosure-Experimental part", Journal of the Acoustical Society of America, Vol. 87, pp. 708-727, 1990.

77. J. Pan, "The forced response of an acoustic-structural coupled system", Journal of the Acoustical Society of America, Vol. 91, pp. 949-956, 1992.

78. J. Pan, "A study of the medium frequency response of sound field in a panel-cavity system", Journal of the Acoustical Society of America, Vol. 103, pp. 1510-1519, 1998.

79. J.G. Ih, J.H. Lee, "A prediction method for the sound transmission loss of finite double partitions at low frequencies", Inter-Noise, Aug. 27-30, 2001.

80. F. Scarpa, G. Curti, "A method for the parametric frequency sensitivity of interior acousto-structural coupled systems", Applied Acoustics, Vol. 58, pp. 451-467, 1999.

81. F.J. Fahy, C. Schofield, "A note on the interaction between a Helmholtz resonator and an acoustic mode of an enclosure", Journal of Sound and Vibration, Vol. 72, pp. 365-378, 1980.

82. A. Cummings, "The effects of a resonator array on the sound field in a cavity", Journal of Sound and Vibration, Vol. 154, pp. 25-44, 1992.

83. A. Gonenc-Sorguc, “Shaping of sound fields inside acoustoelastically coupled enclosed spaces”, Ph.D. Thesis, Mech. Eng. Dept., Middle East Technical University, Feb. 1997.

84. A. Doria, “A simple method for the analysis of deep cavity and long neck acoustic resonators”, Journal of Sound and Vibration, Vol. 232, pp. 823-833, 2000.

85. F.K. Bogner, R.L. Fox, I.A. Schmmit, “The generation of inter-element compatible stiffness and mass matrices by the use of interpolation formulas”, Proceedings of Conference on Matrix Methods in Structural Mechanics, AFDFL-TR-66-80, pp. 397-443, 1965.

86. A. Houmat, “An alternative hierarchical finite element formulation applied to plate vibrations”, Journal of Sound and Vibrations, Vol. 206, pp. 201-215, 1997.

87. D.J. Allman, “A simple cubic displacement element for plate bending”, International Journal for Numerical Methods in Engineering, Vol. 10, pp. 263-281, 1976.

88. D.J. Allman, “A compatible triangular element including vertex rotations for plane elasticity analysis”, Computers and Structures, Vol. 19, pp. 1-8, 1984.

89. D.J. Allman, “Evaluation of the constant strain triangle with drilling rotations”, International Journal for Numerical Methods in Engineering, Vol. 26, pp. 2645-2655, 1988.

90. D.J. Allman, “Analysis of general shells by flat facet finite element approximation”, Aeronautical Journal, Vol. 95, pp. 194-203, 1991.

91. D.J. Allman, “A basic flat facet finite element for the analysis of general shells”, International Journal for Numerical Methods in Engineering, Vol. 37, pp. 19-35, 1994.

92. D.J. Allman, “Implementation of a flat facet shell finite element for applications in structural dynamics”, Computers and Structures, Vol. 59, pp. 657-663, 1996.

93. E.H. Dowell, C.F. Chao, D.B. Bliss, “Absorption material mounted on a moving wall-fluid/wall boundary conditions”, Journal of the Acoustical Society of America, Vol. 70, pp. 244-245, 1981.

94. S. Marburg, H.J. Hardtke, “ A study on the acoustic boundary admittance: determination, results and consequences”, Engineering Analysis with Boundary Elements, Vol. 23, pp. 737-744, 1999.

95. L.L. Beranek, Noise Reduction, McGraw-Hill, Inc., USA, 1960.

96. P. Juhl, “A note on the convergence of the direct collocation boundary element method”, Journal of Sound and Vibration, Vol. 212, pp. 703-719, 1998.

97. S. Marburg, “Six boundary elements per wavelenth: is that enough ?”, Journal of Computational Acoustics, Vol. 10., pp. 25-51, 2002.

98. B. Irfanoglu, M. Caliskan, “Mixed variable direct coupling FEM / BEM approach to structural acoustic coupling problems”, Proc. of the 8-th Int. Congr. On Sound and Vibration, Hong Kong, 2001.

99. B. Irfanoglu, M. Caliskan, A. Gonenc-Sorguc “Analysis of structurally coupled acoustic fields by acoustoelasticity and integrated FEM-BEM approaches”, Proc. of the 9th Int. Congr. on Sound and Vibration, Orlando, USA, 2002.

100. B. Irfanoglu, M. Caliskan, “Application of FEM/BEM method to interior acoustical field shaping by Helmholtz resonators”, Int. Conf. on Theoretical and Computational Acoustics, USA, 2003.

101. D.A. Dunavant, “High degree efficient symmetrical gaussian quadrature rules for the triangle”, International Journal for Numerical Methods in Engineering, Vol. 21, pp. 1129-1148, 1985.

102. M. Abramowitz, I.A. Stegun, Handbook of Mathematical Functions with Formulas, Graphs, and Mathematical Tables, National Bureau of Standards, USA, 1964.

VITA

Bülent İrfanoğlu was born in Ankara on October 24, 1966. He received his B.S. degree in Faculty of Engineering, Department of Mechanical Engineering from the Middle East Technical University and M.S. degree in Engineering Science in 1994. His main areas of interest are computational and experimental studies in acoustics, vibrations, modal analysis and structural dynamics.